Journal of South American Earth Sciences 70 (2016) 115–144

Contents lists available at ScienceDirect

Journal of South American Earth Sciences

journal homepage: www.elsevier.com/locate/jsames

The Itataia phosphate-uranium deposit (Ceará, Brazil) new petrographic, geochemistry and isotope studies

César Ulisses Vieira Veríssimo [a, *], Roberto Ventura Santos [b], Clóvis Vaz Parente [a], Claudinei Gouveia de Oliveira [b], José Adilson Dias Cavalcanti [c], José de Araújo Nogueira Neto [a]

[a] Departamento de Geologia, Universidade Federal do Ceará, CE, Brazil
[b] Instituto de Geociências, Universidade de Brasília, DF, Brazil
[c] CPRM - Companhia de Pesquisa de Recursos Minerais, DGM - REFO-CE, Brazil

ARTICLE INFO

Article history:
Received 7 October 2015
Received in revised form
13 April 2016
Accepted 6 May 2016
Available online 11 May 2016

Keywords:
Isotope geochemistry
Hydrothermal fluids
Phosphorus-uraniferous ores
Itataia deposit
Brazil

ABSTRACT

The Itataia phosphate-uranium deposit is located in Santa Quitéria, in central Ceará State, northeastern Brazil. Mineralization has occurred in different stages and involves quartz leaching (episyenitization), brecciation and microcrystalline phase formation of concretionary apatite. The last constitutes the main mineral of Itatiaia uranium ore, namely collophane. Collophanite ore occurs in massive bodies, lenses, breccia zones, veins or episyenite in marble layers, calc-silicate rocks and gneisses of the Itataia Group.

There are two accepted theories on the origin of the earliest mineralization phase of Itataia ore: syngenetic (**primary**) – where the ore is derived from a continental source and then deposited in marine and coastal environments; and epigenetic (**secondary**) – whereby the fluids are of magmatic, metamorphic and meteoric origin. The characterization of pre- or post-deformational mineralization is controversial, since the features of the ore are interpreted as deformation.

This investigation conducted isotopic studies and chemical analyses of minerals in marbles and calc-silicate rocks of the Alcantil and Barrigas Formations (Itataia Group), as well as petrographic and structural studies. Analysis of the thin sections shows at least three phosphate mineral phases associated with uranium mineralizaton: (1) A prismatic fluorapatite phase associated with chess-board albite, arfvedsonite and ferro-eckermannite; (2) a second fluorapatite phase with fibrous radial or colloform habits that replaces calcium carbonate in marble, especially along fractures, with minerals such as quartz, chlorite and zeolite also identified in calc-silicate rocks; and (3) an younger phosphate phase of botryoidal apatite (fluorapatite and hydroxyapatite) related with clay minerals and probably others calcium and aluminum phosphates. Detailed isotopic analysis carried out perpendicularly to the mineralized levels and veins in the marble revealed significant variation in isotopic ratios. Mineralized zones exhibit a decrease in $\delta^{13}C$ and $\delta^{18}O$ isotope values and a higher $^{87}Sr/^{86}Sr$ ratio toward the center of the vein. In conjunction with petrographic studies, these changes contesting the hypothesis of a sedimentary origin for uranium and suggest a radiogenic Sr input by alkaline to peralkaline fluids from fertile granites of the end of Brasiliano/Pan-African orogeny, located outside the deposit. The origin of the phosphorous is associated with phosphorite deposits in the same depositional environment of the neoproterozoic supracrustal quartz-pelite-carbonate sediments of the Itataia Group.

Considering the studies conducted here and available geological data, three main mineralizing events can be identified in Itataia: (1) an initial high temperature event connected with a sodium metasomatism-related uranium episode, taking place in Borborema Province and its African counterpart; (2) a second lower temperature stage, consisting of a multiphase cataclastic/hydrothermal event limited to fault and paleokarst zones; and (3) a third and final event, developed in frankly oxidizing conditions. The last two involving mixing of hydrothermal and meteoric fluids.

* Corresponding author. Departamento de Geologia, Centro de Ciências, Universidade Federal do Ceará, Fortaleza, CE, Brazil.
E-mail addresses: cesarulisses85@gmail.com, verissimo@ufc.br (C.U.V. Veríssimo).

http://dx.doi.org/10.1016/j.jsames.2016.05.002
0895-9811/

1. Introduction

Uranium has become an important commodity in the global mineral resources market, largely due to the increasing impact of greenhouse gases related to fossil fuel energy production. As such, new nuclear power plants are being considered for future global energy production, even in countries that previously banned these facilities. Brazil, for instance, has announced the construction of new nuclear power plants, which will require a major increase in uranium production.

In the 1970s and early 1980s a major mineral prospecting campaign conducted by the Brazilian government located a number of uranium deposits, including Lagoa Real and Itataia. The latter, which is the focus of this study, is located in Ceara State, Northeast Brazil, and contains a reserve of 142,500 tons of uranium associated with 18 million tons of phosphate ore (Mendonça et al., 1985). Previous studies on the Itataia uranium deposit have reached different conclusions concerning the origin of mineralization.

An early study concluded it is related to convective fluids associated with post-orogenic fertile granites, responsible for widespread episyenization (Angeiras et al., 1978, 1981). However, other studies have concluded that the mineralization of Itataia is a primary sedimentary deposition of uranium-bearing carbonate fluorapatite (Favali and Leal, 1982; Saad et al., 1984). According to these authors, U^{6+} ions were reduced to U^{4+} in marine environments near the coast. Further research by Mendonça et al. (1985) and Castro et al. (2005a) detailed the different types of uranium-phosphate ores and discussed the remobilization of uranium and phosphate-bearing minerals under metamorphic and supergene conditions.

Castro et al. (2005a) also conduct isotopic analysis for $\delta^{18}O$ and $\delta^{13}C$ in marbles samples from a drill-hole of Itataia mineralized zone, correlating isotopic heterogeneity to the percolation of fluids second low-angle ductile shear zone. The nature of the fluids was attributed to meteoric or connate water that migrated a few hundred meters depths.

More recently, data obtained during the Phosphates of Brazil project carried out by *Geological Survey of Brazil* (CPRM) in 2010 indicated alkaline rocks associated with anorogenic magmatism as the primary source of both phosphate and uranium. The results of this project were published by Santos et al. (2014) and Cavalcanti and Bessa (2011), who describe other uranium-phosphate deposits in Ceara state, associated with feldspathic alkaline rocks (albitites) and volcanic rocks related to Mesozoic magmatism (Rio Ceará-Mirim dyke set). These rocks are intrusive into Paleoproterozoic basement gneisses of the Itataia Group (São José do Macaoca) and in Neoproterozoic granites that make up the Santa Quitéria magmatic arc, located west of the Itataia U–P deposit. In the 1980s, the Brazilian company Nuclebrás also investigated some of these occurrences, including Serrotes Baixos, Mandacarú and Taperuaba, which display similar geological features to those found in Itataia (Favali et al., 1984; Leal et al., 1984; Haddad , 1981).

In this regard, the present work is a new contribution to the genetic model of tatiaia deposit based in petrographic, mineral chemistry and isotopic geochemistry data. A better understanding of the genesis of the Itataia ore deposit is also important for planning future exploration campaigns in the area. In this paper, a detailed study of the mineralized zones was carried out to investigate the origin of uranium-phosphate-rich fluids. Field observation, petrography and detailed isotope geochemistry (oxygen, carbon, and strontium isotopes) were used to determine whether or not the mineralization fluids imprinted major isotopic variations on the host rocks.

2. Regional geologic features

The Itataia deposit and other related phosphorus-uraniferous occurrences are located in the Ceará Central Domain (CC), in the northern segment of the Borborema Province and northeastern portion of the South American Platform (Almeida et al., 1981) (Fig. 1).

The Borborema Province (BP) consists mainly of a Neoarchean and Paleoproterozoic migmatitic gneiss complex, representing the basement of the region, which is partially covered by Mesoproterozoic to Neoproterozoic metasedimentary and metavolcanic supracrustal rocks. The latter are intruded by Neoproterozoic to Ordovician granitic bodies (Brito Neves et al., 2001).

The BP was defined as part of the collage of Neoproterozoic Western Gondwana, formed during the collision of an orogenic complex system situated between the Amazonian-São Luis/West Africa and São Francisco-Congo cratons (Brito Neves and Cordani, 1991; Trompette, 1994; Van Schmus et al., 1995; Brito Neves et al., 1999). The province is divided into domains Médio Coreaú (MC), Ceará Central (CC), Orós-Jaguaribe (OJ) and Rio Grande do Norte (RN) by large transcurrent shear zones, namely Transbrasiliano (TBSZ), Senador Pompeu (SPSZ), Portalegre (PASZ) and Patos (PSZ) (Brito Neves et al., 2000; Medeiros, 2004) (Fig. 1).

The Ceará Central Domain (CC) is divided as follows: (1) Archean basement represented by the Cruzeta Complex (Oliveira and Cavalcante, 1993); (2) Paleoproterozoic accretionary terranes that encompass the Canindé Complex (Torres et al., 2008), São José da Macaoca and Algodões units, Sítio dos Bois and Cipó orthogneisses and the Madalena Suite (Cavalcante et al., 2003); (3) the Neoproterozoic metasedimentary passive margin sequence represented by the Ceará Complex, including Quixeramobim and Independência Units (Castro, 2005; Arthaud, 2007; Arthaud et al., 2008, 2015); (4) the Neoproterozoic Tamboril-Santa Quiteria magmatic arc; (5) Neoproterozoic to Cambrian granites; (6) Eopaleozoic molassic basins associated with Brasiliano strike-slip shear zones; and (7) Cretaceous magmatism represented by Rio Ceará-Mirim dykes (Figs. 1 and 2).

3. Sampling and analytical procedures

Quantitative chemical analyses of feldspars, amphiboles and apatites in marbles and calc-silicate rocks of the Itataia Deposit were carried out at the Institute of Geosciences Electron Microprobe Laboratory, University of Brasília. The equipment used was a Jeol JXA-8230 with five WDS spectrometers and EDS. The calibration conditions applied were 20 kV and 25 nA, with a beam diameter of 5 μ and 10 s of exposure time. The structural formulas were calculated using Minpet 2.0 program, observing the procedures developed by Leake et al. (1997).

A total of 117 samples were analyzed for C and O isotopes, and 10 samples for Sr isotopes. Samples were taken from selected outcrops as well as drill cores that crosscut the mineral deposit. In general, the samples were well preserved and show slight signs of weathering. Samples of carbonates for carbon, oxygen, and strontium isotopes were extracted using a hand-drill, enabling detailed sampling such as profiles across mineralized veins.

For oxygen and carbon isotopes, an aliquot of about 300 μg of each sample was placed in glass vials that were subsequently flushed with He at 72 °C. After flushing, the aliquots were attached with concentrated phosphoric acid and the CO_2 released was analyzed for carbon and oxygen isotopes in a Delta V Advantage spectrometer connected to a Gas Bench II apparatus. The $\delta^{18}O$ e $\delta^{13}C$ were calculated using international standards (NBS-18, NBS-19,

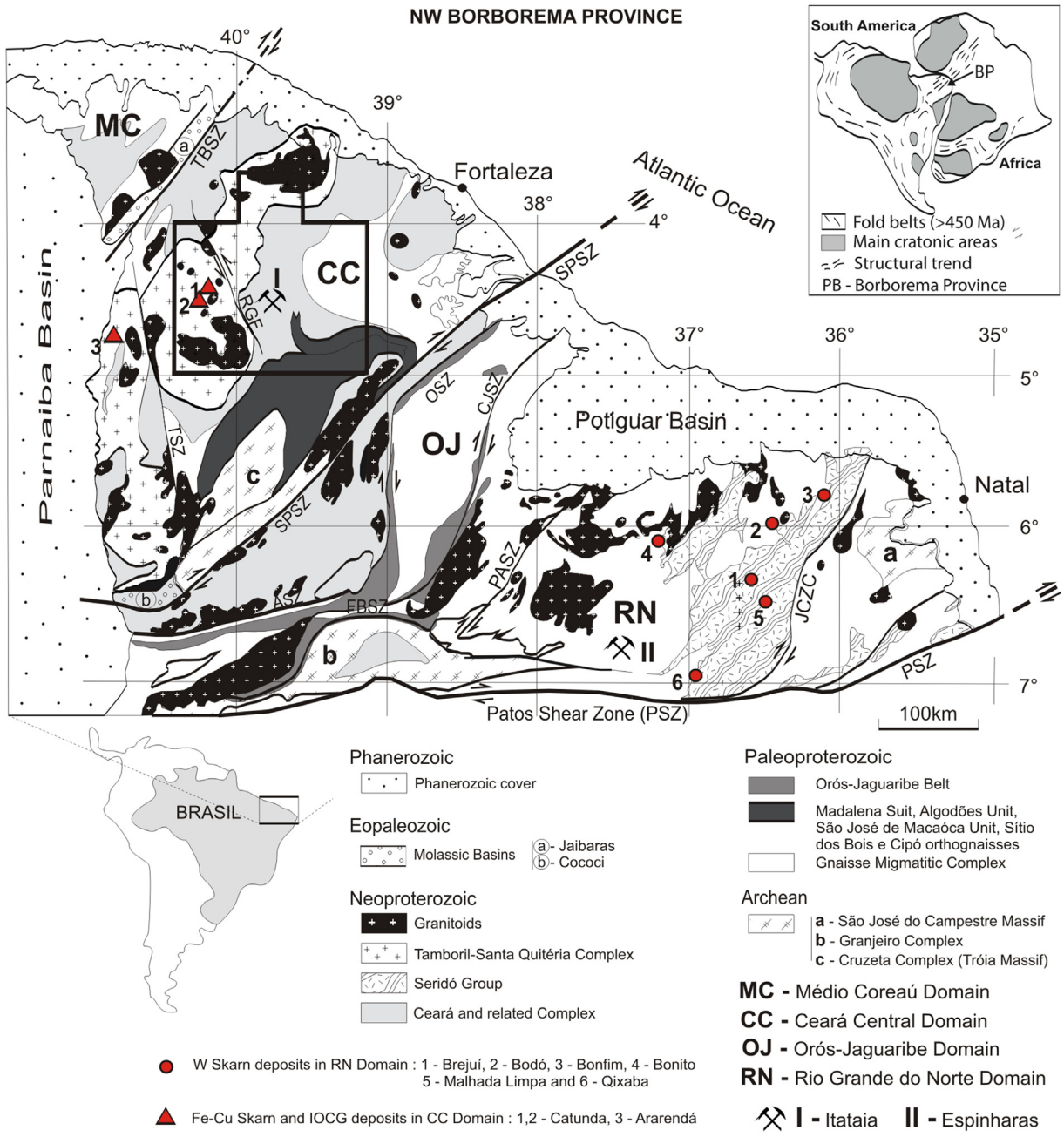

Fig. 1. Simplified geological map of the northwest Borborema Province showing the main geologic units from the Médio Coreaú – MC, Ceará Central – CC, Orós – Jaguaribe – OJ and Rio Grande do Norte–RN domains. Main phosphate-uranium deposits, tungsten skarns deposits, iron-copper skarn and IOCG deposits in the BP. Major shear zones: TBSZ, Transbrasiliano (Sobral-Pedro II); SPSZ, Senador Pompeu; ASZ, Aiuaba, OSZ, Orós; JSZ, Jaguaribe; FBSZ, Farias Brito; PASZ, Porto Alegre; JCSZ, João Câmara; PSZ, Patos; TSZ, Tauá; RGF, Rio Groairas fault. (modified from Mont'Alverne et al., 1998; Cavalcante et al., 2003; Souza Neto et al., 2008, Arthaud et al., 2015 and Parente et al., 2015).

BSC-27, GEFA-28) and reported in permil relative to PDB. For $^{87}Sr/^{86}Sr$ analysis, 50 mg of carbonate powder samples were weighed into Teflon beakers and digested in weak acetic acid to dissolve only the carbonate fraction and avoid leaching Rb from the non-carbonate constituents of the samples. $^{87}Sr/^{86}Sr$ ratios were measured using a Thermo Neptune MC-ICP-MS, at the Geochronos Laboratory of the University of Brasília. Analyses of NBS 987 standard carried out during this study yielded an average value of 0.710230 ± 8 (1σ). Uncertainties in individual analyses were better than 0.01% (2σ).

4. Phosphorus-uraniferous occurrences in the Ceara Central domain

4.1. Additional occurrences around the Itataia deposit

There are several other minor phosphate-uranium occurrences around the Itataia deposit, largely characterized by (1) > 10 ppm anomalous uranium in an aerial gamma spectrometry survey, (2) positive results in phosphate detection tests using ammonium molybdate, and (3) measurements above 1000 cps using a scintillation counter (Cavalcanti and Bessa, 2011).

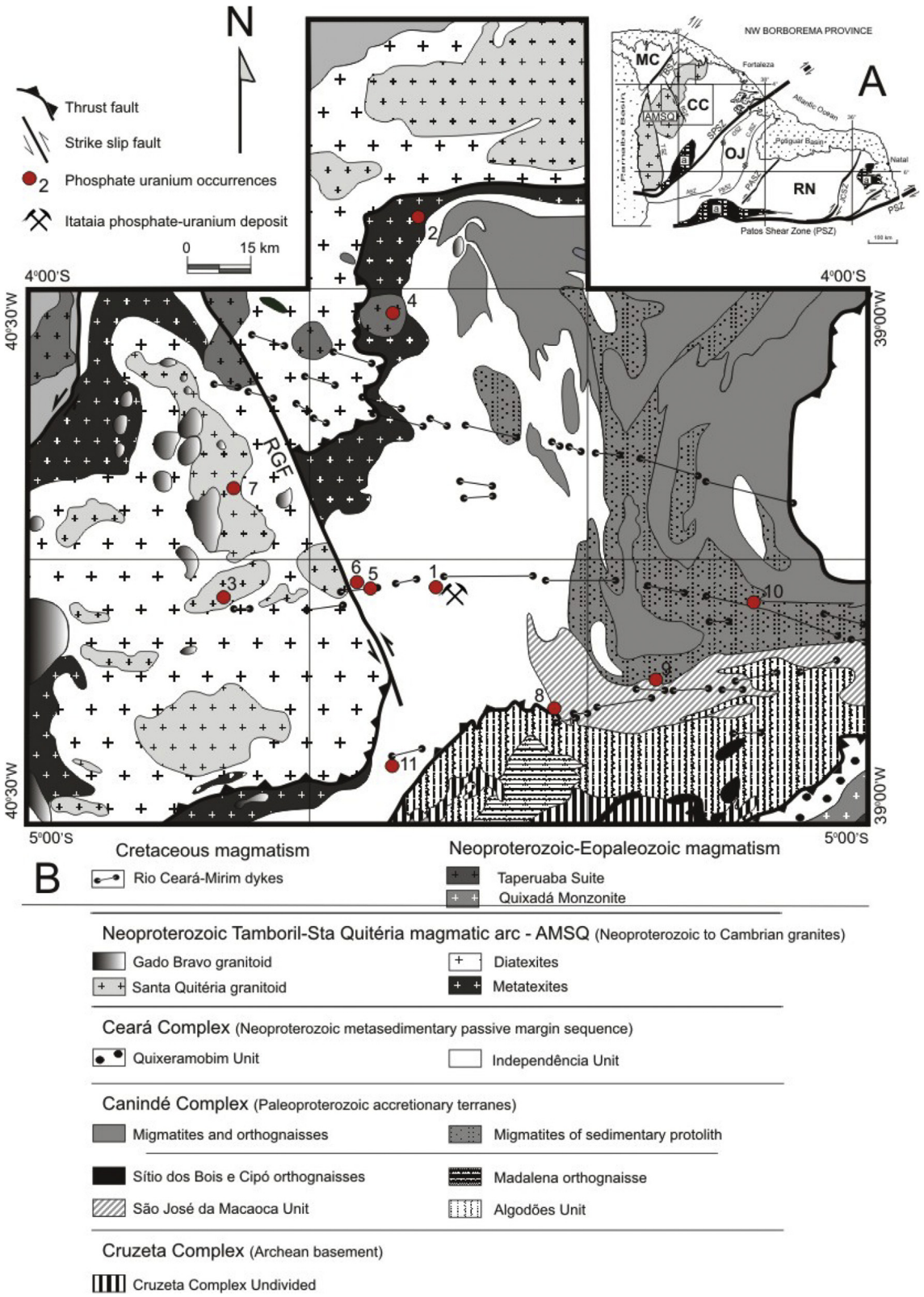

Fig. 2. A) Crustal blocks of the northern Borborema Province (adapted from Brito Neves et al., 2000 and Cavalcante et al., 2003). B) Simplified geological map of the part of the Ceará Central domain, with the location of the Itataia deposit and others phosphate-uranium occurrences (red circles): (1) Itataia Deposit; (2) Mandacarú Farm; (3) Serrotes Baixos; (4) Taperuaba; (5) Itataia oeste 1; (6) Itataia oeste 2; (7) Aquiri Farm; (8) Madalena, (9) Manitoba Farm; (10) Pedra Preta Farm; (11) Águas Belas. Compiled and modified from Cavalcante et al. (2003), Torres et al. (2008), Cavalcanti and Bessa (2011). (For interpretation of the references to colour in this figure legend, the reader is referred to the web version of this article.)

These occurrences are related to episyenite bodies resulting of hydrothermal alteration of Neoproterozoic granitic bodies in the region. Furthermore are recorded albitization processes associated with alkaline magmatism Cenozoic Rio Ceará Mirim (Cavalcanti and Bessa, 2011) (Fig. 2).

Features common to all instances include evidence of Na-metasomatism, iron oxide impregnation and the presence of apatite as prismatic crystals and/or as collophane (microcrystalline apatite), typically filling rock cavities and voids. Fig. 2B illustrates the major occurrences mapped around the Itataia deposit.

4.2. Itataia deposit

4.2.1. Ore occurrence types

They are found five main ore types in the Itataia phosphate-uranium deposit: massive collophanite, stockwork or vein type, carbonaceous breccia, carbonate breccia and episyenite.

Massive collophanite—fine-grained ore, massive, red-colored, formed by amorphous apatite (collophane), exhibiting cavities filled by newly formed pyramidal quartz, altered feldspar, calcite, graphite and clay minerals (Fig. 3A).

Stockwork – network of small, irregular collophanite veins so closely spaced along fractures and foliation plans in marbles. Its occurrence limited to depths of less than 150 m, while decreasing or even absent (Castro et al., 2005a). The proximity and association with fault planes can be seen in galleries and on the escarpment which limits the main uranium anomaly (Figs. 3D and 8).

Carbonaceous breccias—show breccia texture with centimetric fragments of feldspathic rock, marble with graphite lamellae and calc-silicate rock supported by carbonaceous matrix of fine to medium grained. The collophanite occurs or disseminated in the matrix, or filling veins and cavities together with calcite (Fig. 3 B). Distributed in restricted area within the main orebody, limited between the topographic levels 480 and 400 m. The carbonaceous breccias show high uranium and zirconium content, as well as varying amounts of pyrite, zircon, graphite, chlorite, goethite and clay minerals. Uranium occurs both associated with black phosphatic material, as well as the zircon, to much higher levels than in collophanite (NUCLEBRÁS, 1984; Alcântara e Silva, 2003).

Carbonate breccias – correspond to the breccia ores formed by karst processes of dissolution of the marbles (Alcantil Formation) accompanied by calcite recrystallization, with or without fault-related. It contain rounded to subangular fragments of marble and calc-silicate rocks ranging from a few millimeters to 30 cm, surrounded by concentric layers of collophane cemented by calcite. The fragments are impregnated by intergranular collophane coated by a newer reddish collophane phase with colloform habit, indicating more of a mineralization phase (Fig. 3 C). In zones of extensional faults occur both marble fragments as of collophanite rotated and cemented by goethite, collophane and calcite (Fig. 8 C and D).

Episyenites—ores with pegmatoid and vacuolar texture, which contains disseminated collophane and filling voids, often bordering albite crystals. However the presence of coffinite ($USiO_4$) was described in just a sample of apatite analyzed during the mineral exploration of the deposit (NUCLEBRÁS, 1984). The episyenites exhibit light rose to red-brown color, tabular or lenticular geometry, metric thickness, average grain thick, and that cut both gneisses and marbles (Fig. 3 E and F).

4.2.2. Field features and ore structural control

The Itataia uranium-phosphate deposit is hosted by Neoproterozoic supracrustal quartz-carbonate rocks (Santos, 2003; Castro et al., 2005a) that surround the Santa Quitéria Arc (Fetter, 1999). These rocks are within the Itataia Group and, together with the Independence Unit and Ceará Complex, form part of the geotectonic Ceará Central Domain (Arthaud et al., 1998).

The Itataia Group is dominated by high amphibolite grade metamorphosed sedimentary rocks that were strongly deformed during the Brasiliano-Pan-African orogeny. In the area are recorded two deformational events developed in ductile conditions. A first set as D_1, recognized only in the rocks of the Paleoproterozoic basement (São José de Macaoca Unit) and another younger, progressive (D_2) related to Brasilian orogeny that affected the rocks of the Itataia Group (Arthaud et al., 1998 . Santos, 2003). D_2 has been interpreted as a regional compressional episode that resulted in tight isoclinal folds with a low-angle axial plane. These folds trend southwards and are accepted to be related to thrust faults that locally evolved into transcurrent fault zones (Santos, 2003; Santos et al., 2003; Arthaud, 2007). The Itatiaia Group is subdivided into four formations, starting from the bottom to the top by paragneiss migmatized (Serra do Céu Fm) capped by pure and micaceous quartzites, and locally hematite-rich (Laranjeiras Fm) superimposed by another unit of thicker paragneiss (Barrigas Fm) and finally marbles (Alcantil Fm). In metapelitic units (paragneiss) the most common lithotypes are garnet- and sillimanite-bearing gneisses and migmatites. These usually display granitic pegmatitic veins, amphibolitic gneisses and, less often, rhyolitic or dacitic leptinites (Mendonça et al., 1982). The paragneisses of the Barrigas Formation, are thrusted by quartzites of the Laranjeiras Formation, in some instances leading to tectonic intercalation of gneisses and quartzites. The contact between the intermediate gneisses (Barrigas Fm) and marbles of Alcantil Formation is gradational and marked by the occurrence of impure marbles and calc-silicate rocks. In the Alcantil Formation marbles are the main host rock of mineralization (Fig. 4). They are usually calcitic, white to gray in color, and may also contain minerals such as graphite, diopside, scapolite, tremolite and phlogopite. These marbles are usually more than 50 m thick and, in cases of successive tight folding, can be up to 500 m thick. In addition to marbles, gneisses and calc-silicate rocks also host uranium-phosphate mineralization.

Metamorphic parageneses of rocks in the Itataia Group include calcite + phlogopite + tremolite + quartz in marble of the Alcantil Formation; and biotite + feldspar + silimanite + muscovite + garnet in gneiss of the Barrigas Formation. Based on metamorphic parageneses, Santos (2003) estimated that these rocks were subjected to temperatures up to 650 °C and pressures ranging from 5 to 6 kbar.

The main record of uranium ore in the deposit Itataia occurs at the top of a hill, with an altitude of 580 m, along an east-west fault-line scarp. The main orebody stretches 900–1000 m east-west and is 200–300 m wide, with a known thickness around 150–200 m (Saad et al., 1984; Silva, 2003). Inside main collofanite orebody occur: smaller bodies of massive ore, mineralized breccias, stockwork and disseminated ore (Fig. 4).

Other minor occurrences are hosted in NW-SE fractures and along the tectono-metamorphic foliation. The correlation between the east-west fault plane, main ore body and the highest uranium anomalies (4800 to 7100 cps) can be observed when radiometric lines and geological local map are superimposed (Fig. 5). Since uranium is closely associated with phosphorus, brittle control is the same for the phosphorous anomaly. The projection of structural data measured in boreholes and underground research galleries shows that Itataia ore has developed along an important fault and fracture system. The brittle structures include a set of normal faults associated with extensional and shear fractures oriented E-W and NW-SE (Figs. 6 and 7).

The simple fault and sheeted fault planes show a close association with carbonate breccias, calcite veins and collophanite. The spatial distribution of discontinuities are presented in stereoplots

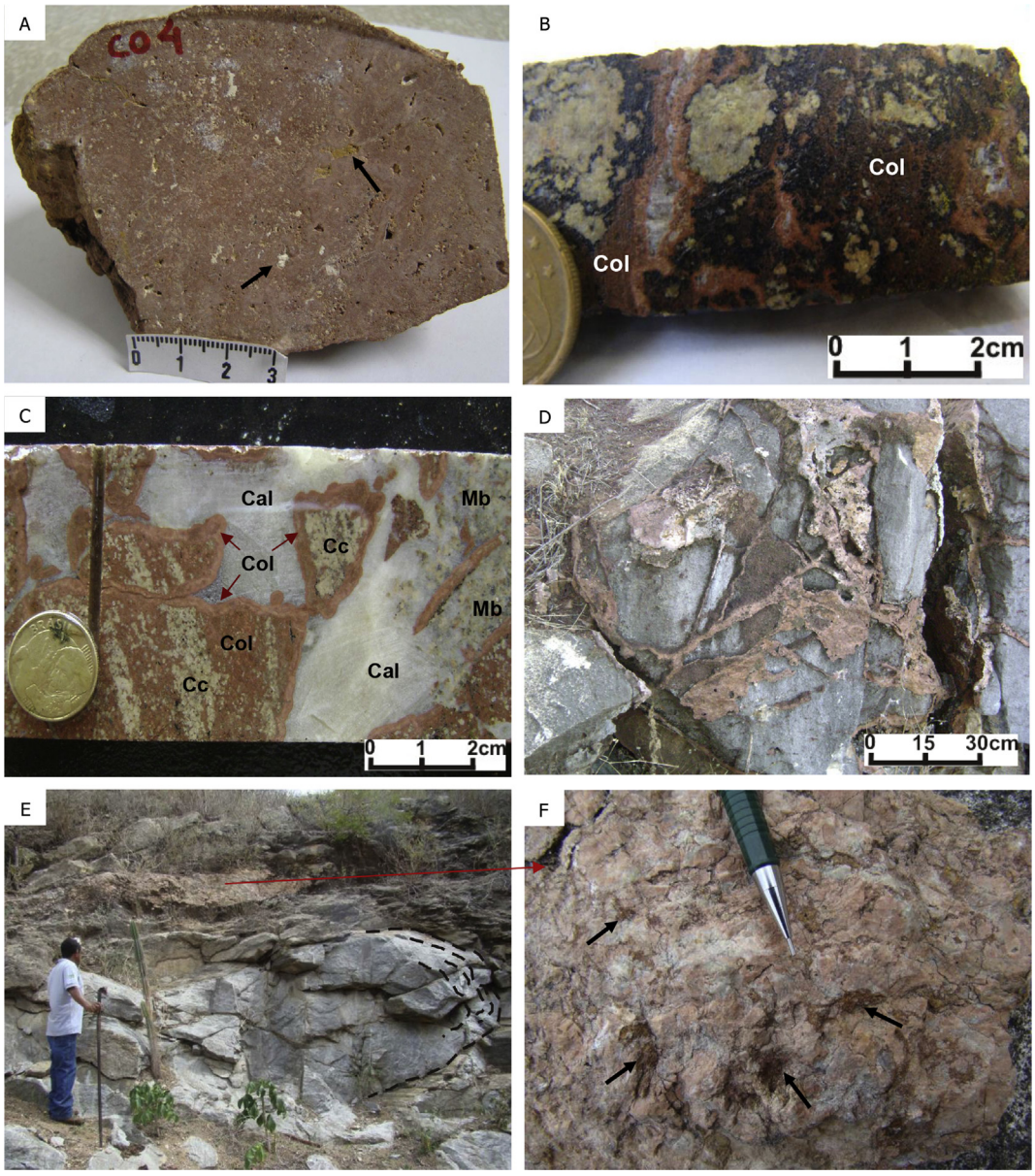

Fig. 3. A: Massive collophanite ore sample containing microcrystalline apatite and clay minerals. The black arrows indicate cavities which may be filled with calcite, quartz, feldspar, graphite or clay minerals. B and C: Drill core showing collophanite associated with carbonaceous and carbonate breccias where clasts are composed of feldspatic rock, marble (Mb), calc-silicate rocks (Cc) and collophanite (Col). The matrix of the breccias may be either a well-crystallized carbonate (Cal) or dark gray carbonaceous rock. D: Collophanite veins crosscutting marbles or Stockwork type ore.E and F: epysyenite ore filling voids (devido a lixiviação de quartzo) by quartz leaching (black arrows).

showing three sets of fracture/fault trending: NNW-SSE, NW-SE and E-W. Inside the subterranean galleries a gradual south to north increase in ore volume was observed, accompanied by brecciation and karstification of Alcantil Formation marbles (Fig. 8).

The east-west fault trace controls the formation of a broad valley and extends regionally toward the Precambrian basement of the Itataia Group, penetrating the Neoproterozoic Tamboril-Santa Quiteria magmatic arc. Several targets or other uranium occurrences were recorded throughout this regional east-west brittle trend with or without phosphates, in the same direction as Cretaceous dykes (see Fig. 2).

At least two important karstification phases were observed inside galleries intercepting the highest uranium anomaly. An early hydrothermal phase enabled the crystallization of calcite megacrystals in cavities and voids suggesting hipogenic carsctification process (Fig. 8 C, D, E and F), while a younger stage developed at a lower temperature, where rainwater rich in phosphate and uranium percolated into discontinuous planes, leading to the precipitation of a microcrystalline phosphate phase containing high levels of uranium–collophane (Fig. 8 E and F).

Large calcite crystals ore monocrystalline speleothems are rare in “normal” (i.e. meteoric) caves. In surface condition, most calcite crystals grows by the competitive enlargement and coalescence of crystallites deposited as syntaxial (axially aligned) overgrowths on previous crystals (Self and Hill, 2003; Ford and Williams, 2007). Usually mega crystals of carbonates (calcite and dolomite) and sulfate (gypsum) are commonly observed in hydrothermal environments or hypogenic caves – often referred to as “thermal caves” (Dong et al., 2013; Bella et al., 2016; García-Ruiz et al., 2007; Forti, 2010; Audra et al., 2010; Otoničar, 2013; Bella et al., 2016).

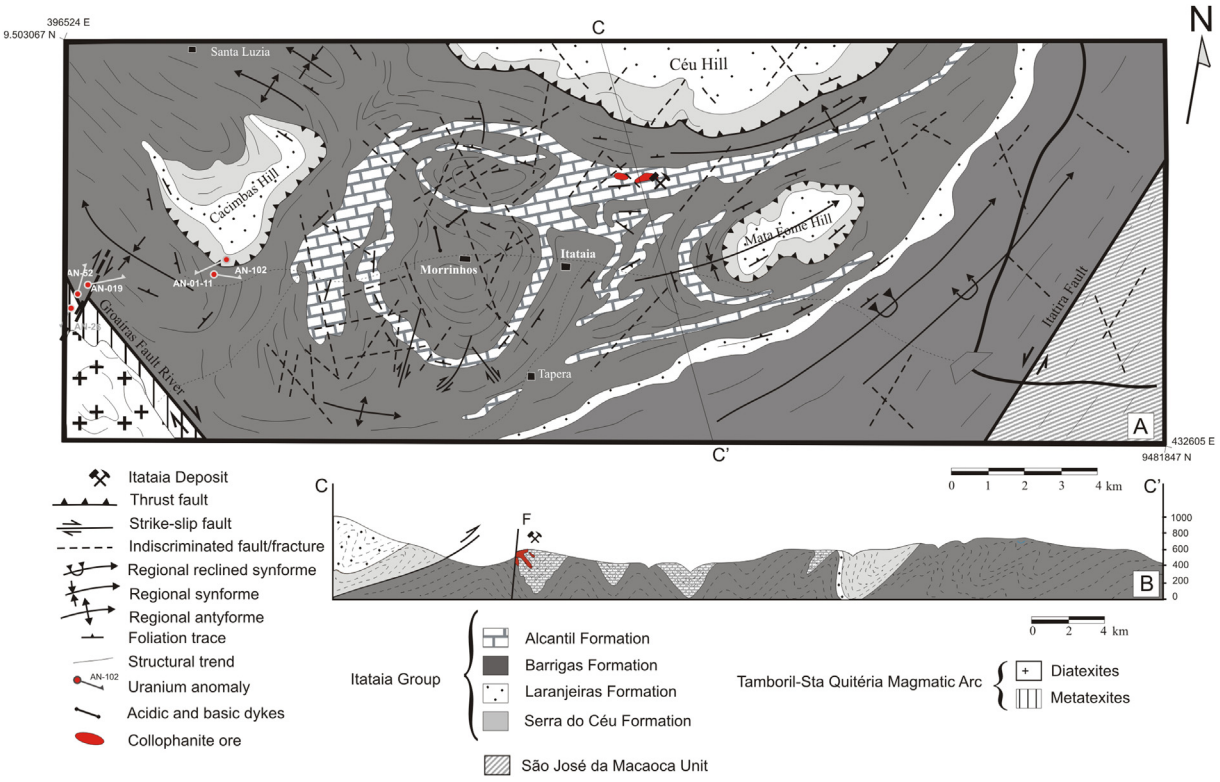

Fig. 4. A) Geological map and location of the Itataia phosphate-uranium deposit (adapted from Mendonça et al., 1985; Santos, 2003 and Pires, 2012). B) Geological section across the Itataia neoproterozic supracrustal Group.

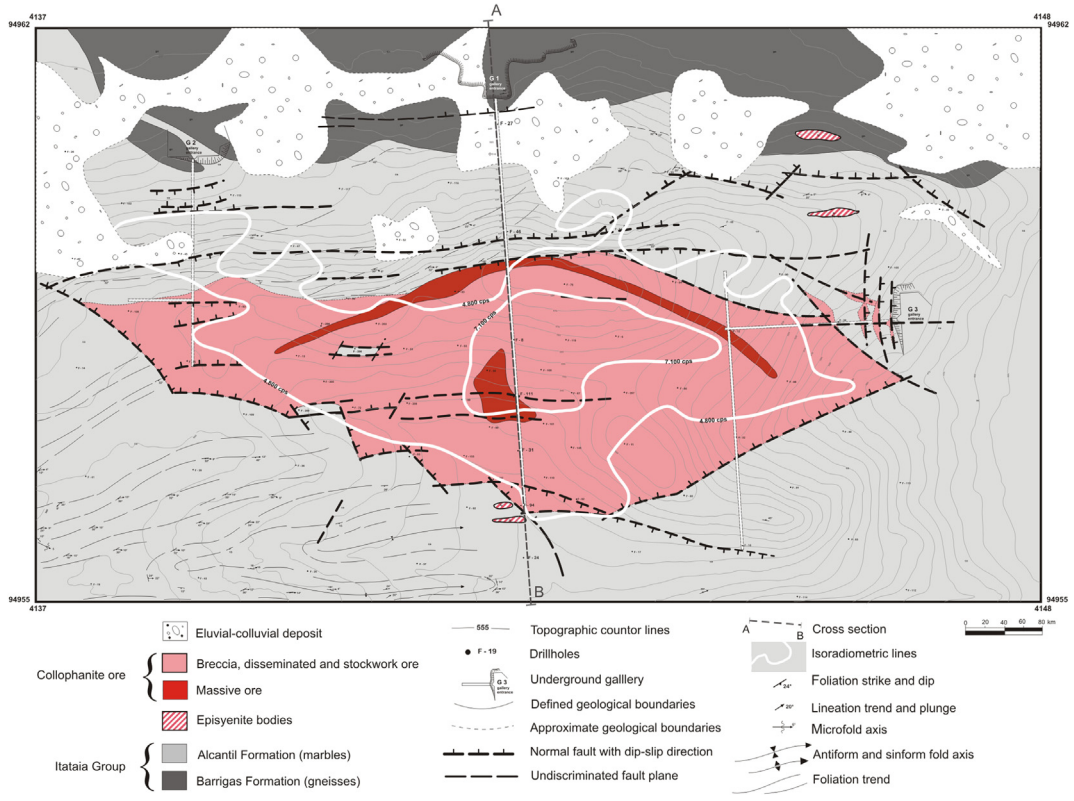

Fig. 5. Geological map of Itataia phosphate-uranium deposit, illustrating the main ore body and its association with fault planes and highest uranium anomalies (4800 to 7100 cps) (modified from NUCLEBRÁS, 1984).

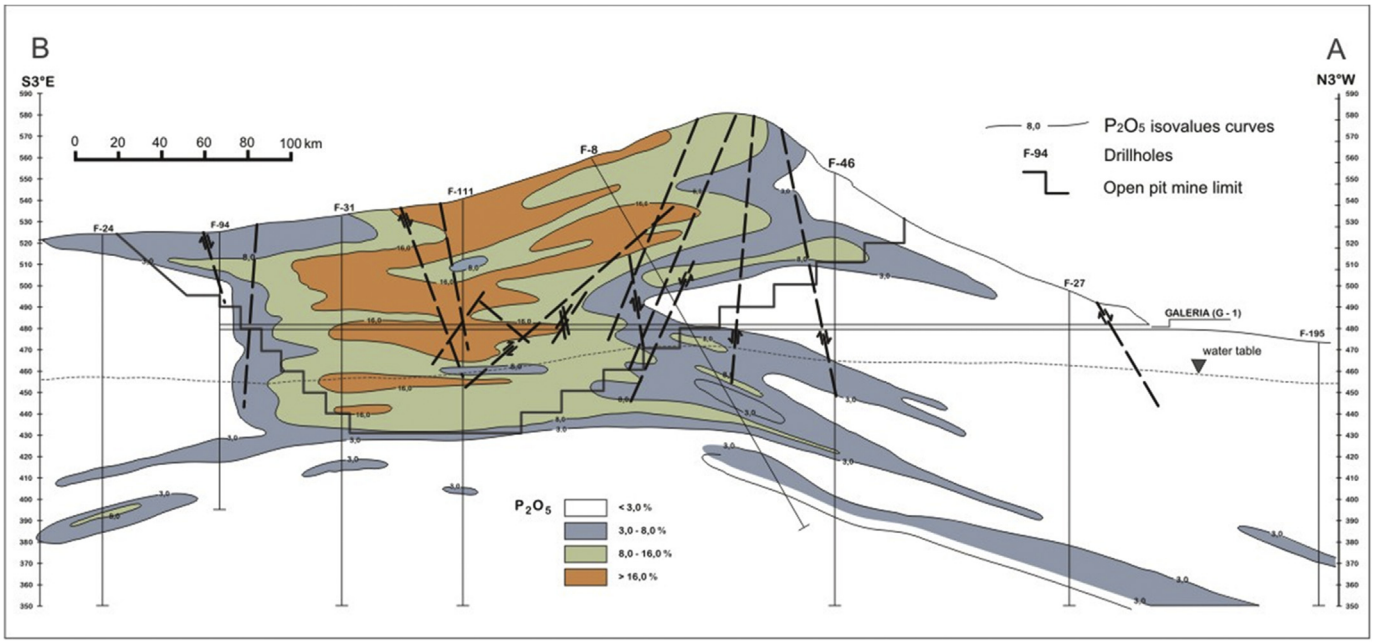

Fig. 6. Cross section through the main uranium mineralized zone with P_2O_5 isovalues curves. The AB section is drawn on the geological map of Fig. 5 and shows the strong correlation between east-west fault line scarp, main collophanite ore body and the P_2O_5 isovalues. Since uranium is closely associated with phosphorus, brittle control is the same for the phosphorous anomaly (adapted from NUCLEBRÁS, 1984 and Alcântara e Silva, 2003).

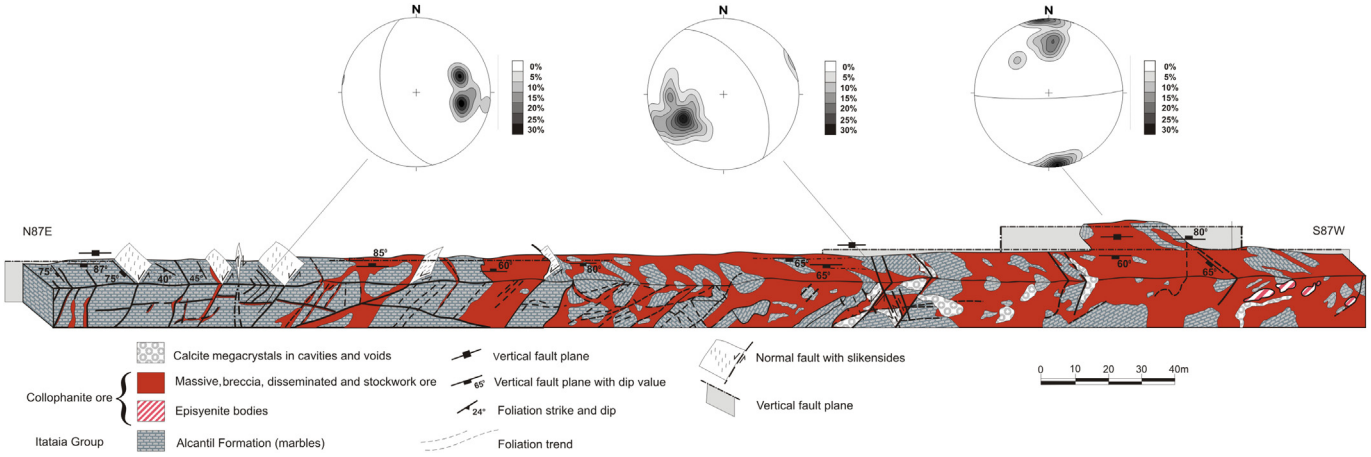

Fig. 7. Detailed geological and structural map of gallery G-3 illustrating the relation of collophanite ore and brittle tectonic. From south to north is noted a gradual increase in ore volume, accompanied by brecciation and karstification of marbles. The spatial distribution of fractures and faults were treated statistically and presented in stereoplots (equal area projection, lower hemisphere). The great circles represent the main orientation of fault/fracture planes measured (modified from NUCLEBRÁS, 1984).

An older, ductile structural control can also be seen in galleries and the drill core. Structural and chemical data (isovalue of Al_2O_3) on the Itataia deposit were used to draw up a schematic geological section to assign mineralization to the hinge zone of isoclinal folds, with foliation planes dipping to the north (Fig. 9). These south-trending folds are related to the most important ductile phase (D_2) of the Brasiliano compressional event, characterized by nappes and basal thrusts (quartzites and migmatites of the Laranjeiras and Serra do Céu Formations) over Barrigas gneisses and Alcantil marbles from the top of the Itataia Group (see Fig. 4).

Itataia ore, commonly called collophanite, also exhibits well-defined topographic control, propagating up to 130 m deep. The lower limit of the supergene alteration is clearly visible in the lithochemical profiles (U_3O_8) of drill holes located in the main mineralized zone () and in a cross-section of the phosphorus isovalue (Fig. 6). High phosphorus concentrations (P_2O_5 >16%) are limited to a topographic altitudes of up to 440 m.

4.2.3. *Petrographic features*

Petrography and field features indicate the existence of three main generations of apatite in Itataia: an older generation associated with hydrothermal Na-metassomatic fluids displaying well-formed crystals, a second related to a low temperature hydrothermal event and a younger apatite generation associated with residual massive ore. The older apatite (Ap_1) is well crystalized and usually associated with neoformed chess-board albite and sodic amphiboles (Fig. 11). In mineralized zones of marble and calc-silicate rocks are common relicts of calcic amphibole (tremolite) showing bluish green rims with strong pleochroism (Fig. 11E) and undeformed apatite crystals replacing calcic plagioclase (Fig. 11 A

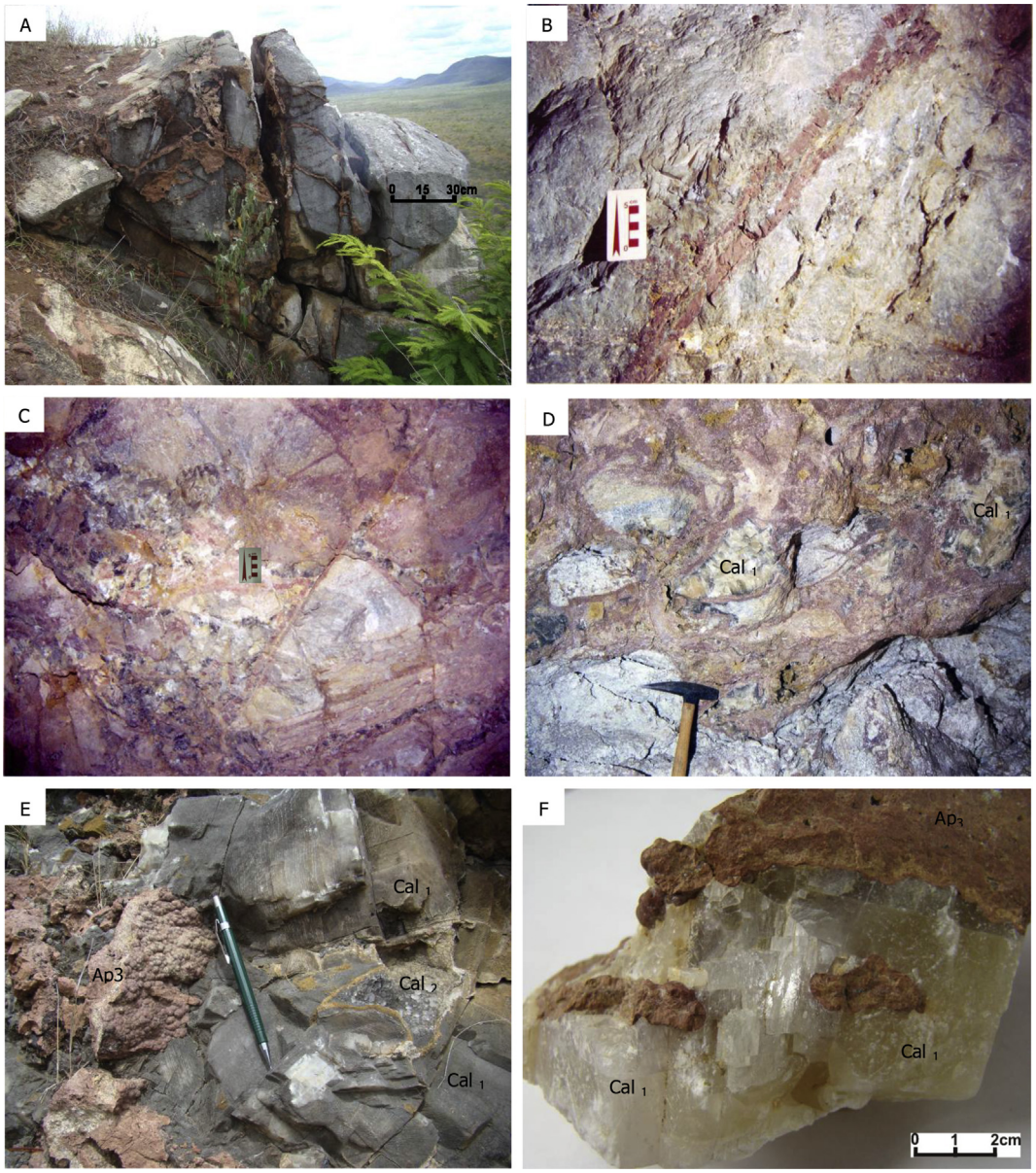

Fig. 8. A: Stockwork collophanite ore in fault scarp located north of the main uranium anomaly of Itataia deposit. B and C: Fractures and faults in the Alcantil Formation marbles inside G3 gallery generating breccias filled by collophanite. D: Breccia collophanite ore and calcite megacrystals (Cal_1) within karstified marbles of Alcantil Formation inside G3 gallery. E and F: Residual collophanite phase (Ap_3) with botryoidal texture covering and filling voids in hydrothermal calcite crystals. Note two stages of calcite formation: megacrystals of hydrothermal calcite (Cal_1) and minor calcite crystals filling voids generated by dissolution of megacrystals (Cal_2) (E).

and B) suggesting strong input of alkaline hydrothermal fluids rich in sodium.

This U-bearing prismatic apatite (Ap_1) often occurs together with colloform apatite (Ap_2) on marble lenses and calc-silicate rocks of the Alcantil Formation. These lenses have been interpreted as Fe–Ca-bearing carbonate rocks that were transformed via metamorphism into marble and calc-silicate rocks made up of diopside, tremolite, biotite-phlogopite, calcium plagioclase, quartz, and titanite (Castro et al., 2005a). In addition to these rocks, the ore zone is also crosscut by centimeter-to meter-thick pegmatite dykes rich in albite, a small amount of quartz and interstitial colloform apatite (Ap_2) (Fig. 12 A and B).

Veins that crosscut these rocks intercepted by drill cores show interaction between the veins and the host rock, as demonstrated by the gradual transition in the amount of collophanite between the center of these veins and the carbonate host rock (Fig. 12 C and D). Collophanite layers are common throughout the ore deposit and vary from a few centimeters to 1 m thick. In some instances they are stratified and folded, suggesting the ore was deformed, probably during the D_2 tectonic event (Fig. 12 A). However, a close look at these rocks also suggests that a metamorphic mineral assemblage of the marble and calc-silicate rocks was modified by the U–P-bearing fluids. This interpretation is not easily reconciled with the existence of folded collophanite layers and lenses within the marble. However, it is supported by the absence of deformed apatite crystal and the low temperature assemblage of the collophanite (Fig. 11 F). Specific topic further on describes the use of C, O and Sr isotopes to determine whether this replacement process imprinted any isotopic change on the host rock.

Collophanites are also commonly found disseminated in

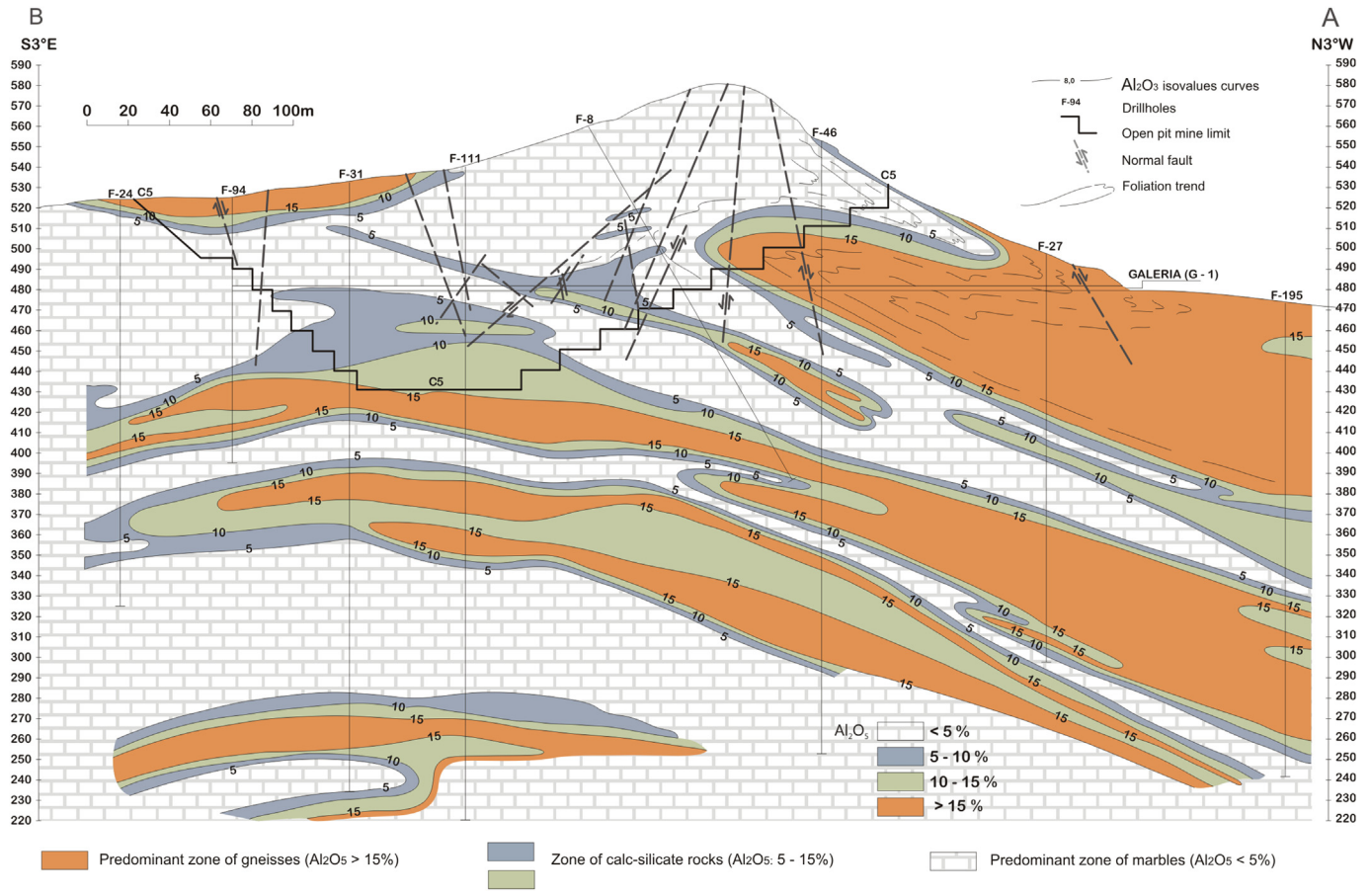

Fig. 9. Cross section through the main uranium mineralized zone with Al_2O_3 isovalues curves. The AB section is drawn on the geological map (Fig. 4) and shows the main ductile and brittle structures and associated geological interpretation (adapted from NUCLEBRÁS, 1984).

feldspatic rocks, marbles and calc-silicates rocks usually connected to collophanite veins. (Fig. 12 A, B and Fig. 13 A).

Petrographic observations indicate that the colloform habit of apatite developed after prismatic apatite. Colloform apatite (Ap_2) fills voids and karst cavities, occurring in association with authigenic quartz, calcite, chlorite and sometimes zeolites (Figs. 13 and 14). This mineral association suggests another hydrothermal event of lower temperature associated with the formation of the second phosphate phase.

Colloform apatite is also associated with breccias and carbonaceous breccias in which the clasts are made up of feldspatic rock, marble, calc-silicate rocks and collophanite itself. The clasts reach up to 30 cm and are usually enveloped by a layered reddish collophane film. The matrix of the breccias can be either well-crystallized carbonate or dark gray carbonaceous rock (Fig. 3 B, C and Fig. 13 B).

It is very common to find fragments impregnated by intergranular collophane coated by a newer reddish collophane phase. Also, more than one generation of calcite crystals encapsulating collophane, suggesting cyclic karstification and mineralization phases (Fig. 3 B, C and Fig. 13 A, B).

A younger apatite phase occurs at the top of the hill and is characterized by reddish and yellowish residual U–P-rich rocks with a typically botryoidal texture. It's associated to massive collophanite ore and except for preserved graphite flakes, there is no evidence of original primary mineral association (Fig. 3 A and Fig. 15 B, C and D). The massive ore is full of voids, some of which are filled with quartz, calcite, graphite, clay minerals and probably by others supergene phosphates.

In the top of Itataia deposit it can be observed the alteration profile of marbles and collophanite ore. A typical lateritic profile, with residual collophanite showing cavernous structure generated by chemical leaching of marbles inside yellowish-brown soil (Fig. 15 A).

X-ray diffractometry analyzes of collophanite ore realized, in this and other works (e.g. Fyfe, 1978; Mendonça et al., 1985) indicates the presence of at least two different apatites: (1) fluorapatite (Ca (PO4)3 F) and (2) hydroxyapatite (Ca5 (PO4)3 (OH)). It is probable that fluorapatite predominates in hydrothermal phases while the hydroxyapatite in residual ores. This fact can be confirmed by more detailed studies including the younger phosphate phases generated in frankly supergene conditions.

4.2.4. *Mineral chemistry*

Mineral chemical analyses were performed on feldspars, amphiboles and apatites present in gneisses from the Barriga Formation and marbles from the Alcantil Formation to study mineral transformations in the host rocks of uranium-phosphorus mineralization.

4.2.4.1. Plagioclase. The crystals analyzed show no chemical zoning and include: (1) newly formed grain together with apatite, quartz and calcite veins filling cavities or fractures in marble and calc-silicate rocks and (2) larger grains associated with biotite, quartz and garnet in the original banded texture of enclosing mineralized gneisses. In the calc-silicate portions containing amphibole and

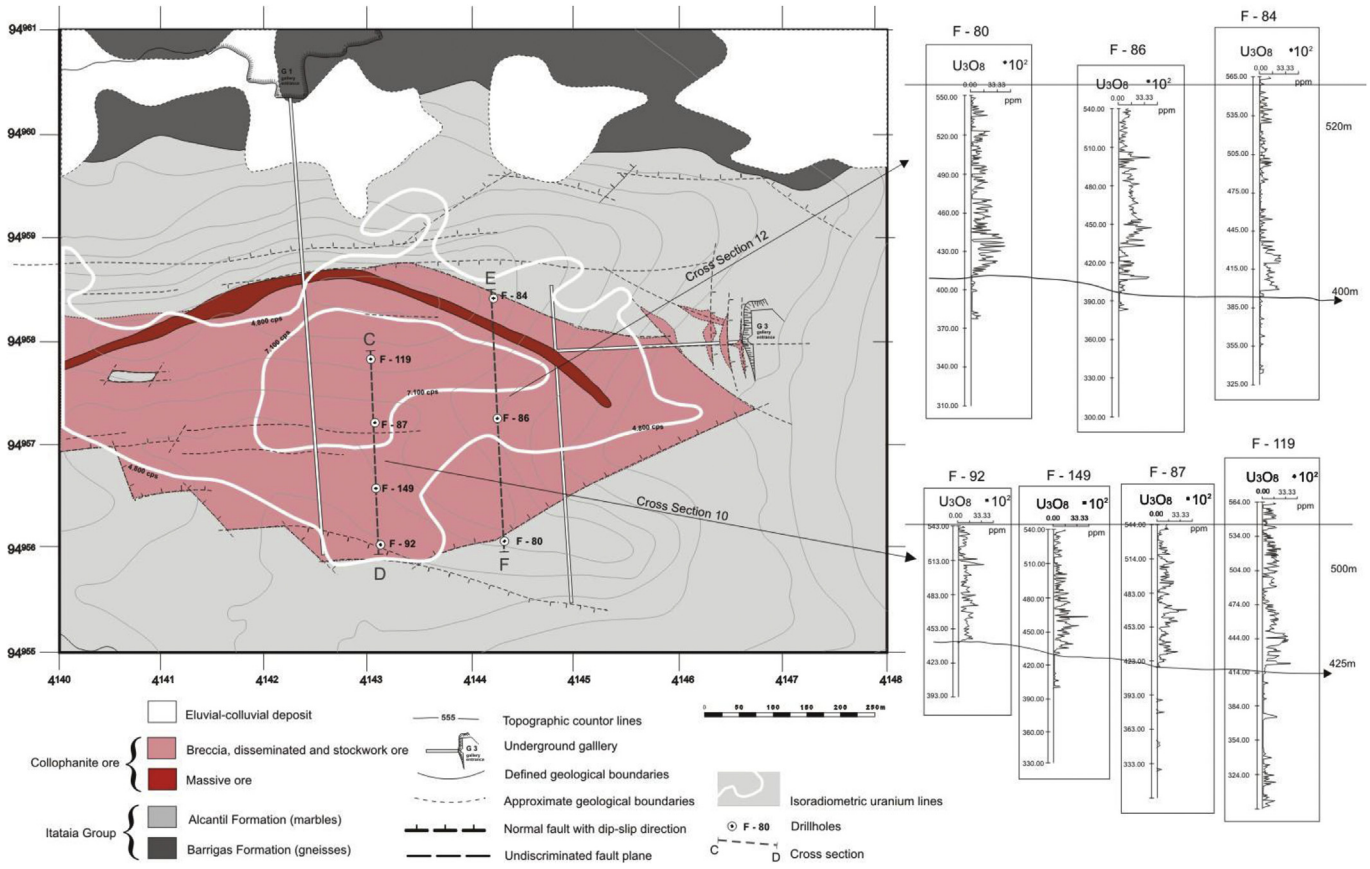

Fig. 10. Lithochemical profiles in different drillholes performed atop the main uranium anomaly showing changes in the levels of U_3O_8 oxide with depth. Uranium concentration was measured by gamma rays (modified from NUCLEBRÁS, 1984).

collophane masses, plagioclase occasionally exhibits chess-board twinning, with microcrystals of albite overlapping larger reddish brown plagioclase crystals (see Fig. 12 A and B). All plagioclase analyzed is composed of albite ($Ab_{95.9 - 99.8}$) with Na_2O content between 11.1 and 12.4% (Table 1). Petrographic observations indicate that most grains have been affected by the albitization process.

4.2.4.2. Amphiboles. Twenty-six punctual analyses were performed on amphibole crystals from four different samples. The structural formulas were calculated on the basis of 24 (O, F, Cl) and the calculation of ferric iron was performed using Minpet 2.0 program. Calcium and sodium groups were identified in marble and calc-silicate gneisses from the Itataia deposit. The calcic amphibole is represented by *actinolite* (Table 2, Fig. 16 and Fig. 17A). These minerals make up the original pre-hydrothermal alteration and mineralization assembly, passing through sodium metasomatism to Na–Ca amphibole and alkali amphibole of the ANa + AK > 0.5 group (Figs. 16 and 17A).

The presence of relict amphibole crystals is common in the mineralized zone, ranging from light green at their center to bluish-green at the rims, exhibiting strong pleochroism and a Fe- and Na-rich composition (Fig. 15). X-ray diffraction analysis performed by Castro (2005) and Castro et al. (2005a) suggested a variety of pargasite slightly enriched in potassium ($(Na,K)Ca_2(Mg,Fe)_4Al(Si_6Al_2)O_{23}$). However, microprobe chemical analysis indicates an amphibole with much higher levels of sodium and iron. While pargasite has an average content of 4% Na_2O and 8% FeO, the amphibole analyzed had compositional range of Na_2O between 7.09 and 8.65% and FeO between 24.3 and 28.9%. Microprobe analysis of the cores and edges of coarser amphibole crystals (0.3–0.5 mm) showed higher lime and magnesia contents in the nucleus and higher sodium, iron and titanium levels toward the edge (Figs. 18 and 19, Tables 2 and 3). These results suggest intake of these elements during sodium metasomatism, turning calcic amphiboles from the *tremolite-actinolite* series (ANa + AK < 0.5; Ti < 0.5) (Table 2 and Fig. 17A) into soda amphiboles (A Na + AK > 0.5) compatible with the composition of *arfvedsonite* ($NaNa_2(Fe^{2+}4Fe^{3+})Si_8O_{22}(OH)_2$) and *iron-eckermannite* ($NaNa_2(Fe^{2+}4Al)Si_8O_{22}(OH)_2$) (Table 3, Fig. 17 B).

Focusing on the mineral chemistry of amphibole (core and edge) it is possible to quantify the removal of Ca and Mg and the approximate contribution of Na and Fe, with the latter increasing more than twice (Fig. 19).

4.2.4.3. Apatite. A total of forty electron microprobe analyses of apatite were performed on four samples of mineralized marbles and calc-silicate gneisses. The structural formulas were calculated on the basis of 26 (O, F, Cl). Two distinct generations of apatite were analyzed: (1) clear prismatic apatite (Ap_1) with a crystal size between 0.05 and 0.1 mm (see Fig. 11 C and D); and (2) cryptocrystalline or amorphous apatite (Ap_2) with a colloform structure (collophane), consisting of concentric spheroidal aggregations (see Fig. 13 C, D and Fig. 14 A, B). Chemical analyses show that both generations correspond to fluorapatite, however, there are some subtle variations observed in relation to their mineral chemistry. The prismatic apatite usually exhibits low uranium content (UO_2 from 0.006 to 0.09% or 2–34 ppm total uranium) and slightly higher average fluorine content, while collophane has higher

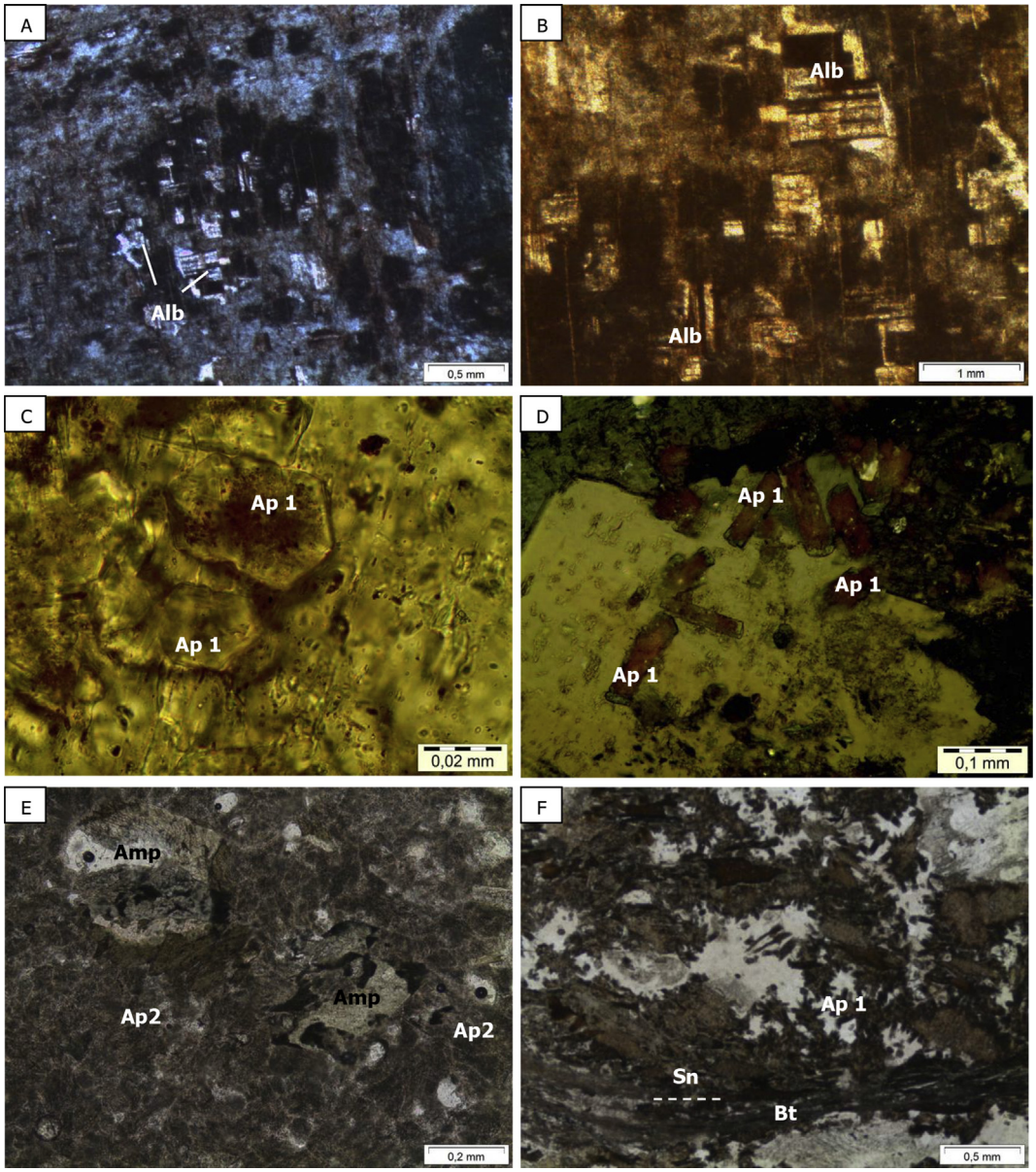

Fig. 11. A and B: Percolation of fluids along fracture and cleavage planes of feldspars, produced albitization and typical chess-board twinning. C and D: Older generation of well-formed apatite crystals associated with hydrothermal fluids. E: Alkali-amphibole (Amp) surrounded by collophorm apatite phase (Ap_2). The amphiboles have a sodium-rich rim relative to their central portion. F: Undeformed apatite crystals (Ap_1) filling voids in calc-silicate rocks. Note the main foliation plane (Sn) defined by biotite flakes (Bt) bypassing the undeformed apatite crystals, indicating it was not affected by the main D_2 regional deformation event. Fig. 11 A, B, D and F were made with crossed nicols while Fig. 11 C and D with parallel.

uranium content (UO_2 from 0.074 to 0.816% or 29–314 ppm total uranium) and lower fluorine content. Prismatic apatite (Ap_1) also has higher P_2O_5 and lower FeO, Na_2O and SrO levels compared to colloform apatite (Tables 4A and 4B). Despite differences all apatites analyzed correspond also to fluorapatite with F contents highest than 2%, indicating the wide prevalence of this mineral during the U–P mineralization phases in hydrothermal conditions.

To younger apatite phases have not been carried out mineral chemical analysis. However, taking the existing diffraction data for colofanitos obtained in this and other previous studies (e.g., Fyfe, 1978; Mendonça et al., 1985). It is possible that besides the fluorapatite there are other phases of calcium (hydroxyapatite, carbonate-hydroxyapatite) and aluminum phosphates formed in frankly supergene conditions.

4.2.5. Isotopic studies

An important aim of Sr isotope studies of hydrothermal deposits is the characterization of the original isotopic composition of the fluid and, therefore, the ultimate source rocks for Sr and also metals. Carbonate minerals are particularly well suited for recording the Sr-isotope signatures of their source fluid, as they readily incorporate Sr but no Rb in their crystal structure (Faure, 1998).

Isotopic studies carried out previously in Itataia match analysis of carbon and oxygen isotopes of thirteen samples collected at different depths along the borehole (F-119) that cuts the mineralized zone (Castro et al., 2005a). Distinct isotopic differences have led the authors to relate the lower $\delta^{18}O$ and $\delta^{13}C$ isotopic ratios with the thrust zone intercepted by drilling, along which fluids would have been channeled. Within the interval of the studied profile

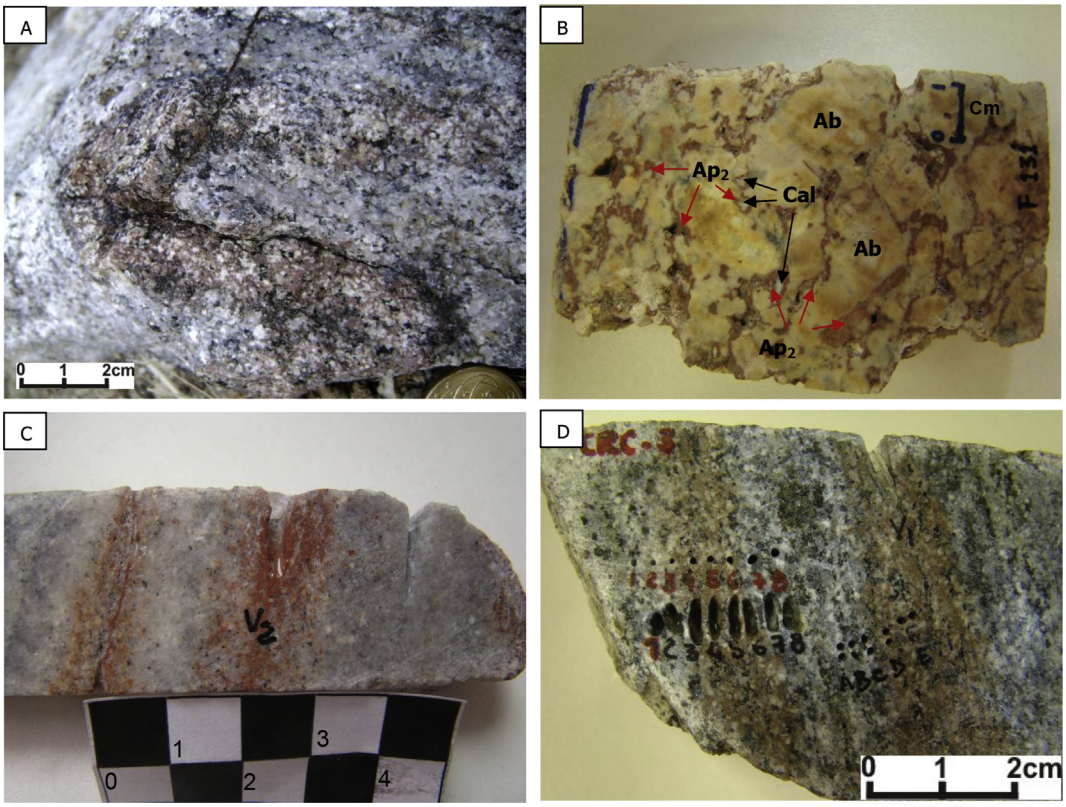

Fig. 12. A: Uranium mineralized pegmatites crosscutting the marbles of the Alcantil Fomation, preserving the structure of the original carbonate rocks. B: Drill core sample of episyenite showing collophanite filling voids left by the leaching of quartz. Colloform apatite phase (Ap_2) and calcite (Cal) filling voids surrounding albite crystals. C and D: Drill cores showing collophanite veins crosscutting marbles and calc-silicate rocks from the Alcantil Formation. Note the gradual transition in the amount of collophanite between the center of these veins and the carbonate rocks, suggesting interaction between the veins and host rocks.

were recognized the presence of mylonite, fault breccias and dissolution associated with karstification processes. The isotopic variations found, much larger than those expected in devolatilization processes, led Castro et al. (2005a) to suggest that the main mechanism responsible for the isotopic heterogeneity in Itataia was channeled percolation fluids. The nature of the fluids was attributed by the authors to meteoric or connate water that migrated a few hundred meters depths.

In order to address the origin of the mineralization fluids in the Itataia deposit, two different set of samples were analyzed. Isotopic data for the first group of samples include were used to evaluate the carbon and oxygen isotopic variations within the scale of the deposit (Fig. 20, Fig. 21). The second group of samples analyzed for carbon, oxygen and strontium isotopes, was used to study small-scale isotopic variations related to the ore-forming fluids (Fig. 22). In the first case it is possible only a comprehensive analysis of data on the deposit of scale without a refined petrographic control. $\delta^{13}C$ ‰ and $\delta^{18}O$‰ diagrams for two drill core samples show similar isotopic results. The most unaltered white and gray marbles have a restricted isotopic composition, with carbon isotopic values ranging between 0‰ and 3‰, and oxygen isotopic values ranging from −6‰ to −8‰. Impure marble and marble samples that present evidence of alteration, such as yellowish color and the presence of clay minerals, display far more variable and negative isotopic values of $\delta^{13}C$‰ and $\delta^{18}O$‰. These samples exhibit carbon isotopic values that fall within the low range for unaltered marbles, but much lower oxygen isotopic values. (Figs. 20 and 21).

Carbonates are also commonly found in other rocks, such as episyenites, breccias, mylonites and calc-silicate rocks. In contrast to marbles, they exhibit lower and more variable carbon and oxygen isotopic values, with carbon ranging between −2‰ and −6‰, and oxygen isotopic values ranging from −10‰ to −14‰. This group of samples also includes well-formed carbonate crystals that fill voids of the residual ore (Figs. 20 and 21). These variations may be related to the original composition of the analyzed rocks, with the temperature changes accompanying the reactions during metamorphism and deformation, or even localized changes generated by the percolation fluids along preferred zones. The latter alternative is considered by Castro et al. (2005a) as the main responsible for the isotopic heterogeneity in Itataia deposit and may indicate the influence of the hydrothermal overprint by fluid with isotopic values quite distinct from those expected when in equilibrium with marble (Figs. 20 and 21).

For detailed isotopic studies were analyzed two drill core samples (marbles and calc-silicate rock), Both cut by veins subconcordant with the tectono-metamorphic foliation, previously assigned to primary mineralization of sedimentary origin.

Fig. 22 shows centimeter-scale isotopic profiles across collophanite veins and their marble host rock. Profiles were performed in order to evaluate whether the mineralization fluids imprinted any carbon, oxygen, or strontium isotopic variation on the marble host rocks. These rocks are particularly suited to this type of study because they have a more homogenous carbon and oxygen isotopic composition, and are expected to have lower radiogenic strontium isotopic ratios. In general, the isotopic profiles show a higher $^{87}Sr/^{86}Sr$ ratio toward the center of the vein, revealing that mineralization fluids were characterized by more radiogenic strontium isotope ratios. In contrast, $\delta^{13}C$‰ and $\delta^{18}O$‰ decreased in the same direction, reinforcing that mineralization fluids were not in isotopic equilibrium with the marble host rocks. This

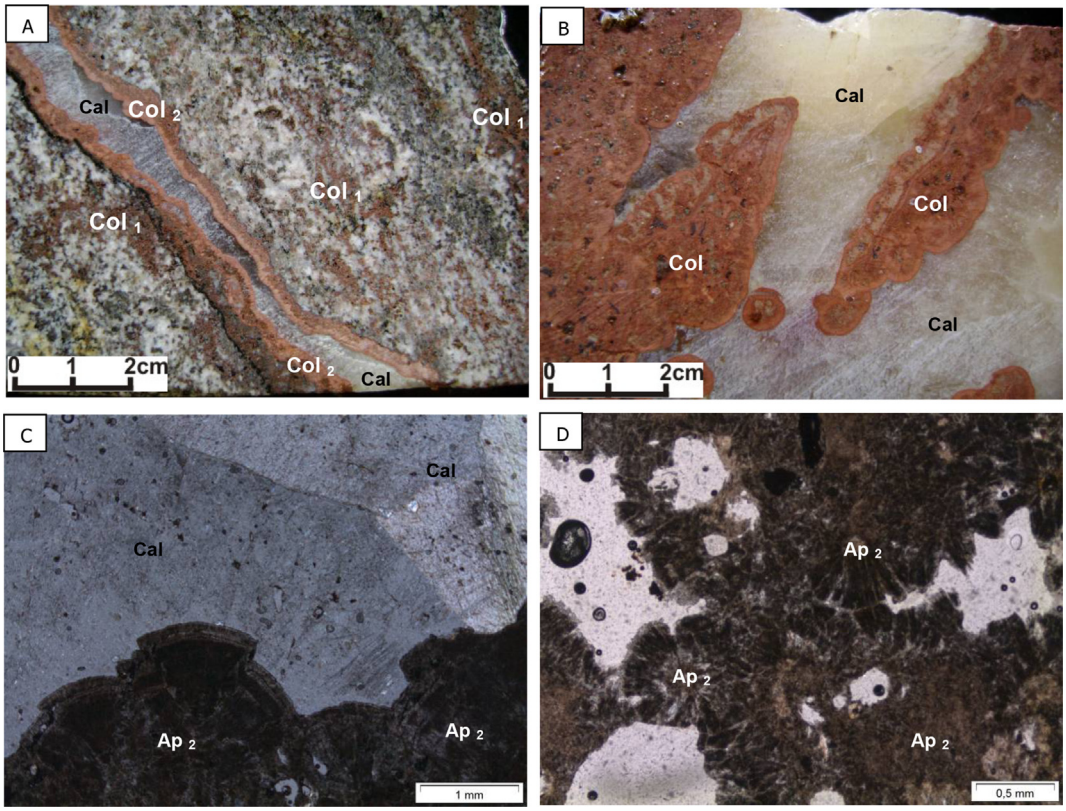

Fig. 13. A: Drill cores showing disseminated collophanite (Col_1) and collophanite veins (Col_2) crosscutting calc-silicate rocks from the Alcantil Formation, B: Drill core showing colloform apatite (Ap_2) filling voids in calcite megacrystals (Cal). C and D: Colloform apatite (Ap_2) filling voids with calcite crystals (Cal) in marble from the Alcantil Formation–plane-polarized light.

indicates the epigenetic nature of the mineralization and calls the sedimentary origin hypothesis into question.

Despite the small number of analyzes, the $^{87}Sr/^{86}Sr$ ratio of marbles and calc-silicates are very uniform and fit into a very tight range (0.7070–70780). The U–P enriched zones is more radiogenic than marble and calc-silicate host rocks, with $^{87}Sr/^{86}Sr$ always greater than 0.7125 suggesting radiogenic Sr influx from magmatic source.

Since collophanite occurs in different types of host rock, it is important to evaluate.

If there are isotopic differences between collophanites and each of the rocks associated. Fig. 23 shows isotopic values of these carbonates and reveals a wide range of isotopic compositions. For instance, carbonate associated with collophanite veins (1 and 2) in marble exhibits $\delta^{18}O‰$ within the same range of the host rock (−7‰ to −13‰), but lower $\delta^{13}C‰$ values (0‰ to −1.3‰). In contrast, collophanite in calc-silicate rocks (3) presents much lower $\delta^{18}O$ (−9‰ to −14‰) and $\delta^{13}C$ (−2‰ to −4.5‰).

5. Discussion and conclusions

Most current classification schemes for uranium deposits emphasize differences in host rock type, host environment, geologic time and geotectonic setting (e.g. Roberson et al., 1978; Bowie, 1979; Nash, 1981; Ferguson, 1987; Dahlkamp, 2009, 1993,1980; Plant et al., 1999; Misra, 2000; Cuney, 2014, 2010,2009). Although these classification schemes remain largely valid and operate with guides and metalogenetic models, it is often difficult to adopt a single model to describe some deposits over time and in different geological settings. This is because most of the known deposits in the world exhibit more than a mineralizing process or various stages of uranium reconcentration.

Different models have been proposed as the primary source of uranium in the Itataia deposit: (1) terrigenous continental source, via adsorption of uranium in organic matter or in marine phosphates accumulated inside localized depressions in shallow marine platform environments (Favali and Leal, 1982; Saad et al., 1984; Mendonça et al., 1985; Castro, 2001; Castro et al., 2005a) and (2) of magmatic origin, related to episyenites formed from fertile post-orogenic granites (Fyfe, 1978; Campos et al., 1979; Angeiras et al., 1981; Angeiras, 1988; Castro, 2005; Castro et al., 2005b). More recent studies highlight the importance of hot spots related to the opening of the South Atlantic in the formation of the Itatiaia deposit and other similar occurrences in the Ceará Central Domain (Santos et al., 2014; Cavalcanti et al., 2013, 2014).

Several authors have suggested different processes in the reconcentration and formation of massive collophanites in Itataia. These include hydrothermal alteration accompanying sodium metasomatism associated with granitogenesis or regional metamorphism, hydrothermal convection systems involving the mixing of meteoric and magmatic fluids, karstification, and supergene enrichment processes.

Analysis of the data presented here and those available in previous studies suggest the multiphase mineralization process for the Itataia deposit, whose primary source is igneous, as already suggested by other researchers (Fyfe, 1978; Campos et al., 1979; Angeiras et al., 1981; Angeiras, 1988; Castro, 2005; Castro et al., 2005b). The distinctly more radiogenic $^{87}Sr/^{86}Sr$ signatures of the mineralized zones as compared to the marble and calc-silicate host rocks, suggest that hydrothermal fluids were derived from a source rock outside de Itataia Group. Probably associated with late to post-collisional granites of the Brasiliano/Pan-African Orogeny.

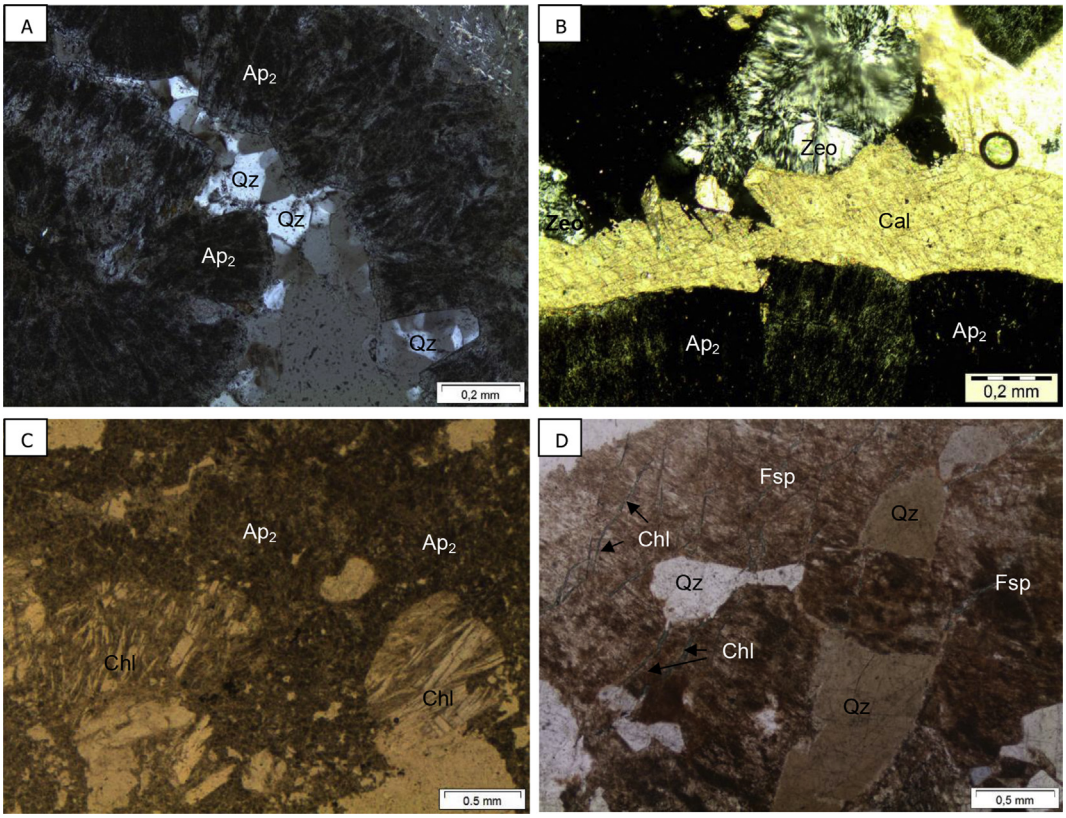

Fig. 14. A: Colloform apatite (Ap_2) filling cavities with authigenic quartz (Qz); B: Apatite associated with zeolite (Zeo) and carbonate (Cal); C: apatite associated with chlorite; and D: Hematitized feldspar (Fsp) containing quartz inclusions (Qz) and fractures filled with chlorite (Chl). Photomicrographs A and B using polarized light and crossed nicols while C and D natural light.

The initial phase was followed by leaching and uranium reconcentration in hydrothermal and supergene conditions, erasing the records of primary uranium mineralogy, probably represented by coffinite and generating an amorphous apatite phase containing uranium (collophane), which predominated and formed mineral ore. The uranium mineral coffinite, commonly associated with epysienites, is described in the internal report of Itataia Project (NUCLEBRÁS, 1984) and in Espinharas deposit (Porto da Silveira et al., 1991) also located in the NW Borborema Province, near of the Patos shear zone.

The main mineralization site coincides with the hinge zone of isoclinal folds and an extensive E-W regional fault, where ore occurs as massive bodies or stockwork filling fractures, faults and carbonate breccias.

5.1. First mineralizing event and regional context

The Itataia deposit is located in the Ceará Central Domain (CC), whose structural framework is the result of a collision between the São Luis-West Africa and São Francisco-Congo cratons during the Brasiliano/Pan-African orogeny, prior to the consolidation of Western Gondwana at the end of the Neoproterozoic period (Arthaud, 2007; Arthaud et al., 2015). The frontal collision between ca 0.66 and 0.60 Ga produced crustal thickening through stacking similar to tectonic nappes described in the Himalayan chain (Caby and Arthaud, 1986). Around 0.59 Ga the frontal collision evolved into an oblique collision, generating north-south continental strike-slip shear zones (Arthaud et al., 2015). This framework was later cut by two dextral EW transcontinental shear zones (Patos and Pernambuco Lineaments), dividing the Borborema Province (PB) into three subprovinces (Caby, 1989; Schobbenhaus and Campos, 1984; Arthaud et al., 2015). Preliminary geochronological data suggest that deformation in the shear zones probably began around 0.60–0.57Ga and continued under decreasing temperature to around 0.50 Ga (Vauchez et al., 1995; Corsini et al., 1998).

Another remarkable feature is the widespread occurrence of Neoproterozoic to Early Paleozoic granitic plutonism (622 Ma to 532 Ma) (e.g. Fetter, 1999; Brito Neves et al., 2003; Neves, 2003).

Similar or correlated structural features and geological evolution are observed between the West Africa and Congo cratons, where extends the Brasiliano/Pan-African orogenic belt based on pre-drift reconstruction (Caby, 1989; Trompette, 1994; Neves and Mariano, 1999; Arthaud et al., 2015).

The rocks of the Itataia Group occur in an area bounded by two strike-slip faults: Groaíras (sinistral) and Itatira (dextral). The former separates the Itataia Group from the Santa Quiteria magmatic arc located to the west, while the latter separates these rocks from their Paleoproterozic basement represented by the San Jose Macaoca Unit.

The main tectonic features of the Itataia group resulted from a southeast to south convergent regime that developed top-to-the-south thrust faults and a stretching lineation over a flat-lying foliation that rotates gradually NW-SE to NE-SW (Santos et al., 2003).

Recent SHRIMP U–Pb zircon ages (0.63 Ga) of paragneisses in the Ceara Complex (Arthaud, 2007; Arthaud et al., 2015) and Sm–Nd isochron age (0.62 Ga) of paragneisses from the Barrigas Formation (Santos et al., 2003) are interpreted to mark the metamorphism time in the Itataia Group.

Petrography and chemical analyses of minerals show that the first Itataia mineralization phase is characterized by severe Na-

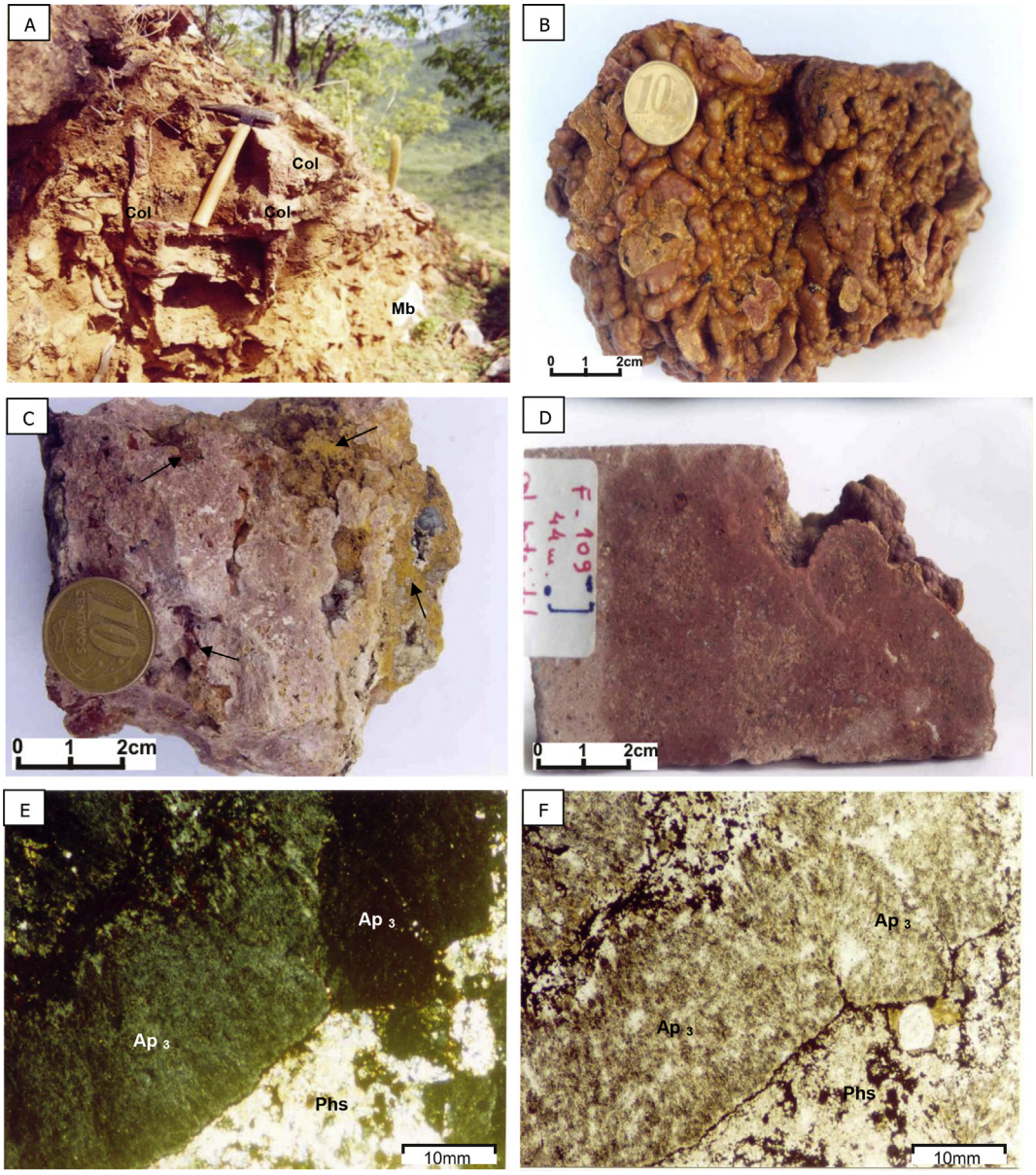

Fig. 15. A: Residual collophanite ore at the top of Itataia deposit. The cavernous structure is similar to other lateritic profiles generated by chemical leaching. Massive collophanite levels (Col) and some marble fragments (Mb) inside yellowish-brown soil. B and C: Massive collophanite ore samples showing botryoidal texture. Note others reddish and yellowish residual phosphate phases not analyzed (black arrows). D and F: Photomicrographs illustrating newest apatite phase (Ap_3) associated with other microcrystalline phosphate phase not analyzed (Phs). E: Using polarized light and crossed nicols while F natural light. (For interpretation of the references to colour in this figure legend, the reader is referred to the web version of this article.)

metasomatism-related episyenitization, hematitization and chloritization, soon after or in the end of deformation and metamorphism that marked the Brasiliano/Pan-African orogenesis.

Uranium mineralization accompanied by hydrothermal alteration connected with quartz dissolution, Na-metasomatism and generation of voids have been reported in several granite-related and/or hydrothermal vein-type U deposits. Hydrothermally altered quartz-depleted rocks are referred to as episyenites, as defined by Lacroix (1920 in René, 2005), due to their syenite-like appearance. The term epysyenitization is typically used to describe a type of subsolidus alteration in Hercynian granites of the Massif Central in France (Poty et al., 1986; Cuney, 1978; Leroy, 1978; Cathelineau, 1987, 1986). Occurrences of the same process in granites connected with uranium mineralization have also been described in: northern Sweden (e.g. Smellie and Laurikko, 1984; Öhlander, 1986), the Bohemian Massif (e.g. Hecht et al., 1999; René, 2005), southern China (Chen et al., 2009; Hu et al., 2008, 2013), southeast Bokan Mountain, the Ross-Adams deposit in Alaska (e.g. Thompson, 1988; Dahlkamp, 1993; Plant et al., 1999), and central Ukraine (e.g., Cuney et al., 2012).

Collophanite ore in the Itataia deposit occurs mainly as massive bodies or as stockwork filling fractures in marble, calc-silicate gneiss, episyenites and carbonate breccias. In veins that cross marble and calc-silicates rocks the colofanito is, as a rule, associated with Na–amphibole and with newly formed albite crystals. The macroscopic features of Itataia episyenites are the same as those described for other well-known episyenites: light rose to red-brown color, equigranular, and medium-grained rock with medium to high porosity. In addition, vugs resulting from hydrothermal leaching of magmatic quartz were filled with newly formed

Table 1
Electron microprobe analyses and mineral formula calculations for selected plagioclase from host rocks of the Itataia deposit. Analyses (1–2): marbles from borehole FS101; (3–7): mineralized zone in marbles from borehole FS34B; (8–12) marbles and calc-silicate rocks from borehole FS35.

Sample	FS101	FS101	FS34B	FS34B	FS34B	FS34B	FS34B	FS35	FS35	FS35	FS35	FS35	
Analysis	1	2	3	4	5	6	7	8	9	10	11	12	
SiO2	67.225	67.942	67.657	68.897	68.485	68.426	68.801	68.916	67.864	68.916	67.263	69.032	
TiO2	0	0	0	0	0	0	0	0.029	0	0	0	0.003	
Al2O3	18.466	18.927	19.337	19.03	18.793	19.094	19.248	19.125	19.023	19.253	18.51	19.138	
FeO	0.072	0.024	0.044	0.02	0.044	0.029	0.035	0.045	0.807	0.069	0.032	0.096	
MgO	0.008	0.006	0	0	0	0.013	0	0	0.662	0	0	0.004	wt. %
BaO	0	0	0.086	0	0.001	0	0	0	0	0.087	0.015	0.036	
CaO	0.032	0.246	0.754	0.019	0	0.054	0.026	0.057	0.043	0.022	0.024	0.012	
Na2O	11.713	11.369	11.145	12.01	11.731	11.652	11.935	12.439	11.705	11.526	11.394	11.979	
K2O	0.03	0.063	0.085	0.031	0.03	0.036	0.035	0.019	0.033	0.058	0.033	0.033	
Total	97.55	98.58	99.11	100.01	99.08	99.3	100.08	100.63	100.14	99.93	97.27	100.33	
O 8													
Sample	FS101	FS101	FS34B	FS34B	FS34B	FS34B	FS34B	FS35	FS35	FS35	FS35	FS35	
Analysis	1	2	3	4	5	6	7	8	9	10	11	12	
Si	3.011	3.008	2.986	3.01	3.016	3.007	3.003	2.999	2.976	3.009	3.017	3.007	
Al	0.974	0.987	1.005	0.979	0.975	0.988	0.989	0.98	0.982	0.99	0.978	0.982	
Ti	0	0	0	0	0	0	0	0.001	0	0	0	0	
Fe2	0.003	0.001	0.002	0.001	0.002	0.001	0.001	0.002	0.03	0.003	0.001	0.003	
Mg	0.001	0	0	0	0	0.001	0	0	0.043	0	0	0	
Ba	0	0	0.001	0	0	0	0	0	0	0.001	0	0.001	a.f.u
Ca	0.002	0.012	0.036	0.001	0	0.003	0.001	0.003	0.002	0.001	0.001	0.001	
Na	1.017	0.976	0.954	1.017	1.002	0.993	1.01	1.049	0.995	0.976	0.991	1.012	
K	0.002	0.004	0.005	0.002	0.002	0.002	0.002	0.001	0.002	0.003	0.002	0.002	
Cations	5.01	4.988	4.99	5.01	4.997	4.995	5.006	5.035	5.03	4.984	4.99	5.009	
Ab	99.6	98.4	95.9	99.7	99.8	99.5	99.7	99.6	99.6	99.6	99.7	99.7	
An	0.2	1.2	3.6	0.1	0	0.3	0.1	0.3	0.2	0.1	0.1	0.1	
Or	0.2	0.4	0.5	0.2	0.2	0.2	0.2	0.1	0.2	0.3	0.2	0.2	

carbonates and albite. In Itataia the only exception is that primary minerals such as uraninite or pitchblende (UO_{2+x}) and coffinite ($USiO_4$), typically present in other granite-related and/or hydrothermal vein-type U deposits, have not been described. The main ore mineral is amorphous apatite (collophane). This is likely due to the multistage nature of mineralization, which includes remobilization and formation of new mineral phases in hydrothermal and supergene conditions, as well as the high solubility of primary uranium minerals in oxidizing conditions, especially in the presence of phosphate ($[PO_4]^{-3}$) and/or carbonate ($[CO_3]^{-2}$) ions, leading to the formation of complex uranyl $[UO_2]^{+2}$ (Langmuir, 1978; Finch and Murakami, 1999). Weathering processes may be particularly effective in leaching uranium, due to the high oxidation state of meteoric waters (Skirrow et al., 2009).

Sodium metasomatism in Itataia is evident in the almost total albitization of episyenites and country rocks and the formation of alkali amphibole group ANa + AK > 0.5. Albitization occurs in at least two stages: first, leading to the formation of albite crystals over k-feldspar (showing chess-board twinning); and second involving the formation of new crystals associated with fluorapatite and carbonates in veins and voids formed by quartz leaching.

Alkali amphiboles are formed by the transformation of *tremolite-actionolite* calcic amphibole into marble, and Fe–Mn–Mg amphibole (*cummingtonite*, *anthopyllite* and *gedrite*) into *arfvedsonite* and *ferro-eckermannite* sodic in calc-silicate gneiss. These changes are accompanied by the formation of fluorapatite, opaque minerals and fluorite.

In uranium deposits related to Na metasomatism, including granite-related or hydrothermal vein-type deposits, temperatures ranging from 350 °C to 550 °C are estimated for the circulation of large volumes of fluids associated with sodic alteration and silica leaching (Skirrow et al., 2009; Cuney, 2010). Experimental synthesis of hydrothermal albite conducted by Martin (1969) suggests that the presence of peralkaline fluids ($Na_2O + K_2O > Al_2O_3$) is essential in order to reach completion in authigenic albite. The alkalinity of fluids related to the first Itataia mineralization event explains the quartz leaching observed, as well as the formation and stability of albite and sodium amphibole.

5.2. Age of the first mineralizing event and other uranium related deposits

Castro (2005) and Castro et al. (2005b) obtained an $^{40}Ar/^{39}Ar$ age of 0.59 Ga for alkali-amphiboles of hydrothermalized rock situated near the entrance of Gallery G-3. Although the potential compositional variation of grain makes the exact meaning of the ages uncertain, the values seem to reflect the age of the metasomatic event, since a significant effect of the crystal's center-edge age would have appeared in the heating phase of the analysis. Based on these ages, the authors suggest that the first mineralizing event at Itataia occurred soon after the regional metamorphism climax (*ca.* 0.60 Ga). This age is compatible with the end of metamorphism, installation of strike-slip regional shear zones and emplacement of post-orogenic granitic bodies in the Brasiliano/Pan-African orogenic belt. As proposed by other authors, this suggests the existence of fertile granitic uranium bodies below the surface in the Itataia region, given the presence of circular structures with radial fractures, interpreted as dome-type structures formed by granitic intrusion (rising pluton) (Fyfe, 1978; Angeiras et al., 1981; Angeiras, 1988).

Additionally, Mendonça et al. (1985) described the occurrence of porous tactite formed from marble in the Alcantil Formation. This occurs due to increased temperature at the edges of the dome-type structure as well as intense muscovitization and turmalinization, suggesting greisenization.

The association between Itataia uranium mineralization and post-Brasiliano granite genesis was also pointed out by Haddad and Leonardos (1980); Haddad (1981), Castro (2005), Castro et al. (2005b) and, more recently, Cavalcanti and Bessa (2011) and Santos et al. (2014). These authors suggest that alkaline granitic

Table 2
Electron microprobe analyses and mineral formula calculations for calcic amphiboles from host rocks of the Itataia deposit. Analyses (1–8): CRC 3; (9–13): F34A and (14):GN2.

Sample	CRC3	CRC3	CRC3	CRC3	CRC3	CRC3	CRC3	CRC3	F34A	F34A	F34A	F34A	F34A	GN2	
Analysis	1	2	3	4	5	6	7	8	9	10	11	12	13	14	
Location	core	core	core	core	core	core	core	core	core	core	core	core	core	core	
SiO2	55.303	56.457	52.883	54.436	53.044	53.04	53.159	54.76	55.713	54.064	53.556	54.446	55.073	51.712	
TiO2	0.025	0.027	0.056	0.021	0	0.023	0.008	0	0	0.343	0.72	0.072	0.067	0.102	
Al2O3	1.662	1.071	1.337	2.903	0.88	0.99	1.31	2.449	1.459	1.531	1.663	2.063	1.099	1.194	
FeO	11.276	10.13	10.827	11.005	10.85	10.586	10.565	11.916	8.077	12.661	12.78	11.974	13.601	9.319	
Cr2O3	0.025	0.01	0.015	0	0.031	0.06	0.103	0.059	0.033	0.05	0.02	0.053	0.018	0	
MnO	0.058	0	0.083	0.049	0.019	0.015	0.049	0	0.014	0.047	0.01	0.04	0.012	0.043	
MgO	16.365	17.989	11.112	16.393	11.291	11.286	10.852	15.584	18	15.077	14.812	15.651	15.027	11.415	wt.%
CaO	12.683	12.725	23.025	12.46	23.289	23.954	22.841	12.184	12.686	11.01	9.769	11.804	8.797	22.702	
Na2O	0.124	0.108	0.502	0.329	0.359	0.317	0.426	0.399	0.201	1.108	1.552	0.438	2.334	0.407	
K2O	0.064	0.048	0	0.099	0	0.018	0	0.072	0.056	0.095	0.131	0.083	0.123	0.028	
V2O3	0.006	0.004	0.019	0	0.099	0.034	0.002	0.063	0.081	0.008	0.086	0.082	0.042	0.057	
BaO	0.031	0.032	0	0	0.016	0.053	0.046	0.151	0	0	0.061	0	0	0	
F	0.259	0.105	0	0.101	0.01	0	0	0.186	0.384	0.198	0.189	0.159	0.406	0	
Cl	0.001	0	0.018	0.018	0.002	0	0	0.018	0.014	0.002	0.019	0.009	0.019	0.012	
Total	97.86	98.7	99.86	97.81	99.86	100.32	99.26	97.78	96.69	96.14	95.35	96.82	96.6	96.99	
O_F_Cl	0.11	0.04	0	0.05	0	0	0	0.08	0.16	0.08	0.08	0.07	0.18	0	
CTotal	97.75	98.66	99.86	97.76	99.86	100.32	99.26	97.7	96.53	96.06	95.27	96.75	96.42	96.99	
24 (O,F,Cl)															
Sample	CRC3	CRC3	CRC3	CRC3	CRC3	CRC3	CRC3	CRC3	F34A	F34A	F34A	F34A	F34A	GN2	
Analysis	1	2	3	4	5	6	7	8	9	10	11	12	13	14	
Location	core	core	core	core	core	core	core	core	core	core	core	core	core	core	
TSi	7.902	7.914	8.068	7.757	8.098	8.078	8.15	7.867	7.97	7.949	7.962	7.881	8.113	8.096	
TAl	0.098	0.086	0.113	0.243	0.074	0.083	0.111	0.133	0.03	0.063	0.082	0.119	0.032	0.103	
TFe3	0	0	0.105	0	0.136	0.151	0.067	0	0	0	0	0	0	0.108	
Sum_T	8	8	8.286	8	8.308	8.312	8.328	8	8	8.012	8.044	8	8.145	8.307	
CAl	0.181	0.091	0.128	0.244	0.084	0.095	0.126	0.282	0.216	0.202	0.209	0.233	0.159	0.117	
CCr	0.003	0.001	0.002	0	0.004	0.007	0.012	0.007	0.004	0.006	0.002	0.006	0.002	0	
CFe3	0.011	0.096	0.142	0.076	0.159	0.183	0.112	0.029	0	0.072	0.176	0.092	0.267	0.14	
CTi	0.003	0.003	0.006	0.002	0	0.003	0.001	0	0	0.038	0.081	0.008	0.007	0.012	
CMg	3.486	3.759	2.527	3.482	2.57	2.562	2.48	3.338	3.839	3.305	3.283	3.378	3.3	2.664	
CFe2	1.313	1.05	1.134	1.193	1.09	1.014	1.175	1.345	0.941	1.375	1.248	1.281	1.264	0.972	
CMn	0.004	0	0.011	0.003	0.002	0.002	0.006	0	0.001	0.003	0.001	0.002	0.001	0.006	
CCa	0	0	1.05	0	1.091	1.134	1.087	0	0	0	0	0	0	1.089	a.f.u.
Sum_C	5	5	5	5	5	5	5	5	5	5	5	5	5	5	
BFe2	0.024	0.041	0	0.043	0	0	0	0.058	0.025	0.11	0.165	0.077	0.145	0	
BMn	0.004	0	0	0.003	0	0	0	0	0.001	0.003	0.001	0.002	0.001	0	
BCa	1.942	1.911	2	1.902	2	2	2	1.876	1.944	1.734	1.556	1.831	1.388	2	
BNa	0.017	0.015	0	0.045	0	0	0	0.055	0.028	0.153	0.265	0.061	0.466	0	
Sum_B	1.986	1.967	2	1.993	2	2	2	1.989	1.998	2	1.986	1.971	2	2	
ACa	0	0	0.713	0	0.718	0.775	0.665	0	0	0	0	0	0	0.719	
ANa	0.017	0.015	0.149	0.046	0.106	0.094	0.127	0.056	0.028	0.163	0.183	0.062	0.201	0.124	
AK	0.012	0.009	0	0.018	0	0.003	0	0.013	0.01	0.018	0.025	0.015	0.023	0.006	
Sum_A	0.029	0.023	0.862	0.064	0.825	0.872	0.791	0.069	0.038	0.181	0.208	0.077	0.224	0.848	
Sum_cat	15.015	14.99	16.148	15.057	16.133	16.183	16.119	15.058	15.036	15.193	15.238	15.048	15.369	16.155	
CCl	0	0	0.005	0.004	0.001	0	0	0.004	0.003	0	0.005	0.002	0.005	0.003	
CF	0.117	0.047	0	0.046	0.005	0	0	0.085	0.174	0.092	0.089	0.073	0.189	0	

intrusions belonging to the Quintas Ring Complex, originally described by Haddad (1981) as the Taperuaba Ring Complex, may be the primary source of Itataia uranium. The Taperuaba syenogranite, located *ca*. 60 km N-NW of Itataia, shows albitization and uranium mineralization (700–820 ppm U_3O_8), and was dated by Castro (2005) at 0.478 Ga (U–Pb zircon age).

There are other deposits similar to and associated with post-collisional granites at the time of the closing of the Brasiliano/Pan-African orogeny. The São José de Espinharas uranium deposit and occurrences in Sítio Bravo/Pocinhos, Araras, CB-62, Pilões, Cajá and Barra de Santa Rosa, located in southern Borborema Province in Paraiba state, are all the result of Na metasomatism accompanied by silica leaching, albitization, hematitization and uranium enrichment (e.g. Santos, 1985; Santos and Anacleto, 1985; Porto da Silveira et al., 1991; Barbosa, 2011; Gomes et al., 2003; Souza et al., 2012).

Geochemical and mineralogical studies carried out by Porto da Silveira et al. (1991) indicates a hydrothermal/metasomatic origin for U mineralization of the Espinharas deposit and coffinite as the only mineral of uranium ore found. As in the Itataia deposit, sodium metasomatism in Espinharas is characterized by quartz dissolution, albitization, neoformation of sodium amphibole, hematitization, chloritization, and phosphate and uranium enrichment (Porto da Silveira et al., 1991; Barbosa, 2011). Likewise, most of the known radiometric anomalies within the Seridó belt are confined to alkali-granites and associated granitic bodies, with some found in the vicinity of Espinharas (Ballhorn et al., 1978).

Similar genetic aspects can be observed across the Atlantic Ocean, within the Central African Fold Belt on the northern edge of the Congo craton. The Kitongo uranium deposit, adjacent to the Patos and Pernambuco (Central Cameroon) shear zones on the African continent, can be classified as Na-metasomatism-related, showing albitization, hematitization and uranium mineralization (Kouske et al., 2012).

U occurrence is hosted by granitic rocks associated with Kogué granitic batholith, one of several granitic intrusions of Pan-African age from Sudanese mobile belt. An Rb–Sr age of ca 0.59 Ga for biotite from granite intrusion is considered the approximate massif

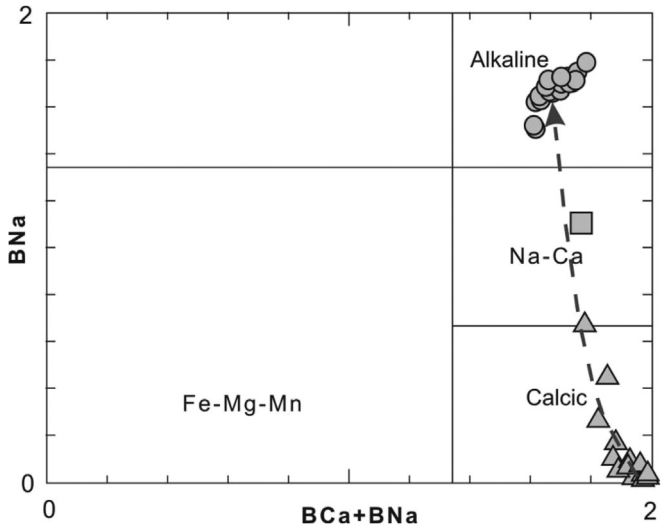

Fig. 16. General classification diagram of amphibole from marble and calcium-silicate rocks from the Itataia deposit according to Leake et al. (1997) (drillholes: CRC 3, FS34A and GN2). The dashed arrow suggests metasomatic trend with calcium leaching and sodium intake.

emplacement age (Bessoles and Trompette, 1980). Thus, the Itataia uranium deposit and other uranium occurrences in the Borborema Province and its African counterpart do not point to an isolated phenomenon, but rather are likely part of the same mineralizing event that occurred in the transition between the late Neoproterozoic and early Paleozoic periods (Cambrian-Ordovician).

The proposed existence of a regional mineralizing event involving the formation of the Itataia, Espinharas and West African deposits was first suggested by Ballhorn et al. (1978) and Angeiras et al. (1978), and more recently by Cuney (2010). The last author suggests that a uranium mineralization episode associated with Na metasomatism occurred during the Brasiliano/Pan-African event (~500 Ma).

In the Borborema and Benin-Nigeria provinces, basement and sedimentary cover were involved in a frontal collision between ca. 0.66 and 0.60, evolving into an oblique collision and generating a continental strike-slip shear zone around 0.59 Ga (Arthaud et al., 2015).

The first contractional phase of Brasiliano/Pan-African orogeny is marked in the study area for nappe and thrust development in the Itataia Group toward SSW. After 0.6 Ga, a second deformation event occurred in both provinces, producing transcurrent shear zones accompanied by the intrusion of large volumes of mantle-

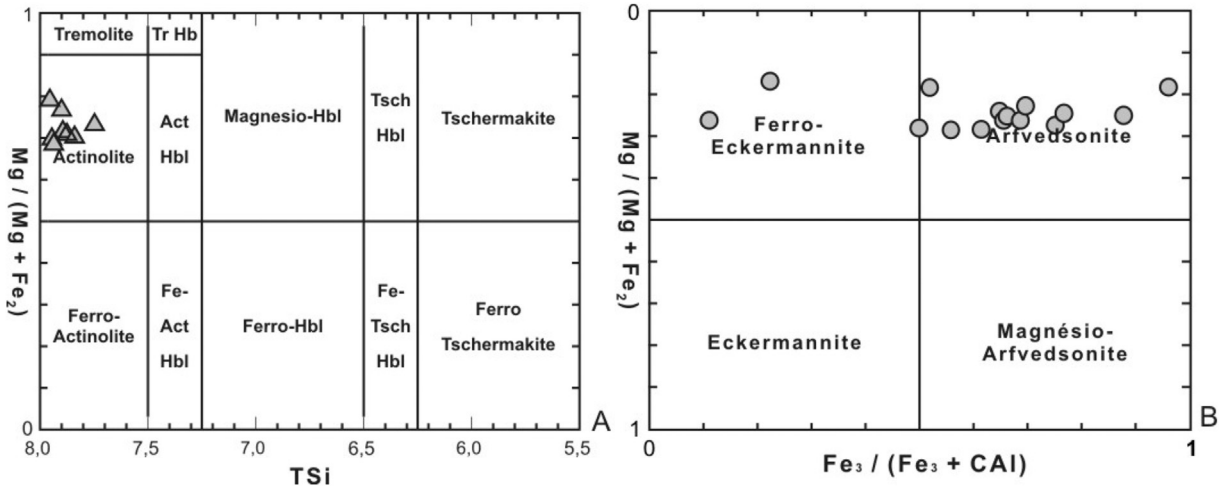

Fig. 17. Classification diagrams for the analyzed amphiboles according to Leake et al. (1997). A: calcic amphiboles—CaB ≥1.5; (Na + K)A < 0.50 and Ti < 0.50; B: alkali amphiboles—NaB ≥ 1.34; (Na + K)A > 0.50.

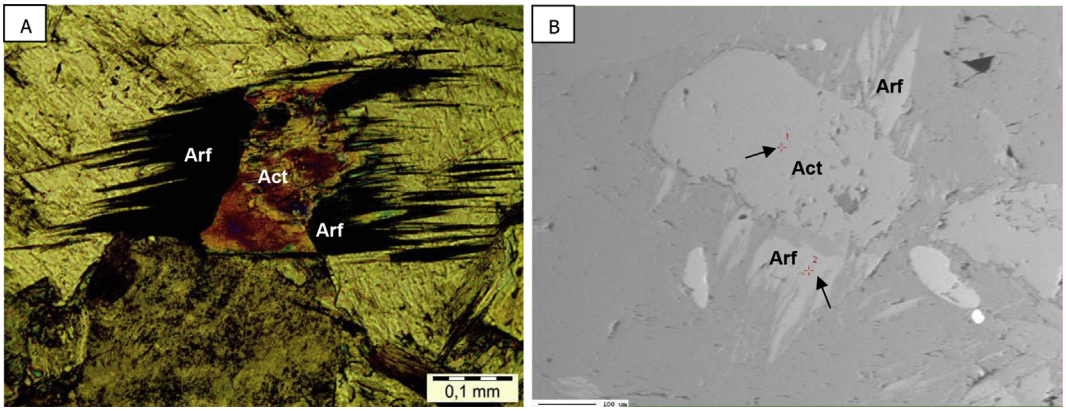

Fig. 18. A: Photomicrograph of relic core of calcic amphibole (*actinolite*—Act) and sodic rims (*arfvedsonite*—Arf) generated by sodium metasomatism (transmitted light; crossed nicols); B. SEM image illustrating the location of points with chemical microanalysis. Black arrows indicate the points 1 (core) and 2 (edge) analyzed.

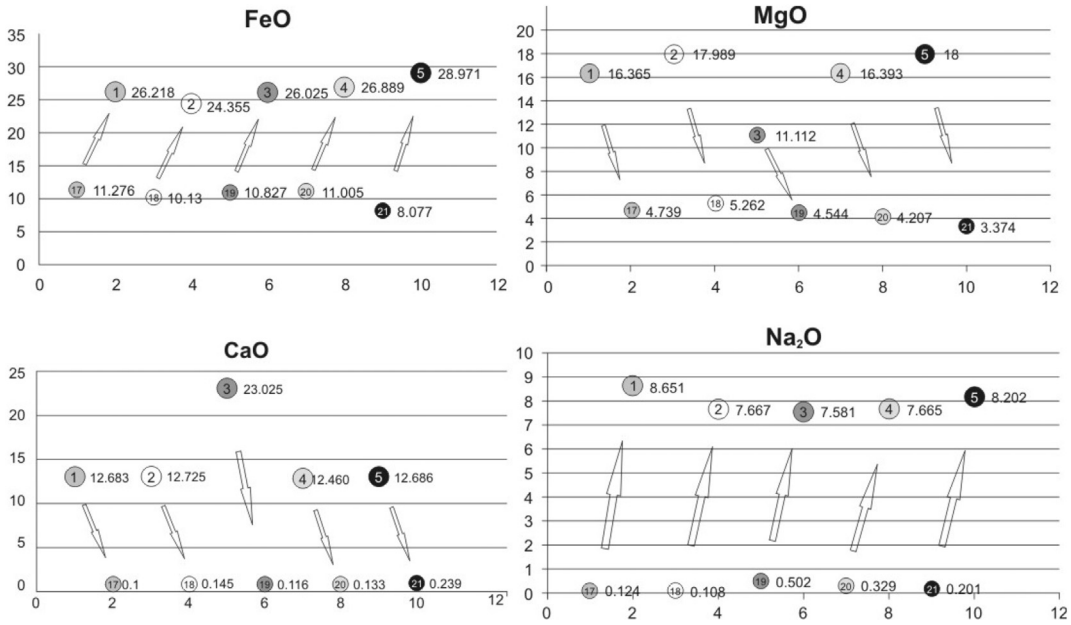

Fig. 19. Electron microprobe analyses for the core (small circles) and edge (large circles) of Na-amphiboles from host rocks of the Itataia deposit. Arrows up indicate the supply and arrows down the removal of the element during the metasomatism. Data from the chemical analyzes of core (1–5) and edge (17–21) of amphiboles (samples CRC3 and F34A–Tables 2 and 3).

and crustal-derived magmas (e.g. Ferreira et al., 1998; Neves et al., 2000). In the Ceara Central (CC) and Médio Coreaú (MC) Domains granites associated with strike-slip shear zones were dated between 0.56 and 0.59 Ga (U–Pb zircon age) (Nogueira, 2004; Santos et al., 2008). The strike-slip phase of the Brasiliano cycle was followed by rapid unroofing and deposition of supracrustal sequences within small transtensional-type molasse basins, accompanied in part by bimodal volcanism (Brito Neves, 1998; Arthaud, 2007). The Rb–Sr ages for the volcanic rocks of one of these basins, situated on the northwest boundary of the CC (Jaibaras basin), suggest intervals of 0.56–0.53 Ga for the basal and 0.53–0.44 Ga for the upper sequence (e.g. Parente et al., 2004).

Granitic intrusive rocks with varying compositions and ranging from the end of the Neoproterozoic to Lower Cambrian periods (0.54–0.52 Ga) are partly contemporaneous to the formation of the basins, and are linked to extrusion processes at the end of the Brasiliano Cycle (Brito Neves et al., 2003). Several other granitic intrusions, including the Quintas Ring Complex and Pajé suite, are also post-Brasiliano and exhibit Ordovician ages (0.47–0.48 Ga) (Castro, 2005; Arthaud, 2007; Teixeira, 2005).

Considering the ages obtained for sodic amphibole and those of Quintas Ring Complex granites, recognized as fertile, the age interval of the first mineralizing event in Itataia is between 0.59 and 0.47 Ga. One possibility is an association with late manifestations of the Brasiliano event, contemporaneous to the development of transcurrent shear zones accompanied by granitic intrusion. A second possibility is an association between mineralization and post-Brasiliano magmatism.

The Rio Grande do Norte Domain (RN) of the Borborema Province, to the north of the Patos Shear Zone, contains other ore deposits formed by the infiltration of the fluids produced by igneous intrusions. Most BP skarn deposits exhibit a close relationship with Brasiliano plutons (igneous suite) (600–530 Ma) and are W – skarns, forming the Tungsten Province of Seridó. Considering existing geochronological data for the Brejui (W) skarn deposit, the maximum age of these skarns is estimated to be between 555 and 480 Ma (e.g. Souza Neto et al., 2008). The oldest is related to Acari granite, considered to be the source of fluids involved in the skarn formation (e.g. Legrand et al., 1991) and the youngest corresponds to the age obtained for pegmatite bodies that crosscut some skarns in the Brejui deposits (e.g., Salim, 1993).

Sodic alteration is not only associated with uranium mineralization, but may also occur as regional alteration zones in some IOCG, VHMS, skarn districts, deeper parts of porphyry cooper systems or associated with some alkaline igneous complexes. In the Ceará Central Domain (CC) west of the Itataia deposit occurrences of skarns and IOCG deposits were first described related to Brasiliano granite genesis inside and on the western edge of AMSQ, respectively (Parente et al., 2014 and Parente et al., 2015). Although there is no geochronological data on the new skarn and IOCG occurrences discovered, some of them are likely related to the first Itataia mineralizing event. This confirms the importance of late to post-Brasiliano granitogenesis in Borborema Province, as a source of mineralizing events genetically related to granitic intrusions. Most of them, taking place during the hydrothermal event that normally follows the magma emplacement. With the polymetallic potential depending on the chemism of granites and reactivity of the host rocks.

5.3. Structural control of mineralization – the second event

The interrelationship between fold hinge and U–P mineralization in Itataia deposit indicates that the architecture of the mineralizing site was established at the end of the Brasiliano orogeny. In our view, the metallogenic history of Itataia begins soon after the thrust and nappes of the basal pelitic unit (Fm Barrigas) in the Itataia Group over the chemical sequence (Fm Alcantil), generating south-trending isoclinal folds. The mineralization site of uranium and phosphorus coincides with the hinge zone of the decametric isoclinal fold. Hinge zones include ductile and brittle plans that usually operate as conduits for fluid percolation.

Although the control observed in drill cores and galleries is essentially brittle and mineralization is post-tectonic, folded features and the correlation between mineralized levels and plans of

Table 3
Electron microprobe analyses and mineral formula calculations for soda amphiboles from host rocks of the Itataia deposit. Analyses (15–18): CRC 3; (19): F34A; (20–21): GN2Na and (22–26):GN2.

Sample	CRC3	CRC3	CRC3	CRC3	F34A	GN2Na	GN2Na	GN2	GN2	GN2	GN2	GN2	
Analysis	15	16	17	18	19	20	21	22	23	24	25	26	
Location	edge	edge	edge	edge	edge	core	core	core	core	core	core	core	
SiO2	52.793	53.739	53.652	53.206	52.625	51.96	53.116	53.208	51.74	52.611	52.135	51.37	
TiO2	3.209	5.685	4.577	4.49	0.437	4.154	3.863	3.826	5.235	3.374	4.455	4.402	
Al2O3	0.131	0.489	0.321	0.537	0.069	0.406	0.398	0.294	0.641	0.255	0.577	0.584	
FeO	26.218	24.355	26.025	26.889	28.971	26.449	25.113	24.327	26.609	24.864	25.335	25.467	
Cr2O3	0.094	0.088	0.097	0.059	0	0.097	0.085	0.046	0	0.058	0.088	0.06	
MnO	0	0.007	0.023	0.011	0.038	0.034	0.096	0.053	0.038	0.064	0.034	0.038	
MgO	4.739	5.262	4.544	4.207	3.374	3.272	4.763	4.806	2.985	4.851	4.805	4.284	
CaO	0.1	0.145	0.116	0.133	0.239	0.133	0.105	0.099	0.006	0.076	0.062	0.078	wt.%
Na2O	8.651	7.667	7.581	7.665	8.202	7.614	7.74	8.326	7.774	8.423	7.096	7.6	
K2O	0.257	0.165	0.194	0.147	0.232	0.234	0.296	0.212	0.227	0.179	0.165	0.162	
V2O3	0.293	0.206	0.228	0.257	0.114	0.574	0.386	0.618	0.657	0.468	0.575	0.759	
BaO	0.015	0.108	0.13	0.014	0.008	0.101	0	0.13	0	0	0.014	0	
F	0	0.087	0.094	0.072	0.101	0.061	0.044	0	0.077	0.011	0.161	0.013	
Cl	0	0	0.004	0.005	0	0.003	0.004	0	0.006	0	0.023	0.009	
Total	96.41	97.92	97.49	97.63	94.41	95	95.92	95.9	95.99	95.18	95.44	94.77	
O_F_Cl	0	0.04	0.04	0.03	0.04	0.03	0.02	0	0.03	0	0.07	0.01	
CTotal	96.41	97.88	97.45	97.6	94.37	94.97	95.9	95.9	95.96	95.18	95.37	94.76	
24 (O,F,Cl)													
Sample	CRC3	CRC3	CRC3	CRC3	F34A	GN2Na	GN2Na	GN2	GN2	GN2	GN2	GN2	
Analysis	15	16	17	18	19	20	21	22	23	24	25	26	
Location	edge	edge	edge	edge	edge	core	core	core	core	core	core	core	
TSi	8.748	8.651	8.716	8.651	8.934	8.792	8.769	8.86	8.709	8.809	8.622	8.646	
TAl	0	0	0	0	0	0	0	0	0	0	0	0	
Sum_T	8.748	8.651	8.716	8.651	8.934	8.792	8.769	8.86	8.709	8.809	8.622	8.646	
CAl	0.026	0.093	0.061	0.103	0.014	0.081	0.077	0.058	0.127	0.05	0.112	0.116	
CCr	0.012	0.011	0.012	0.008	0	0.013	0.011	0.006	0	0.008	0.011	0.008	
CFe3	0.148	0.119	0.199	0.24	0.312	0.087	0.167	0.007	0.036	0.094	0.334	0.21	
CTi	0.4	0.688	0.559	0.549	0.056	0.529	0.48	0.479	0.663	0.425	0.554	0.557	
CMg	1.171	1.263	1.101	1.02	0.854	0.825	1.172	1.193	0.749	1.211	1.185	1.075	
CFe2	3.178	2.804	3.016	3.06	3.607	3.377	3.012	3.138	3.379	3.116	2.796	3.015	
CMn	0	0	0.001	0.001	0.003	0.002	0.006	0.003	0.003	0.004	0.002	0.003	
CCa	0.008	0.012	0.009	0.011	0.02	0.011	0.009	0.008	0.001	0.006	0.005	0.007	a.f.u
Sum_C	4.944	4.991	4.959	4.991	4.865	4.926	4.934	4.892	4.957	4.915	5	4.99	
BFe2	0.307	0.355	0.321	0.356	0.194	0.278	0.288	0.243	0.331	0.271	0.374	0.36	
BMn	0	0.001	0.002	0.001	0.003	0.003	0.007	0.004	0.003	0.005	0.003	0.003	
BCa	0.01	0.013	0.011	0.012	0.023	0.013	0.01	0.009	0.001	0.007	0.006	0.008	
BNa	1.684	1.631	1.666	1.631	1.779	1.706	1.695	1.743	1.666	1.717	1.617	1.63	
Sum_B	2	2	2	2	2	2	2	2	2	2	2	2	
ANa	1.096	0.762	0.722	0.786	0.921	0.792	0.783	0.945	0.872	1.018	0.658	0.851	
AK	0.054	0.034	0.04	0.03	0.05	0.051	0.062	0.045	0.049	0.038	0.035	0.035	
Sum_A	1.15	0.796	0.762	0.816	0.971	0.842	0.845	0.99	0.921	1.056	0.693	0.885	
Sum_cat	16.842	16.439	16.438	16.458	16.771	16.56	16.549	16.741	16.587	16.779	16.316	16.522	
CCl	0	0	0.001	0.001	0	0.001	0.001	0	0.002	0	0.006	0.003	
CF	0	0.044	0.048	0.037	0.054	0.033	0.023	0	0.041	0.006	0.084	0.007	

tectonic-metamorphic foliation suggest the use of inherited structures in uranium and phosphate concentration.

The influence of the Brasiliano tectonic event on local relief configuration is evident; so much so that residual plateaus developed on quartzites of the basal units of the Itataia Group (Laranjeiras and Serra do Céu Fm), evident in klippe structures and front portions of the nappes overlying top units of the Itataia Group (Barrigas and Alcantil Fm).

The main body of massive collophanite has elongated geometry and follows the subvertical fault-line scarp that limits uranium and phosphate occurrences to the north.

The main radiometric anomaly and higher uranium content overlap with the relief ridge and more intensely fractured and faulted area. In the underground galleries that cross-cut the main fault plane, there is clear north-south ore zoning, with higher uranium content and higher massive collophanite volume in the more intensely faulted, brecciated and karstified zones. These zones transition into stockwork collophanite ore and then into portions where marble exhibits preserved tectonic-metamorphic foliation and collophane is limited to filling small faults and fractures.

These evidences point out the importance of a second U–P mineralizing event, of lower temperature, characterized by the concentration of hydrothermal fluid along the extensional faults with neoformation of phosphates, quartz, carbonates and chloritization. Associated with this event occurs the formation of a second apatite phase (Ap_2) and the generation of the stockwork ores, the mineralized breccias (carbonaceous and carbonate) and probably the filling of the voids left by quartz leaching in episyenites ores by colloform apatite (Ap_2).

Electron microprobe analyses reveal that clear prismatic apatite has low uranium and slightly higher fluorine contents, while colloform apatite has higher average contents of uranium and lower fluorine levels. The chemical formulas suggest that prismatic and colloform apatite related to hydrothermal stages is fluorapatite, and prismatic apatite represents the oldest phase of hydrothermal origin that persists to greater depths. It occurs in veins that have clearly interacted with the host rock, setting reaction edges

Table 4.A
Electron microprobe analyses and mineral formula calculations for selected apatite from host rocks of the Itataia deposit. Analyses (1–12): sample CRC 3 and (13–19): sample F34A.

Sample	CRC3	CRC3	CRC3	CRC3	CRC3	CRC3	CRC3	CRC3	CRC3	CRC3	CRC3	CRC3	F34A	F34A	F34A	F34A	F34A	F34A	F34A	
Analysis	1	2	3	4	5	6	7	8	9	10	11	12	13	14	15	16	17	18	19	
SiO2	1.531	0.063	1.073	0.904	0.241	0.055	0.538	0	0.059	0.859	0.021	0.647	0.405	2.208	0	0.025	2.675	0.247	0.056	
FeO	3.3806	0.248	0.625	3.146	0.377	0.429	0.354	0.151	1.031	0.346	0.138	0.277	0.77	0.844	0.041	0.09	1.551	0.391	0.33	
MnO	0	0.026	0.024	0.031	0.015	0	0.032	0.007	0.02	0.018	0.028	0	0.039	0.066	0.037	0.02	0.038	0.047	0.054	
MgO	0.068	0.008	0.06	0.125	0.067	0.017	0.012	0	0.002	0.125	0	0.055	0.083	0.415	0	0	0.404	0.101	0	
SrO	0.571	0.592	0.745	0.416	0.529	0.401	0.74	0.597	0.529	0.747	0.728	0.573	0.395	0.402	0.318	0.222	0.474	0.443	0.5	
CaO	49.221	51.942	52.327	50.351	50.921	52.636	53.494	53.593	53.093	50.93	52.276	51.995	51.593	50.459	53.258	52.258	48.809	52.325	51.863	wt.%
Na2O	0.794	0.88	1.105	0.679	0.728	0.573	0.389	0.379	0.386	0.983	0.849	0.854	0.175	0.958	0.181	0.27	1.407	0.761	1.087	
K2O	0	0.028	0	0.066	0	0	0	0	0	0.002	0.008	0.002	0.005	0	0.003	0.003	0.033	0.009	0.023	
P2O5	36.868	37.097	36.268	36.156	37.029	38.307	38.62	39.464	38.596	35.893	37.698	37.033	39.203	37.108	39.965	40.313	36.242	38.668	38.448	
SO3	0.392	0.547	0.581	0.381	0.477	0.36	0.393	0.346	0.418	0.532	0.561	0.527	0.076	0.387	0.093	0.079	1.051	0.356	0.664	
UO2	0.301	0.239	0.108	0.266	0.437	0.099	0.275	0.186	0.097	0.275	0.189	0.18	0.112	0.074	0.156	0.121	0.508	0.295	0.671	
F	3.264	3.803	3.729	3.458	3.203	3.453	3.518	3.38	3.296	3.444	3.502	3.1	3.134	3.23	2.735	2.658	2.902	2.926	3.384	
Cl	0.022	0.006	0.012	0.029	0.162	0.007	0.014	0.006	0.023	0.01	0.016	0.019	0	0	0.022	0	0.004	0.011	0.01	
Total	96.41	95.48	96.66	96.01	94.19	96.34	98.38	98.11	97.55	94.16	96.01	95.26	95.99	96.15	96.81	96.06	96.1	96.58	97.09	
O_F_Cl	1.38	1.6	1.57	1.46	1.39	1.46	1.48	1.42	1.39	1.45	1.48	1.31	1.32	1.36	1.16	1.12	1.22	1.23	1.43	
CTotal	95.03	93.88	95.09	94.55	92.8	94.88	96.9	96.69	96.16	92.71	94.53	93.95	94.67	94.79	95.65	94.94	94.88	95.35	95.66	
26(O,Cl,F)																				
Sample	CRC3	CRC3	CRC3	CRC3	CRC3	CRC3	CRC3	CRC3	CRC3	CRC3	CRC3	CRC3	F34A	F34A	F34A	F34A	F34A	F34A	F34A	
Analysis	1	2	3	4	5	6	7	8	9	10	11	12	13	14	15	16	17	18	19	
Fe2	0.491	0.036	0.088	0.45	0.056	0.062	0.05	0.022	0.147	0.05	0.02	0.04	0.114	0.123	0.006	0.013	0.226	0.056	0.047	
Mn	0	0.004	0.003	0.004	0.002	0	0.005	0.001	0.003	0.003	0.004	0	0.006	0.01	0.005	0.003	0.006	0.007	0.008	
Mg	0.018	0.002	0.015	0.032	0.018	0.004	0.003	0	0.001	0.032	0	0.014	0.022	0.108	0	0	0.105	0.026	0	
Sr	0.058	0.059	0.073	0.041	0.054	0.04	0.073	0.059	0.052	0.075	0.072	0.057	0.04	0.041	0.032	0.023	0.048	0.044	0.05	
Ca	9.165	9.601	9.458	9.235	9.621	9.704	9.74	9.793	9.672	9.507	9.617	9.603	9.753	9.395	9.893	9.87	9.131	9.612	9.526	
Na	0.268	0.294	0.361	0.225	0.249	0.191	0.128	0.125	0.127	0.332	0.283	0.285	0.06	0.323	0.061	0.092	0.476	0.253	0.361	a.f.u
K	0	0.006	0	0.014	0	0	0	0	0	0	0.002	0	0.001	0	0.001	0.001	0.007	0.002	0.005	
Si	0.266	0.011	0.181	0.155	0.042	0.009	0.091	0	0.01	0.15	0.004	0.112	0.071	0.384	0	0.004	0.467	0.042	0.01	
P	5.424	5.418	5.18	5.24	5.528	5.581	5.556	5.699	5.556	5.294	5.48	5.404	5.856	5.46	5.866	6.017	5.358	5.613	5.58	
U	0.01	0.01	0	0.01	0.02	0	0.01	0.01	0	0.01	0.01	0.01	0	0	0.01	0	0.02	0.01	0.03	
S	0.051	0.071	0.073	0.049	0.063	0.046	0.05	0.044	0.053	0.069	0.072	0.068	0.01	0.05	0.012	0.01	0.138	0.046	0.085	
Cations	15.751	15.512	15.432	15.455	15.653	15.637	15.706	15.753	15.621	15.522	15.564	15.593	15.933	15.894	15.886	16.033	15.982	15.711	15.702	
CF	1.794	2.075	1.989	1.872	1.786	1.879	1.891	1.823	1.772	1.897	1.902	1.69	1.749	1.775	1.5	1.482	1.602	1.587	1.835	
CCl	0.006	0.002	0.003	0.008	0.048	0.002	0.004	0.002	0.007	0.003	0.005	0.006	0	0	0.006	0	0.001	0.003	0.003	

Table 4.B
Electron microprobe analyses and mineral formula calculations for selected apatite from host rocks of the Itataia deposit. Analyses (20–28): FS34A; (29–37): sample FS131 and (38–40):sample GN2. Analyses 24 to 28 of clear prismatic apatites (Ap_1).

Sample	F34A	F34A	F34A	F34A	F34A	F34A	F34A	F34A	F34A	FS131	FS131	FS131	FS131	FS131	FS131	FS131	FS131	FS131	GN2	GN2	GN2	
Analysis	20	21	22	23	24	25	26	27	28	29	30	31	32	33	34	35	36	37	38	39	40	
SiO2	1.612	0.163	5.146	0.05	0	0.021	0.12	0.091	0.069	0.023	0.119	0.036	0.157	0.016	0.048	0.073	0.606	0	0.286	2.349	0.142	
FeO	0.648	0.267	2.374	0.035	0.012	0.035	0.079	0.043	0.013	0.341	0.842	0.306	0.278	0.343	0.126	0.801	6.126	0.111	0.673	1.224	0.595	
MnO	0	0.017	0.028	0	0.063	0	0	0	0	0.064	0.009	0.07	0	0.051	0.056	0.019	0.007	0	0.017	0.04	0.009	
MgO	0.56	0.018	0.706	0.016	0.03	0	0	0.004	0	0.007	0.01	0	0	0	0.041	0	0.039	0.009	0.026	0.144	0	
SrO	0.427	0.388	0.382	0.202	0.259	0	0.027	0.074	0.01	0.35	0.307	0.287	0.429	0.431	0.293	0.465	0.209	0.571	0.258	0.268	0.207	
CaO	49.927	52.588	45.928	53.785	53.287	54.783	54.837	55.046	54.703	52.881	52.384	52.597	52.456	52.42	52.327	52.334	48.827	51.47	52.253	50.052	52.775	wt.%
Na2O	0.817	0.584	1.188	0.006	0.264	0.007	0	0.008	0	0.605	0.33	0.584	0.595	0.676	0.748	0.749	0.521	1.08	0.71	0.758	0.464	
K2O	0.154	0.006	0.035	0.013	0	0	0	0	0	0.01	0.001	0	0.007	0	0	0.009	0.009	0	0.002	0	0.207	
P2O5	37.166	38.734	35.605	39.939	40.011	40.523	40.728	41.758	41.722	37.935	36.77	37.047	36.673	37.618	37.215	36.363	34.335	36.4	39.386	37.402	39.719	
SO3	0.823	0.147	0.461	0	0.155	0.067	0.005	0.003	0	0.159	0.206	0.149	0.047	0.054	0.313	0.3	0.278	0.926	0.338	0.184	0.141	
UO2	0.334	0.166	0.132	0.124	0.012	0.007	0.006	0.09	0.009	0.23	0.204	0.332	0.816	0.495	0.499	0.483	0.377	0.476	0.524	0.344	0.542	
F	2.838	2.406	2.693	3.156	3.106	4.095	3.865	3.784	4.454	2.874	3.084	2.8	2.528	2.774	2.819	2.606	2.413	3.024	2.987	2.883	2.437	
Cl	0.018	0.032	0.01	0.106	0.011	0.091	0.074	0.013	0.06	0	0.004	0.007	0	0.019	0.011	0.011	0.017	0	0.016	0	0	
Total	95.32	95.52	94.69	97.43	97.21	99.63	99.74	100.91	101.04	95.48	94.27	94.21	93.99	94.9	94.5	94.21	93.76	94.07	97.48	95.65	97.24	
O_F_Cl	1.2	1.02	1.14	1.35	1.31	1.74	1.64	1.6	1.89	1.21	1.3	1.18	1.06	1.17	1.19	1.1	1.02	1.27	1.26	1.21	1.03	
CTotal 26(O,Cl,F)	94.12	94.5	93.55	96.08	95.9	97.89	98.1	99.31	99.15	94.27	92.97	93.03	92.93	93.73	93.31	93.11	92.74	92.8	96.22	94.44	96.21	
Sample	F34A	F34A	F34A	F34A	F34A	F34A	F34A	F34A	F34A	FS131	FS131	FS131	FS131	FS131	FS131	FS131	FS131	FS131	GN2	GN2	GN2	
Analysis	20	21	22	23	24	25	26	27	28	29	30	31	32	33	34	35	36	37	38	39	40	
Fe2	0.095	0.039	0.362	0.005	0.002	0.005	0.011	0.006	0.002	0.049	0.122	0.044	0.04	0.049	0.018	0.115	0.874	0.016	0.097	0.181	0.085	
Mn	0	0.002	0.004	0	0.009	0	0	0	0	0.009	0.001	0.01	0	0.007	0.008	0.003	0.001	0	0.002	0.006	0.001	
Mg	0.147	0.005	0.192	0.004	0.008	0	0	0.001	0	0.002	0.003	0	0	0	0.011	0	0.01	0.002	0.007	0.038	0	
Sr	0.044	0.039	0.04	0.02	0.026	0	0.003	0.007	0.001	0.035	0.031	0.029	0.043	0.043	0.029	0.046	0.021	0.057	0.026	0.027	0.021	
Ca	9.403	9.721	8.972	9.967	9.866	9.993	9.987	9.986	9.998	9.7	9.733	9.72	9.715	9.675	9.685	9.588	8.92	9.562	9.632	9.488	9.693	
Na	0.278	0.195	0.42	0.002	0.088	0.002	0	0.003	0	0.201	0.111	0.195	0.199	0.226	0.251	0.248	0.172	0.363	0.237	0.26	0.154	a.f.u
K	0.035	0.001	0.008	0.003	0	0	0	0	0	0.002	0	0	0.002	0	0	0.002	0.002	0	0	0	0.045	
Si	0.283	0.028	0.938	0.009	0	0.004	0.02	0.015	0.012	0.004	0.021	0.006	0.027	0.003	0.008	0.012	0.103	0	0.049	0.416	0.024	
P	5.531	5.658	5.496	5.848	5.854	5.841	5.861	5.986	6.026	5.499	5.399	5.41	5.367	5.486	5.443	5.264	4.957	5.343	5.737	5.603	5.764	
U	0.01	0.01	0.01	0	0	0	0	0	0	0.01	0.01	0.01	0.03	0.02	0.02	0.02	0.01	0.02	0.02	0.01	0.02	
S	0.108	0.019	0.063	0	0.02	0.009	0.001	0	0	0.02	0.027	0.019	0.006	0.007	0.041	0.038	0.036	0.12	0.044	0.024	0.018	
Cations	15.934	15.717	16.505	15.858	15.873	15.854	15.883	16.004	16.039	15.531	15.458	15.443	15.429	15.516	15.514	15.336	15.106	15.483	15.851	16.053	15.825	
CF	1.578	1.313	1.553	1.726	1.697	2.205	2.078	2.026	2.403	1.556	1.691	1.527	1.382	1.511	1.54	1.409	1.301	1.658	1.625	1.613	1.321	
CCl	0.005	0.009	0.003	0.031	0.003	0.026	0.021	0.004	0.017	0	0.001	0.002	0	0.006	0.003	0.003	0.005	0	0.005	0	0	

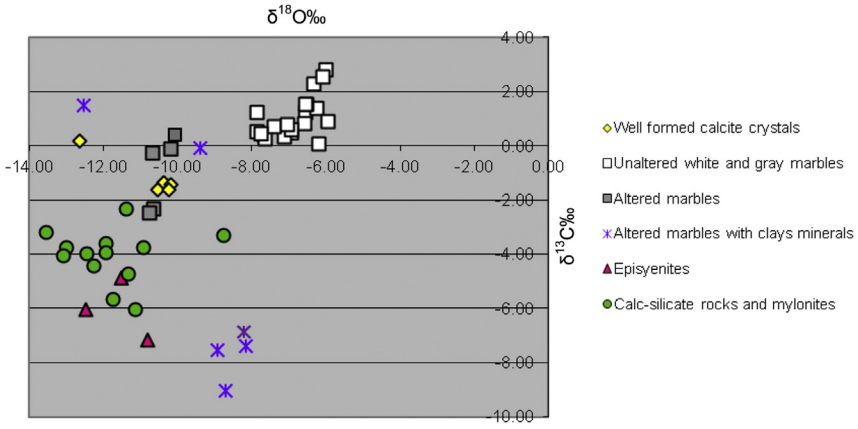

Fig. 20. $\delta^{18}O‰$ versus $\delta^{13}C‰$ diagram with isotopic data from drill core samples (FS-119), including different types of marble, episyenites, calc-silicate and mylonite rocks and well-formed carbonate crystals. $\delta^{18}O$ and $\delta^{13}C$ reported in permil relative to PDB.

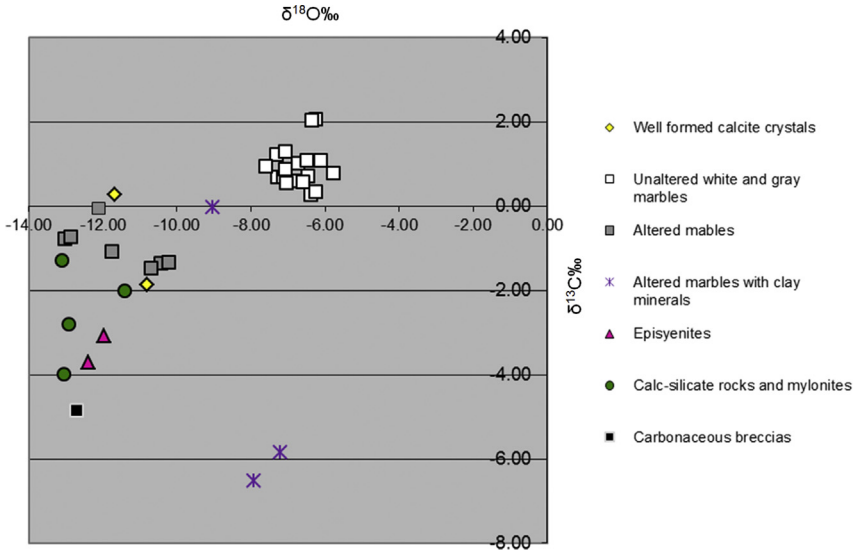

Fig. 21. $\delta^{18}O‰$ versus $\delta^{13}C‰$ diagram with isotopic data from drill core samples (FS-34), including different types of marble, episyenites, calc-silicates and mylonite rocks, carbonaceous breccias and well-formed carbonate crystals. $\delta^{18}O$ and $\delta^{13}C$ reported in permil relative to PDB.

demonstrated by the gradual replacement of carbonate by collophanite from the edges to the center. The occurrence of brecciated zones containing prismatic crystals of fluorapatite next to colloform apatite, as well as phosphate engulfed by carbonates and deposited on the surface of the latter, indicate the existence of cyclical dissolution phases and karstification brecciation related to second hydrothermal phase.

Fluid inclusion studies for younger hydrothermal minerals conducted by Fuzikawa (1978) in quartz, feldspar, carbonate and phosphate from the Itataia deposit indicated that the mineralizing fluids were saline solutions rich in chlorides, mainly CaCl2. Additionally, the temperatures recorded by Fuzikawa (1978) suggest interaction between hydrothermal and meteoric fluids in the formation of Itataia collophanite ore, in addition to the gradual reduction of fluid salinity (CaCl2) over time.

The main fault plane that controls uranium mineralization coincides with regional E-W lineaments visible on remote sensing images. These propagate over the Precambrian basement of the Itataia Group and the Neoproterozoic granitic rocks of the AMSQ. This regional east-west brittle trend contains phosphorus-uraniferous occurrences in albitized and mineralized volcanic acid rocks in the same direction as Rio Ceara Mirim (RCM) cretaceous dikes (e.g. Santos et al., 2014; Cavalcanti et al., 2013; Cavalcanti and Bessa, 2011). This fact, combined with the ca ages of 91 Ma obtained by Netto et al. (1991) for Itataia collophanite led these authors to correlate their origin with the same Cretaceous hot spots responsible for Rio Ceará Mirim (RCM) magmatism.

RCM dykes are similar in composition and tectonic setting to tholleitic dyke swarms from the Benue Trough, and are related to the opening of the equatorial Atlantic Ocean (e.g. Sial et al., 1981; Almeida et al., 1988; Maluski et al., 1995; Coulon et al., 1996). A common explanation for the Benue Trough's formation is that it is an abandoned arm (aulacogen) of a three-armed radial rift system. The other two arms continued to spread during the break-up of Gondwana, as South America separated from Africa (Petters, 1978). This tectonic evolution follows the most widely accepted ideas on riftogenesis, involving the rise of a mantle plume or mantle upwelling, emplacement of intrusive igneous material into the crust, crustal stretching and thinning and, consequently, rifting (Ofoegbu, 1984; Benkhelil, 1989; O'Connor and Le Roex, 1992).

In the Borborema Province, Neojurassic-Early Cretaceous rifting was accompanied and followed by a number of magmatic events in

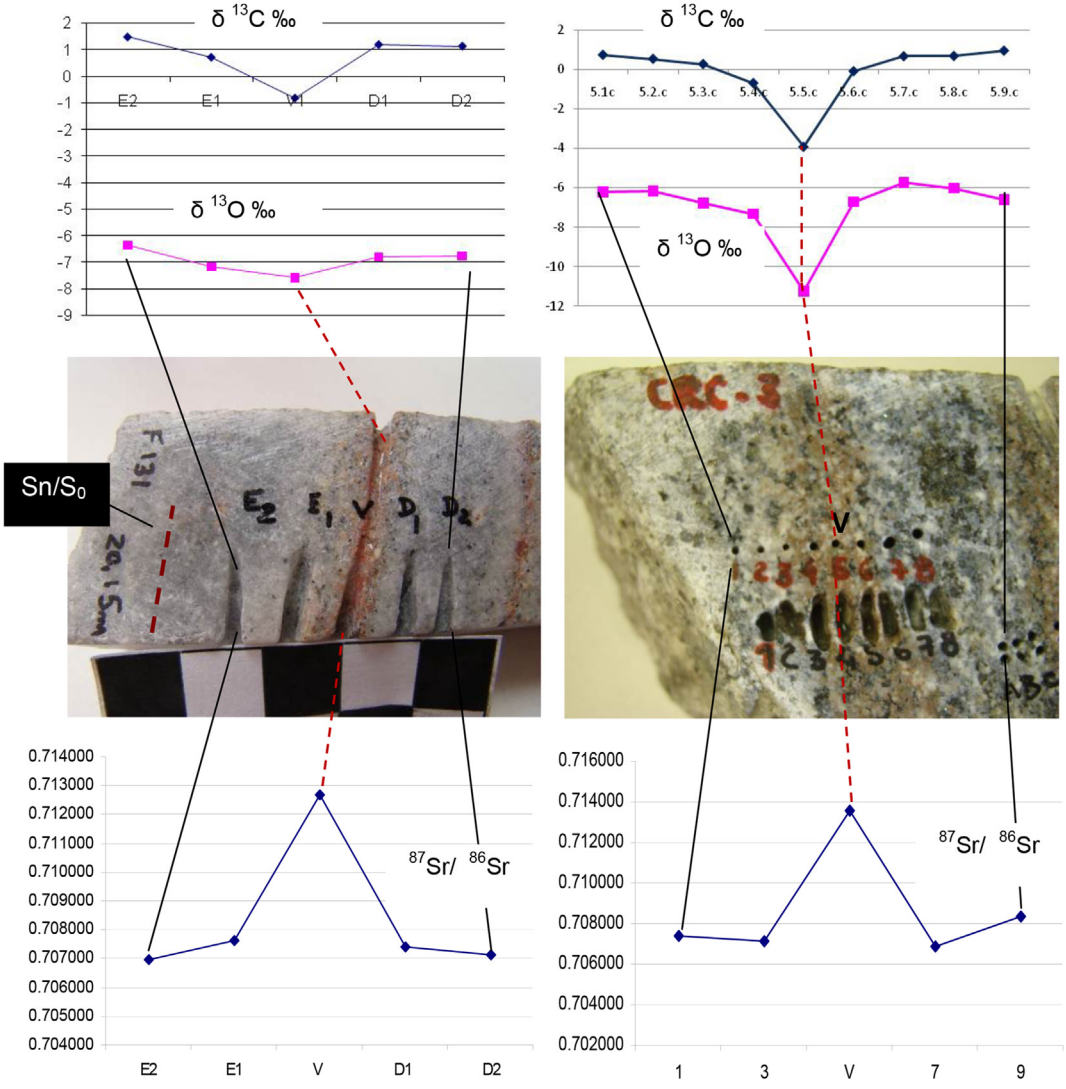

Fig. 22. $\delta^{13}C‰$, $\delta^{18}O‰$ e $^{87}Sr/^{86}Sr$ ratio diagrams showing centimeter-scale isotopic profiles across collophanite veins in marbles (F131) and calc-silicate (CRC-3) host rocks from drill core samples. At the top of the figure, isotopic profiles show a decrease of $\delta^{13}C‰$ and $\delta^{18}O‰$ in isotope values contrasting with the increased $^{87}Sr/^{86}Sr$ ratio toward the center of the vein at the bottom of the figure.

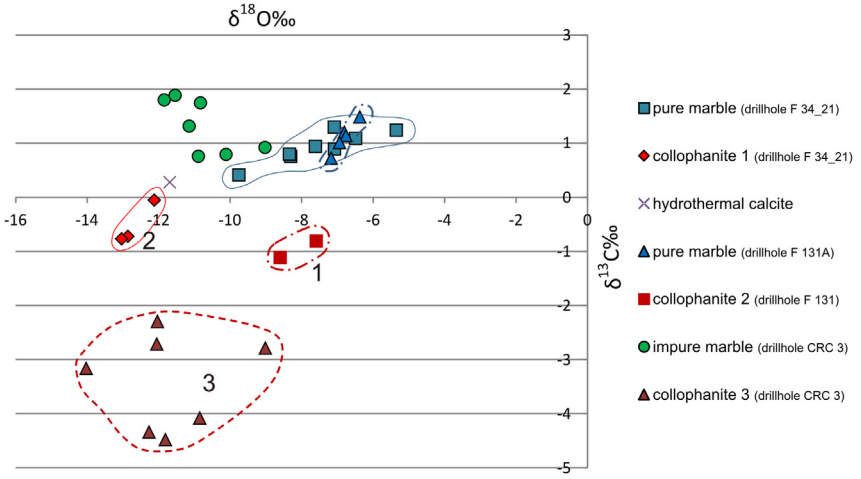

Fig. 23. $\delta^{18}O‰$ versus $\delta^{13}C‰$ diagram with isotopic results on cross-sections of the collophanite mineralized zones of marbles (1 and 2) and calc-silicate (3) rocks (adapted from Veríssimo et al., 2010).

sedimentary basins of the Equatorial Brazilian margin (Ceará, Potiguar, etc.), in the structural heights that separate them, and in adjacent intraplate regions (Almeida et al., 1996).

The Early Cretaceous (145–125 Ma) Rio Ceará Mirim dyke swarm (RCM) intruded the basement of the Borborema Province during rifting events. The dykes infill a set of E-W trending fractures near the southern border of the Potiguar Basin and propagate within-plate E-W/NE-SW for more than 800 km (Sial et al., 1981; Almeida et al., 1988; Archanjo et al., 2000).

According to Santos et al. (2014), Cavalcanti et al. (2013) and Cavalcanti and Bessa (2011) the large gravity faults and fractures that hosted mineralization emerged during RCM magmatism and the hot spots then generated a convective hydrothermal system involving a mixture of meteoric and magmatic fluids. These removed phosphorous and uranium from the alkaline rocks, depositing uranium-rich apatite as collophane.

The genetic model proposed by these authors is plausible to explain only the second Itataia mineralizing event, considering the regional expression of magmatism as a source of heat and fluids; mineral paragenesis indicative of low temperature; and structural control determined by the fault. However, more detailed geochronological and structural studies are needed to consolidate this model.

Other uranium deposits of different ages but in similar tectonic contexts are associated with extensional tectonism post-dating collisional events in China (late Yanshanian tectonism) (e.g. Hu et al., 2008; Hu et al., 2013) in the Czech Republic during the Permian extensional phase of late Variscan evolution of the Bohemian Massif (e.g. René, 2005) or in West Central Spain, related to Alpine age shear zones generated by the reactivation of old Variscan faults (Martin-Izard et al., 2002).

The connection between fault development and the second uranium mineralization in Itataia is also evident in other known epithermal fault- or breccia-hosted uranium deposits. Examples include the Ralston Creek Mine in Colorado (USA), Coles Hill Virginia (USA), Fé Mine (Salamanca, Spain) and hydrothermal uranium deposits in South China (e.g. Wallace and Karlson, 1985; Jerden, 2001; Both et al., 1984; Pérez del Villar et al., 2002; Martin-Izard et al., 2002; Li et al., 2002).

Uranium mineralization in these deposits is episodic, suggesting that cataclastic zones acted as hydrothermal fluid percolation paths flowing cyclically during brittle deformation as conceived by seismic pumping hypothesis (Sibson et al., 1975).

5.4. Age of the second mineralization event

Geochronological data available for the second mineralizing event in Itataia are still limited to the age 91 +–6 Ma obtained by fission tracking in collophanite apatites (eg. Netto et al., 1991). Cavalcanti and Bessa (2011) and Santos et al. (2014) associated this age with the hot spot that generated Rio Ceará Mirim (RCM) magmatism. However, it should be noted that the Mesozoic magmatism activity in NE Brasil (RCM) and its African counterpart is characterized by more than one magmatic event between the Middle Jurassic and Earty Cretaceo periods (e.g. Bellieni et al., 1992; Martins and Oliveira, 1992). In the Benue Trough, three major periods of volcanic action have been identified (e.g. Binks and Fairhead, 1992; Maluski et al., 1995; Coulon et al., 1996): (1) during the Late Jurassic to Albian (147–106 Ma) before the onset of seafloor spreading, when the Equatorial Atlantic was still closed; (2) during the Cenomanian to Santonian (97–81 Ma), postdating the break-up of the South American and African continents; (3) between the Late Maastrichtian and Eocene (68–49 Ma), linked to a subsidence regime interpreted as the isostatic response to the post-rift thermal relaxation of the lithosphere.

The first magmatic event is represented by bimodal volcanism (alkaline basalts and peralkaline rhyolites) and tholeiitic basalts. It is considered broadly contemporaneous with the tholeiitic flood basalts of Parana (Brazil) and Etendeka (Namibia) (Renne et al., 1992; Turner et al., 1994) and with the RCM dyke swarm (Bellieni et al., 1992; Martins and Oliveira, 1992; Almeida et al., 1996). Marzoli et al. (2000) considered this magmatism as a single global activity known as the Equatorial Circum-Atlantic event (EQA), whose origin has been attributed to the result of African plate migration over the St Helena hot spot (Morgan, 1983; Maluski et al., 1995; Coulon et al., 1996).

The second is represented by largely intrusive alkaline rocks emplaced during a decreasing extensional regime, following the major Late Jurassic – Albian rifting phase. Although described as restricted to the southern Benue (e.g., Mascle et al., 1986; Nurnberg and Muller, 1991), ages and composition suggest a correlation between this magmatism and the alkali basalts flows of Serra do Cuo, dated in the PB between 83+-6 Ma and 94 Ma (e.g. Sial et al., 1981; Souza et al., 2003), very close to the age obtained for Itataia collophanites (ca 91 Ma).

This does not exclude the possibility of other mineralizing phases associated with the main peak of Mesozoic magmatic activity in PB, related to the RCM dyke swarm (ca 130 Ma or even younger). Investigating this will require careful petrographic and geochronological studies, due to the microcrystalline nature of hydrothermal and supergenic apatite of Itataia. The episodic character of the mineralization is a common feature in this and other faults or breccia-hosted uranium deposits, marked by various stages of mineral formation due to cyclical percolation of hydrothermal and meteoric fluids channeled by cataclastic zones of faults during brittle deformation.

5.5. Younger mineralization event

The youngest apatite is characterized by botryoidal habit and predominates in the upper portions of the deposit. Formed in oxidizing conditions, it propagates to depths of around 400 m along fault surfaces, fractures and voids generated by solution under karstic conditions.

All structural controls mentioned in previous mineralizing events, especially those related to the second, play important hole in the last U–P mineralizing event. In this case, the extensional failure and related E-W fractures that slice up the fold hinge mineralized, in addition to all empty and open spaces by hypogene karst processes of hydrothermal phase. The karstification process probably continued in phreatic and vadose conditions, as suggested by the sharp topographic boundary that limits the background of the phosphorous-uranium rich ore to a quota of 400 m.

The great majority of publications on the Itataia deposit acknowledge the importance of supergene processes in the genesis of the deposit. However, there are no detailed studies of the supergene mineral phases or previous reports about the existence of aluminous phosphates. The younger mineral phases were not also studied in this work, but the petrographic and XRD analyzes suggest the presence of hydroxyapatite, other aluminous phosphates associated with fluorapatite besides clay minerals, generated in frankly oxidizing conditions.

5.6. Conclusions and summary of the genetic model

The genesis of phosphorous-uraniferous Itataia deposit is marked by various mineralizing stage, which ultimately form the larger phosphate-uranium deposit known in South America. The eighteen million tons of phosphate compared with the little more than hundred and forty thousand tons of uranium measures clearly

suggest the existence of a phosphatic primary repository. Unlike other uranium deposits known in NW Borborema Province, in Itataia the phosphorus and uranium enrichment was a multiphase mineralization process over geological time. The first step begins with the primary phosphate deposition probably in coastal environment formed by delta and lagoons in the presence of organic matter, with calcareous mud, psammites, pelites and chemical sediments. A genetic model for the mineralization U–P events and ore genesis of Itataia deposit is summarized in Table 5.

Linking the studies presented in this work with the available geological data for Itataia uranium-phosphorus deposit, the following conclusions can be drawn.

At least three main events were involved in Itataia ore genesis. The first is a high-temperature hydrothermal-metasomatic event similar to those observed in other granite U-related deposits known in the world, characterized for the circulation of large volumes of fluids associated with sodic alteration and silica leaching. The petrographic and mineral chemical analyses of feldspars, amphiboles and apatites of mineralized zones suggest an alkaline to peralkaline composition of the fluids leading to the almost total albitization, quartz leaching (episyenitization), hematitization and the formation of sodium amphiboles (*arfvedsonite* and *iron-eckermannite*), and a prismatic fluorapatite phase (Ap_1) with low uranium content (2 a 34 ppm). The centimeter-scale isotopic profiles realized across mineralized veins in marbles and calc-silicate rocks of the Itataia Group show a higher $^{87}Sr/^{86}Sr$ ratio followed by $\delta^{13}C‰$ and $\delta^{18}O‰$ decreased toward the center of the zone. The highest $^{87}Sr/^{86}Sr$ value (>0.7125) when compared with the obtained to the marble and calc-silicate host rocks (0.7070–70780) indicate a supply of radiogenic strontium and suggest an external magmatic source for the hydrothermal overprint.

This source is related with late to post-collisional granites of the Brasiliano/Pan-African Orogeny and is responsible by the first high-temperature hydrothermal-metasomatic uranium mineralization episode in Itataia deposit. This event is most likely part of a Na-metasomatic uranium mineralization episode that occurred in NW Borborema Province and its African counterpart. There is great similarity in process and ages obtained for the emplacement of "fertile" granites related to Espinharas uranium deposit (north of Patos Shear Zone) and Kitongo uranium deposits within the Central African Fold Belt on the northern edge of the Congo craton. These ages match those obtained for the sodic amphibole existing hidrotermalitos in Itatiaia Group (0.59 Ga).

Therefore the age of the first U–P mineralizing event of Itataia is well defined and related to the end of the Brasiliano/Pan-African orogeny, contemporaneous to the development of transcurrent shear zones accompanied by granitic intrusion. The Taperuaba syenogranite, located N-NW of Itataia deposit dated at 0.47 Ga (U–Pb zircon age) marks the end of the mineralizing phase.

The second event has located extent, structural controlled by extensional "fault of Itataia" and is characterized by several mineralizing phases of cataclastic/hydrothermal fluid flux/input on fault/fracture and paleokarst zones, which need to be better defined. The connection between fault development and the phosphorous-uranium mineralization in Itataia is also evident in other known epithermal fault- or breccia-hosted uranium deposits in USA (Ralston Creek Mine in Colorado and Coles Hill Virginia), Spain (Fé Mine, Salamanca) and hydrothermal uranium deposits in South China.

Previous fluid inclusion studies for hydrothermal minerals indicated that the mineralizing fluids were saline solutions rich in chlorides and suggest interaction between hydrothermal and meteoric fluids in the formation of Itataia apatite collophane (Ap_2), with a gradual reduction of fluid salinity over time. The petrographic analysis conducted at this work indicates minerals formed at lower temperatures, with a predominance of a second fluorapatite U-rich phase (Ap_2) (29–314 ppm) having fibrou-radious and colloforme habit. This hydrothermal apatite, fill voids and karst cavities in association with authigenic quartz, large calcite crystals, chlorite and zeolite. Associated with this event occurs the generation of the stockwork ores, the mineralized breccias (carbonaceous and carbonate) and the filling of the voids left by quartz leaching in episyenites ores by colloform apatite.

The high porosity resulting from quartz leaching by episyenitization during the first mineralizing event and from hypogene karst processes mixing hydrothermal fluid with heated meteoric waters acting along ductile/brittle planes developed in a big structural and lithoestratigraphic trap.

The Itataia deposit coincides with the hinge zone of a decametric isoclinal fold linked to the Brasiliano compressional event formed by thrust of the basal unit (Fm Barrigas) over the chemical (Fm Alcantil) unit of the Itataia Group. The thrust caused the local increase of marble thickness producing a major trap for mineralization. A second step in the control of mineralization was the

Table 5
Proposed genetic model for the mineralization U–P events and ore genesis of Itataia deposit.

Past events and mineralization U–P events	Mineralogy and related processes in the hot rocks	Typology of phosphorous-uraniferous ores
Phosphate deposition in coastal environment formed by delta and lagoons in the presence of organic matter, with calcareous mud, psammites pelites and chemical sediments shallow marine platform	Primary phosphate	Sedimentar phosphate deposits (phosphorite)
Metamorphism, deformation and granitogene tardi to post Brasiliano/Pan-African orogeny	phosphate formation and recrystallization in metamorphic conditions	
Event 1 Hydrothermal/metasomatic high temperature peralcaline to alkaline fluid circulation of magmatic origin along open spaces foliation, extensional zones and faults planes	Albita from calcic plagioclase Arfvedsonite and fe-eckermannite from tremolita-actinolita Fluorapatite (Ap_1) from igneous and sedimentary apatite widespread episienitization process (Na-metassomatism with quartz lixiviation, Na, Fe and Ti supply and Ca, Mg remotion) precipitation of coffinite formation vugs and larger cavities in structural traps (foliation, extensional zones and faults planes)	Episyenites Uranium and phosphate phases in vugs, voids and structural traps
Event 2 Hydrothermal low temperature heated meteoric waters mixed with a hydrothermal fluid	fluorapatite (Ap_2) with fibro-radious and collophorm habit large calcite crystals and drusy calcite (generation I), autigenic quazrtz, chorite and zeolite karstification in hypogenic conditions	Stockwork and veins of collophanite ore Carbonate and carbonaceous mineralized breccias
Event 3 supergene phreatic phase (probably meteoric waters) and vadose phase (meteoric waters)	fluorapatite and hydroxyapatite (Ap_3) with botryoidal habit drusy and microcristaline calcite (generation II) clay minerals and probably others calcium and aluminous phosphates	Massive collophanite ore

development of E-W extensional failure, which is the current northern boundary of the main orebody.

The relationship between fault development and the second uranium-phosphate phases is clearly observed by the ore zoning in the galleries crossing the mineralized zone. The rich ore intensely brecciated and faulted near the fault scarp, decreases in volume and U–P content to the south.

Considering the existing geochronological data the main period of hydrothermal activity and fluid percolation occurred during the Cenomanian to Santonian (91–81 Ma) postdating the break-up of the South American and African continents. The only age available for the second mineralizing event is compatible with the alkali basalts flows of Serra do Cuo (ca. 91 Ma), after to Rio Ceara-Mirim (RCM) magmatism.

However, considering that the Mesozoic magmatism activity in NE Brasil is characterized by more than one magmatic event, it's quite likely that others volcanic magmatic periods has contributed to the mineralizing stages of Itataia deposit, between the Middle Jurassic and Early Cretaceous periods. Thus, more detailed geochronological and structural studies are needed to better define the relationship between the second U–P mineralizing event with Mesozoic magmatic activity in BP.

The third and last mineralizing event identified in Itataia develops in frankly superficial conditions and was responsible for the generation of the massive reddish and yellowish collophanite ore with the high phosphorus concentrations (P_2O_5 >16%) limited to a topographic altitudes up to 440 m. Besides fluorapatite occurs also other phases of calcium (hydroxyapatite, carbonate-hydroxyapatite) and aluminum phosphates together with clay minerals. The youngest apatite (Ap_3) has botryoidal habit and prevails in the upper portions of the deposit but propagates along the faults, fractures, foliation, vugs and voids created by solution caused both by the infiltration of rainwater in vadose conditions as the associated with seasonal oscillation of water table.

The strong overlap of supergene processes is confirmed by well-defined topographic control reaching depths between 110 and 130 m, which may correspond to an ancient water table limiting the cut-off grade for the ore exploitation.

The Itataia phosphate-uranium deposit has a tectonic and metallogenic complex history characterized by overlapping mineralizing events in different geological times dating back to the deposition of the neoproterozoic supracrustal quartz-pelite-carbonate sediments of the Itataia Group containing phosphorite deposits associated–the primary main source of phosphorus. The primary source of uranium is located outside the mine and was channeled by alkaline-peralkaline fluids from fertile granites of the end of Brasiliano/Pan-African orogeny. The main reason that explains the almost current lack of primary uranium minerals in Itataia is due to the cyclical nature of the mineralizing phase and its high solubility in oxidizing conditions, especially in the presence of phosphate and carbonate, abundant in the Itataia phosphate-uranium deposit.

Acknowledgments

This paper is part of research carried out in cooperation between the Department of Geology of the Federal University of Ceará and the Geosciences Institute of UNB. The authors wish to thank the CAPES (Coordenação de Aperfeiçoamento de Pessoal de Nível Superior) for funding of academic cooperation project entitled: 'Contexto Geológico/Geotectônico dos Recursos Minerais do Estado do Ceará". PROCAD-NF. Thanks also the staff of the geochronology laboratory at the University of Brasilia, especially to doctors Elton L. Dantas, Luis H. Mancini, Nilson F. Botelho and lab technician Barbara A.F. Lima for the technical support.

We are grateful to Givaldo L. Castro, José R. Lima Verde e José R. de Alcântara e Silva for their many constructive discussions during various stages of this project, and to Indústria Nucleares Brasileiras–INB and Grupo Galvani, for providing field support.

References

Alcântara e Silva, J.R.A., 2003. Characterização hidrogeológica da jazida de Itataia-CE. Universidade Federal do Ceará, p. 100. Dissertação de Mestrado.
Almeida, F.F.M., Hasui, Y., Brito Neves, B.B., Fuck, R.A., 1981. Brazilian structural provinces: an introduction. Earth-Science Rev. 17, 1–29.
Almeida, F.F.M., Carneiro, C.D.R., Dehira, L.K., Machado Jr., D.L., 1988. Magmatismo pós-paleozóico no nordeste oriental Brasileiro. Rev. Bras. Geociências 18 (4), 451–462.
Almeida, F.F.M., Carneiro, C.D.R., Mizusaki, A.M.P., 1996. Correlação do Magmatismo das Bacias da Margem Continental Brasileira com o das Áreas Emersas Adjacentes. Rev. Bras. Geociências 26 (3), 125–138.
Angeiras, A.G., 1988. Geology and metallogeny of the northeastern Brazil uranium-phosphorous province emphasizing the Itataia deposit. Ore Geol. Rev. 3, 211–225.
Angeiras, A.G., Neto, A.M., Campos, M., 1978. Mineralização fósforo-uranífera associada a epissienitos sódicos no pré-cambriano. An. do 30º Congr. Bras. Geol. 3, 159–179.
Angeiras, A.G., Netto, A.M., Campos, M., 1981. Phosphoro-Uraniferous Mineralization associated with sodium episyenites in the Ceara precambrian (Brazil). In: Uranium Deposits in Latin America: Geology and Exploration. IAEA Proceedings 162/29, Vienna, pp. 555–577.
Archanjo, C.J., Trindade, R.I., Macedo, J.W.P., Araújo, M.G., 2000. Magnetic fabric of a basaltic dyke swarm associated with Mesozoic rifting in northeastern Brazil. J. South Am. Earth Sci. 13, 179–189.
Arthaud, M.H., 2007. Evolução Neoproterozóica do Grupo Ceará (Domínio Ceará Central, NE Brasil): da sedimentação à colisão continental brasiliana. Tese de doutorado. Universidade de Brasília, p. 132.
Arthaud, M.H., Vasconcelos, A.M., Nogueira Neto, J.A., Oliveira, F.V.C., Parente, C.V., Monié, P., Liégeois, J.P., Caby, R., Fetter, A.H., 1998. Main structural features of precambrian Domains from Ceará (NE Brazil). In: DEGEO/UFOP – IBTA, International Conference on Basement Tectonics, 14th, Ouro Preto, Abstracts, pp. 84–85.
Arthaud, M.H., Caby, R., Fuck, R.A., Dantas, E.L., Parente, C.V., 2008. Geology of the northern Borborema province, NE Brazil and its correlation with Nigeria, NW Africa. In: Pankhurst, R.J., Trouw, R.A.J., Brito Neves, B.B., DeWit, M.J. (Eds.), West Gondwana: Pre-cenozoic Correlations across the South Atlantic Region. Geol. Soc. London. Special Publications, 294.I.
Arthaud, M.H., Fuck, R.A., Dantas, E.L., Santos, T.J.S., Caby, R., Armstrong, R., 2015. The Neoproterozoic Ceara Group, Ceara Central domain, NE Brazil: depositional age and provenance of detrital material. New insights from U–Pb and Sm -Nd geochronology. J. South Am. Earth Sci. 58, 223–237.
Audra, P., Dántoni-Nobecourt, J.-C., Bigot, J.-Y., 2010. Hypogenic caves in France. Speleogenesis and morphology of the cave systems. Bull. Soc. Géol. Fr. 4, 327–335.
Ballhorn, R.K., Thakur, V.K., Da Fonte, J.E.C., Suckau, V., 1978. Geology of the espinharas uranium deposit, Brazil. In: Uranium Deposits in Latin America: Geology and Exploration. IAEA Proceedings 162/27, Vienna, pp. 521–531.
Barbosa, B.M.A., 2011. Estudo do Depósito Uranífero de São José de Espinharas (PB): Avaliação do potential mineral para U-ETR com base na geoquímica e química mineral. Dissertação de mestrado. Universidade Federal de Pernambuco, p. 95.
Bella, P., Gaál, Lovít, Šucha, V., Koděra, P., Milovský, R., 2016. Hydrothermal speleogenesis in carbonates and metasomatic silicites induced by subvolcanic intrusions: a case study from the Štiavnické vrchy Mountains, Slovakia. Int. J. Speleol. 45 (1), 11–25.
Bellieni, G., Macedo, M.H.F., Petrini, R., Piccirillo, E.M., Cavazzini, G., Comim-Chiaramonti, P., Ernesto, M., Macedo, J.W.P., Martins, G., Melfi, A.J., Pacca, I.G., De Min, A., 1992. Evidence of magmatic activity related to Middle Jurassic and Lower Cretaceous rifting from northeastern Brazil (Ceará-Mirim): K/Ar age, palaeomagnetism, petrology and Sr-Nd isotope characteristics. Chem. Geol. 97, 9–32.
Benkhelil, J., 1989. The origin and evolution of the cretaceous Benue Trough (Nigeria). J. Afri. Earth Sci. 8, 251–282.
Bessoles, B., Trompette, R., 1980. Géologie de l' Afrique, la chaîne panafricaine, zone mobile d'Afrique Centrale (partie sud et zone mobile soudanaise). Mémoire du Bureau de Recherches Géologiques Minières 92.
Binks, R.M., Fairhead, J.D., 1992. A plate tectonic setting for Mesozoic rifts of West and Central Africa. Tectonophysics 213, 141–151.
Both, R.A., Arribas, A., Saint-André, B., 1984. The origin of breccia-hosted uranium deposits in carbonaceous metasediments of the Iberian Peninsula: U-Pb geochronology and stable isotope studies of the Fé deposit, Salamanca Province, Spain. Econ. Geol. 89, 584–601.
Bowie, S.H.U., 1979. The mode of occurrence and distribution of uranium deposits: royal Society of London,. Philos. Trans. Ser. 291, 289–300.
Brito Neves, B.B., 1998. The cambro-ordovician of the Borborema province. Rev. Inst. Geociências – Usp. Série Científica, São Paulo 29, 175–193.
Brito Neves, B.B., Cordani, U.G., 1991. Tectonic Evolution of South America during the Late Proterozoic, 53. Precambrian Research, pp. 23–40.

Brito Neves, B.B., Campos Neto, M.C., Fuck, R.A., 1999. From rodinia to western Gondwana: an approach to the Brasilaino-Pan African cycle and orogenic collage. Episodes 22, 155–166.
Brito Neves, B.B., Santos, E.J., Van Schmus, W.R., 2000. Tectonic history of the Borborema province. In: Cordani, U.G., Milani, E.J., Thomaz Filho, A., Campos, D.A. (Eds.), Tectonic Evolution of South America. 31st International Geological Congress, Rio de Janeiro, Brazil, pp. 151–182.
Brito Neves, B.B., Campos Neto, M.C., Van Schmus, W.R., Santos, E.J., 2001. O sistema Pajeú-Paraíba e o maciço São José do Campestre no leste da Borborema. Rev. Bras. Geociências 31, 1–15.
Brito Neves, B.B., Passarelli, C.R., Basei, M.A.S., Santos, E.J.S., 2003. Idades U-Pb em Zircão de Alguns Granitos Clássicos da Província Borborema. Rev. Inst. Geociências – USP. Série Científica, São Paulo 3, 25–38.
Caby, R., 1989. Precambrian terranes of Benin-Nigeria and northeast Brazil and the late Proterozoic South Atlantic fit". Geol. Soc. Am. 145–158. Special Paper 230.
Caby, R., Arthaud, M.H., 1986. Major precambrian nappes of the Brazilian belt, Ceará, northeast Brazil. Geology 14, 871–874.
Campos, M., Braga, A.P.G., Mello, A.A., Souza, E.M., Silva, F.A.F., França, J.B., 1979. Projeto Rio Jaguaribe. DNPM, Brasília, p. 150.
Castro, G.L., 2001. Litogeoquímica e isótopos estáveis de carbono e oxigênio das rochas metassedimentares hospedeiras da jazida fósforo-uranífera de Itataia-Santa Quitéria, Ceará. Dep. Geologia, Universidade Federal do Ceará, p. 195. Dissertação de Mestrado.
Castro, N.A., 2005. Evolução Geológica Proterozóica da Região entre Madalena e Taperuaba, Domínio Tectônico Ceará Central (Província Borborema). Tese de doutorado. Inst. Geociências, Universidade de São Paulo, p. 221.
Castro, G.L., Parente, C.V., Veríssimo, C.U.V., Sial, A.N., Garcia, M.G.M., Santos, R.V., Castro, R.M., Santos, A.A., 2005a. Isótopos de Carbono e Oxigênio dos Mármores Associados com o Depósito Fósforo Uranífero de Itataia, Ceará. Rev. Bras. Geociências 35, 199–208.
Castro, N.A., Basei, M.A.S., Onoe, A.T., 2005b. Phosphorous-uraniferous mineralization at Itataia (Ceará state, Brazil): geological aspects and $^{40}Ar/^{39}Ar$ age. V. SSAGI Abstr. 603, 1–4.
Cathelineau, M., 1986. The hydrothermal alkali metasomatism effects on granitic rocks: quartz dissolution and related subsolidus changes. J. Petrol. 27, 945–965.
Cathelineau, M., 1987. U-Th-REE mobility during albitization and quartz dissolution in granitoids: evidence from south-east French Massif Central. Bull. Minéral. 110, 249–259.
Cavalcante, J.C., Vasconcelos, A.M., Medeiros, M.F., Paiva, I.P., Gomes, F.E.M., Cavalcante, S.N., Cavalcante, J.E., Melo, A.C.R., Duarte Neto, V.C., Benevides, H.C., 2003. Mapa Geológico Do Estado Do Ceará – Escala 1:500.000. CPRM-SGB Serviço Geológico do Brasil, Fortaleza.
Cavalcanti, J.A.D., Bessa, M.D.M.R., 2011. A pesquisa de Fosfato na área Ceará Central. In: Abram, M.B., Bahiense, I.C., Porto, C.G., Brito, R.S.C. (Eds.), Projeto Fosfato do Brasil – Parte I, Capítulo IX. 1ed. Salvador: CPRM, Programa Geologia do Brasil. Informe de Recursos Minerais, Série Insumos Minerais para a Agricultura, 13, pp. 487–518.
Cavalcanti, J.A.D., Veríssimo, C.U.V., Bessa, D.M.R., Parente, C.V., 2013. Contribution of the Karstic Environment on the Origin of the Collophanites of Itataia Uranium-phosphorous Deposit, Borborema Province, Brazil. In: 16th International Congress of Speleology. 2013, Praga, 3, pp. 173–178. Proceedings.
Chen, Y.W., Bi, X.W., Hu, R.Z., 2009. Comparison of geochemical characteristic of uranium- and non-uranium-bearing Indosinian granites in Guidong composite pluton. J. Min. Petrol 29, 106–114.
Corsini, M., Figueiredo, L.L., Caby, R., Feraud, G., Ruffet, G., Vauchez, A., 1998. Thermal history of the Pan-African/Brasiliano Borborema province of the northeast Brazil deduced from $^{40}Ar/^{39}Ar$ analysis. Tectonophysics 285, 103–117.
Coulon, C., Vidal, P., Dupuy, C., Baudin, P., Popoff, M., Maluski, H., Hermitte, D., 1996. The Mesozoic to early Cenozoic magmatism of the Benue Trough (Nigeria); geochemical evidence for the involvement of the St. Helena plume. J. Petrol 37, 1341–1358.
Cuney, M., 1978. Geologic environment, mineralogy, and fluid inclusions of the Bois Noirs-Limouzat uranium vein, Forez, France. Econ. Geol. 73, 1567–1610.
Cuney, M., 2009. The extreme diversity of uranium deposits. Min. Dep. 44, 3–9.
Cuney, M., 2010. Evolution of uranium fractionation process through time: driving the secular variation of uranium deposit types. Econ. Geol. 105, 553–569.
Cuney, M., 2014. Felsic magmatism and uranium deposits. Bull. Soc. Géol. Fr. 2, 75–92.
Cuney, M., Emetz, A., Mercadier, J., Mykchaylov, V., Shunko, V., Yuslenko, A., 2012. Uranium deposits associated with Na-metasomatism from central Ukraine: a review of some of the major deposits and genetic constraints. Ore Geol. Rev. 44, 82–106.
Dahlkamp, F.J., 1980. The time related occurrence of uranium deposits. Min. Dep. 15, 69–79.
Dahlkamp, F.J., 1993. Uranium Ore Deposits. Springer-Verlag, Berlim, p. 460.
Dahlkamp, F.J., 2009. Uranium Deposits of the Word Asia. Springer, p. 493.
Dong, S., Chen, D., Qing, H., Zhou, X., Wang, D., Guo, Z., Jiang, M., Qian, Y., 2013. Hydrothermal alteration of dolostones in the Lower Ordovician, Tarim Basin, NW China: Multiple constraints from petrology, isotope geochemistry and fluid inclusion microthermometry. Mar. Petroleum Geol. 46, 270–286.
Faure, G., 1998. Principles and Applications of Geochemistry, second ed. Prentice Hall, p. 625.
Favali, J.C., Leal, J.R.L.V., 1982. Contribuição ao estudo das mineralizações fosfáticas e uraníferas da jazida de Itataia, Ceará. In: Anais do 32° Congresso Brasileiro de Geologia, SBG, Salvador, pp. 2022–2034.
Favali, J.C., Netto, R.M., Silva, J.R.A., Oliveira, J.A.D., 1984. Ocorrência fósforo-uranífera de Serrotes Baixos-CE. In: Anais do 33° Congresso Brasileiro de Geologia, SBG, Rio de Janeiro, pp. 1452–1462.
Ferguson, J., 1987. The uranium cycle. In: Ferguson, J., Goleby, A.B. (Eds.), Recognition of Uranium Provinces. IAEG, Vienna, pp. 3–16.
Ferreira, V.P., Sial, A.N., Jardim de Sá, E.F., 1998. Geochemical and isotopic signatures of Proterozoic granitoids in terranes of the Borborema structural province, northeastern Brazil. J. South. Am. Earth Sci. 11, 439–455.
Fetter, A.H., 1999. U-pb and Sm-nd Geocronological Constraints on the Crustal Framework and Geologic History of Ceará State, NW Borborema Province, NE Brazil: Implications for the Assembly of Gondwana. Ph.D. thesis. University of Kansas, p. 164.
Finch, R., Murakami, T., 1999. Systematics and paragenesis of uranium minerals. In: uranium: mineralogy, geochemistry and the environment. In: Burns, Finch (Eds.), Reviews in Mineralogy, 38, pp. 91–166.
Ford, D., Williams, P., 2007. Karst Hydrogeology and Geomorphology. John Wiley & Sons Ltd, p. 562.
Forti, P., 2010. Genesis and evolution of the caves in the naica mine (chihuahua, Mexico). Z. für Geomorphol. Suppl. issue 54 (2), 285–306.
Fuzikawa, K., 1978. Estudo preliminar de inclusões flúidas em amostras do Projeto Itatira. Relatório Interno. Nuclebrás, Rio de Janeiro, p. 26.
Fyfe, W.S., 1978. Notes on the Itataia deposit. Relatório de Consultoria DNPM/DIAOP. Nuclebrás, Rio de Janeiro, p. 34.
García-Ruiz, J.M., Villasuso, R., Ayora, C., Canals, A., Otálora, F., 2007. Formation of natural gypsum megacrystals in Naica, Mexico. Geology 35 (4), 327–330.
Gomes, A.J.P., Cruz, P.R., Borges, L.P., 2003. Recursos Minerais Energéticos; Carvão e Urânio. In: Bizzi, L.A., Schobbenhaus, C., Vidotti, R.M., Gonçalves, J.H. (Eds.), Geologia, Tectônica e Recursos Minerais do Brasil, 3. CPRM-SGB, Brasília, 577–528.
Haddad, R.C., 1981. Mineralização uranífera no Complexo Anelar de Taperuaba-CE. Dissertação de mestrado. Universidade de Brasília, p. 73.
Haddad, R.C., Leonardos, O.H., 1980. Granitos anelares de Taperuaba (Ceará) e processos metassomáticos associados. In: Anais do 31° Congresso Brasileiro de Geologia, SBG, Camboriú, pp. 2626–2631.
Hecht, L., Thuro, K., Plinninger, R., Cuney, M., 1999. Mineralogical and geochemical characteristics of hydrothermal alteration and episyenitization in the Königshain granites, northern Bohemian Massif. Ger. Int. Journ. Earth Sci. 88, 236–252.
Hu, R.Z., Bi, X.W., Zhou, M.F., et al., 2008. Uranium metallogenesis in south China and its relationship to crustal extension during the Cretaceous to Terciary. Econ. Geol. 103, 583–598.
Hu, H., Wang, R., Chen, W., Chen, P., Ling, H., Liu, G., 2013. Timing of hydrothermal activity associated with the Douzhashan uranium-bearing granite and its significance for uranium mineralization in northeastern Guangxi, China. Chin. Sci. Bull. 58, 4319–4328.
Jerden Jr., J.L., 2001. Origin of Uranium Mineralization at Coles Hill Virginia (USA) and its Natural Attenuation within an Oxidizing Rock-soil-ground Water System. Ph.D. thesis. Virginia Polytechnic Inst. and State University, 145.
Kouske, A.P., Suh, C.E., Ghogomu, R.T., Ngako, V., 2012. Na-metasomatism and uranium mineralization during a two-stage albitization at Kitongo, Northern Cameroon: structural and Geochemical evidence. Int. J. Geosci. 3, 258–279.
Langmuir, D., 1978. Uranium solution-minerals equilibria at low temperatures with applications to sedimentary ore deposits. Geochim. Cosmochim. Acta 42, 547–569.
Leake, B.E., Woolley, A.R., Arps, C.E.S., Birch, W.D., Gilbert, M.C., Grice, J.D., Hawthorne, F.C., Kato, A., Kisch, H.J., Krivovichev, V.G., Linthout, K., Laird, J., Mandarino, J.A., Maresch, W.V., Nickel, E.H., Rock, N.M.S., Schumacher, J.C., Smith, D.C., Stephenson, N.C.N., Ungaretti, L., Whittaker, E.J.W., Youzhi, G., 1997. Nomenclature of amphiboles. Report of the subcommittee on amphiboles of the international mineralogical association commission on new minerals and mineral names. Am. Mineralogist 82, 1019–1037.
Leal, J.R.L.V., Azevedo, L.F., Castro, G.L., Silva, J.R.A., 1984. Mineralização fósforo-uranífera da Fazenda Mandacaru, Irauçuba-CE. In: Anais do 33° Congresso Brasileiro de Geologia, SBG, Rio de Janeiro, pp. 1437–1451.
Legrand, J.M., Deutsch, S., Cunha de Souza, L., 1991. Datação U-Pb e granitogênese do maciço de Acari, RN. In: Anais do 14° Simpósio de Geologia do Nordeste, SBG/NN, Recife, 12, pp. 172–174.
Leroy, J., 1978. The Margnac and Fanay Uranium Deposits of the La Crouzille District (Western Massif Central, France). Geologic and Fluid Inclusion Studies.
Li, J., Zhou, M., Li, X., Fu, Z., Li, Z., 2002. Structural control on uranium mineralization in South China: implications for fluid flow in continental strike-slip faults. Sci. China Series D 45, 851–864.
Maluski, H., Coulon, C., Popoff, M., Baudin, P., 1995. 40Ar/39Ar chronology, petrology and geodynamic setting of Mesozoic to early Cenozoic magmatism from the Benue Trough, Nigeria. J. Geol. Soc. Lond 152, 311–326.
Martin, R.F., 1969. The hydrothermal syntesis of low albite. Contrib. Mineral. Petrol. 23, 323–339.
Martin-Izard, A., Arribas Sr., A., Arias, D., Ruiz, J., Fernández, F.J., 2002. The Fe deposit, west-central Spain: tectonic-hydrothermal uranium mineralization associated with transpressional faulting of alpine age. Can. Mineralogist 40, 1505–1520.
Martins, G., Oliveira, D.C., 1992. O enxame de diques Rio Ceará-Mirim (EDCM) no contexto da abertura do oceano Atlântico. Rev. Geol. 5, 51–78.
Marzoli, A., Renne, P.R., Piccirillo, E.M., 2000. Ar/Ar Geochronology of Mesozoic Continental Basaltic Magmatism, and the Opening of the Central, Equatorial and Southern Atlantic Ocean. Penrose 2000, Volcanic Rifted Margins. University of

London, p. 54.
Mascle, J., Marhino, M., Wanesson, J., 1986. The structure of the Guinean continental margin: implications for the connection between the Central and the South Atlantic Oceans. Geol. Rundsch. 75, 57–70.
Medeiros, V.C., 2004. Evolução Geodinâmica e Condicionamento Estrutural dos Terrenos Piancó-Alto Brígida e Alto Pajeú, Domínio da Zona Transversal, NE do Brasil. Tese de doutorado, p. 190.
Mendonça, J.C.J.S., Campos, M., Braga, A.P.G., Souza, E.M., 1982. Caracterização estratigráfica dos metassedimentos da região de Itataia-CE (Grupo Itataia). In: Anais do 32º Congresso Brasileiro de Geologia, vol. 1. SBG, pp. 325–338.
Mendonça, J.C.J.S., Campos, M., Braga, A.P.G., Souza, E.M., Favali, J.C., Leal, J.R.L.V., 1985. Jazida de urânio de Itataia-Ceará. In: Principais Depósitos Minerais Do Brasil, I. DNPM/CVRD, pp. 121–131.
Misra, K.C., 2000. Understanding Mineral Deposits. Kluwer Academic Publishers, Dordrecht/Boston/London, pp. 613–659. Cap 14: Uranium Deposits.
Mont'Alverne, A.A.F., Jardim de Sá, E.F., Derze, G.R., Dantas, J.R.A., Ventura, P.E.O., 1998. Mapa Geológico do Rio Grande do Norte e 1:500.000. Departamento Nacional da Produção Mineral/Universidade Federal do Rio Grande do Norte/PETROBRÁS/CRM.
Morgan, W.J., 1983. Hotspot tracks and the early rifting of the Atlantic. Tectonophysics 94, 123–139.
Nash, J.T., 1981. Geology and genesis of major word hard-rock uranium deposits. An overview: U.S. Geological Survey Open-File Report 81-166, p. 123.
Neves, S.P., 2003. Proterozoic history of the Borborema province (NE Brazil): correlations with neighboring cratons and Pan-African belts and implications for the evolution of the western Gondwana. Tectonics 34, 1031. http://dx.doi.org/10.1029/2001TC001352.
Neves, S.P., Mariano, G., 1999. Assessing the tectonic significance of a large-scale transcurrent shear zone system: the Pernambuco lineament, northeastern Brazil. J. Struct. Geol. 21, 1369–1383.
Neves, S.P., Mariano, G., Guimarães, I.P., Silva Filho, A.F., Melo, S.C., 2000. Intralithospheric differentiation and crustal growth: evidence from the Borborema Province, northeastern Brazil. Geology 28, 519–522.
NUCLEBRÁS, 1984. Jazida de Itataia – Relatório de Pesquisa Mineral,. Circulação Interna, Indústria Nucleares do Brasil S/A–INB, Fortaleza, p. 330 vol. 1.
Nurnberg, D., Muller, R.D., 1991. The tectonic evolution of the south Atlantic from late Jurassic to present. Tectonophysics 131, 27–53.
O'Connor, J.M., Le Roex, A.P., 1992. South Atlantic hot spot-plume systems: 1. Distribution of volcanism in time and space. Earth Planet. Sci. Lett. 113, 343–364.
Ofoegbu, C.O., 1984. A model for the tectonic evolution of the Benue Trough of Nigeria. Geol. Rundsch. 73, 1007–1018.
Öhlander, B., 1986. Proterozoic mineralizations associated with granitoids in northern Sweden. Sver. Geol. Unders. 65, 1–39.
Oliveira, J.F., Cavalcante, J.C., 1993. Mombaça, Folha SB.24-V-D-V, Estado Do Ceará, Texto Explicativo. DNPM, Brasília-DF, p. 200.
Otoničar, B., 2013. Large calcite crystals from Cok cave (abandoned iron mine), Jelovica Plateau, NW Slovenia. Mine Caves/Grotte Miniera Mem. Ist. Ital. Speleol. 28, 75–76.
Parente, C.V., Silva Filho, W.F., Almeida, A.R., 2004. Bacias do Estágio da Transição do Domínio Setentrional da Província Borborema. In: Mantesso-Neto, V., Bartorelli, A., Carneiro, C.D.R., Brito Neves, B.B. (Eds.), Geologia do Continente Sul-Americano: Evolução da obra de Fernando Flávio Marques de Almeida, Ed. Beca, São Paulo, pp. 525–536.
Parente, C.V., Verissimo, C.U.V., Botelho, N.F., Oliveira, C.G., Lira Jr., J.A., Martins, D.T., 2014. Caracterização geológica, petrográfica e tipológica dos primeiros Skarns de ferro e cobre encontrados no Arco Magmático de Santa Quitéria-Ceará, Brasil. In: 47º Congresso Brasileiro de Geologia, 2014, Salvador, Ba. Anais do 47º Congresso Brasileiro de Geologia, 2014.
Parente, C.V., Veríssimo, C.U.V., Botelho, N.F., Santos, T.J.S., Oliveira, C.G., Lira Jr., J.A., Martins, D.T., 2015. Depósitos de escarnitos mineralizados em ferro e cobre do arco magmático de Santa Quitéria, Ceará, Província Borborema do nordeste do Brasil. Braz. J. Geol. 45, 359–382.
Pérez del Villar, L., Bruno, J., Campos, R., Gómez, P., Cózar, J.S., Garralón, A., Buil, B., Arcos, D., Carretero, G., Ruiz Sánchez-Porro, J., Hernán, P., 2002. The uranium ore from Mina Fe (Salamanca, Spain) as a natural analogue of processes in a spent fuel repositor. Chem. Geol. 190, 395–415.
Petters, S.W., 1978. Stratigraphic evolution of the Benue Trough and its implications for the upper cretaceous Paleogeography of West Africa. J. Geol. 86, 311–322.
Pires, F.R.M., 2012. Urânio no Brasil: geologia, jazidas e ocorrências. Vitrina Comunicação, INB, Rio de Janeiro, p. 264.
Plant, J.A., Simpson, P.R., Smith, B., Windley, B.F., 1999. Uranium ore deposits: products of the radioactive earth. Rev. Mineralogy Geochem. 38, 255–319.
Porto da Silveira, C.L., Schorscher, H.D., Miekeley, N., 1991. The geochemistry of albitization and related uranium mineralization, Espinharas, Paraiba (PB), Brasil. J. Geochem. Explor 40, 329–347.
Poty, B., Leroy, J., Cathelineau, M., Cuney, M., Friedrich, M., Lespinasse, M., Turpin, L., 1986. Uranium deposits spatially related to granites in the French part of the Hercynian orogeny. In: Fuchs, H.D. (Ed.), Vein Type Uranium Deposits, 361, pp. 246–251. TEC DOC.
René, M., 2005. Geochemical constraints of hydrothermal alterations of two-mica granites of the Moldanubian batholith at the Okrouhlá Radoun uranium deposit. Acta Geodyn. Geomater. 140, 63–79.
Renne, P.R., Ernesto, M., Pacca, I.G., Coe, R.S., Glen, J.M., Prevot, M., Perrin, M., 1992. The age of Parana flood volcanism, rifting of Gondwanaland, and the Jurassic-Cretaceous boundary. Science 258, 975–979.
Roberson, D.S., Tilsley, J.E., Hogg, G.M., 1978. The time-bound character of uranium deposits. Econ. Geol. 73, 1409–1419.
Saad, S., Munne, A.L., Tanaka, A.Y., 1984. Proposição de um novo modelo genético para a jazida de Itataia. In: Anais do 33° Congresso Brasileiro de Geologia. SBG, Rio de Janeiro, pp. 1410–1423.
Salim, J., 1993. Géologie, pétrologie et géochimie des skarns à scheelite de la Mine Brejuí, Currais Novos, région du Seridó, NE du Brésil. DrSc thesis. Univ Catholique de Louvain, Belgium, p. 272.
Santos, L.C.S., 1985. Mineralização de urânio ligada a metassomatismo sódico, espinharas-PB. Revista Bras. Geociências 15, 9–17.
Santos, A.A., 2003. Caracterização litoestrutural e geocronológica da região fósforo-uranífera de Itataia-CE. Dissertação de Mestrado. Universidade Federal do Ceará, p. 100.
Santos, L.C.S., Anacleto, R., 1985. Jazida de urânio de Espinharas – Paraíba. In: Brasil DNPM. Principais Depósitos Minerais Do Brasil. Brasília, 1, pp. 143–165 cap. 10.
Santos, T.J.S., Santos, A.A., Dantas, E.L., Fuck, R.A., Parente, C.V., 2003. Nd isotopes and provenance of metassediments of the Itataia group, northwest Borborema province, NE Brazil. In: IV South American Symposium on Isotope Geology, Salvador, Brazil, pp. 286–289. Short Papers.
Santos, T.J.S., Fetter, A.H., Hackspacher, P.C., Van Schmus, W.R., Nogueira Neto, J.A., 2008. Neoproterozoic tectonic and magmatic episodes in the NW sector of Borborema Province, NE Brazil, during assembly of Western Gondwana. J. South Am. Earth Sci. 25, 271–284.
Santos, E.J., Souza Neto, J.A., Silva, M.R.R., Beurlen, H., Cavalcanti, J.A.D., Silva, M.G., Dias, V.M., Costa, A.F., Santos, R.B., 2014. Metalogênese das porções norte e central da Província Borborema. In: Silva, M.G., Rocha Neto, M.B., Jost, H., Kuyumjian, R.M. (Eds.), Metalogênese das Províncias Minerais do Brasil. Programa Geologia do Brasil. Rec. Minerais. Série Metalogenia. Belo Horizonte, CPRM, pp. 343–388.
Schobbenhaus, C., Campos, D.A., 1984. A evolução da PlataForma Sul-Americana no Brasil e suas principais concentrações minerais. In: Schobbenhaus, C., Campos, D.A., Derze, G.R., Asmus, H.E. (Eds.), Geologia do Brasil. Ministério das Minas e Energia. Departamento Nacional da Produção Mineral, Brasília, pp. 9–53.
Self, C.A., Hill, C.A., 2003. How speleothems grow: a guide to the ontogeny of cave minerals. J. Cave Karst Stud. 65 (2), 130–151.
Sial, A.N., Long, L.E., Pessoa, D.A.R., Kawashita, K., 1981. Potassium-argon ages and strontium isotope geochemistry of Mesozoic and Tertiary basaltic rocks, Northeastern Brazil. An. Acad. Bras. Ciênc 53, 115–122.
Sibson, R.H., Moore, J., Mc Rankin, A.H., 1975. Seismic pumping – a hydrothermal fluid transport mechanism. J. Geol. Soc. 131, 653–659.
Skirrow, R.G., Jaireth, S., Huston, D.L., Bastrakov, E.N., Schofield, A., Wielen, S.E., Barnicoat, A.C., 2009. Uranium Mineral Systems: Process, Exploration Criteria and a New Deposit Framework, p. 44. Geoscience Australia Record 2009/20.
Smellie, J.A.T., Laurikko, J., 1984. Skuppeasavon, northern Sweden: an uranium mineralization associated with alkali metasomatism. Min. Deposita 19, 183–192.
Souza, Z.S., Vasconcelos, P.M., Nascimento, M.A.L., Silveira, F.V., Paiva, H.S., Dias, L.G.S., Thiede, D., Carmo, I.O., 2003. ^{40}Ar-^{39}Ar geochronology of Mesozoic and Cenozoic magmatism in NE Brazil. In: 4th South American Symposium on Isotope Geology, Proceedings, pp. 691–694.
Souza, E.M., Farias, E.E., Silva Filho, C.A., Villar, H.P., França, E.J., Hazin, C.A., 2012. Ocorrência de urânio em Pocinhos, Paraíba – a anomalia de Sítio Bravo: petrografia e radiometria. Estud. Geol. 22, 94–103.
Souza Neto, J.A., Legrand, J.M., Volfinger, M., Pascal, M.L., Sonnet, P., 2008. W-Au skarns in the Neo-Proterozoic Seridó mobile belt, Borborema Province in northeastern Brazil: an overview with emphasis on the Bonfim deposit. Mineral. Deposita 43, 183–205.
Teixeira, M.L.A., 2005. Integração de dados aerogeofísicos, geológicos e isotópicos do limite norte do Complexo Tamboril-Santa Quitéria – CE (Província Borborema). MSc thesis. Inst. de Geociências, Brasília, p. 91.
Thompson, T.B., 1988. Geology and uranium-thorium mineral deposits of the Bokan Mountain Granite complex, southeastern Alaska. Ore Geol. Rev. 3, 193–210.
Torres, P.F.M., Cavalcante, J.C., Forgiarini, L.L., Palheta, E.S.M., Vasconcelos, A.M., 2008. Nota explicativa da Folha Quixadá, escala 1:250.000. Serviço Geológico do Brasil. CPRM, Fortaleza.
Trompette, R., 1994. Geology of Western Gondwana, Pan-African – Brasiliano Aggregation of South America and Africa. A.A. Balkema, Rotterndam, Brookfield, p. 350.
Turner, S., Regelous, M., Kelly, S., Hawkesworth, C., Mantovani, M., 1994. Magmatiim and continental break-up in the South Atlantic: high precision 40Ar-39Ar geochronology. Earth Planet. Sci. Lett. 121, 333–348.
Van Schmus, W.R., Brito Neves, B.B., Hackspacher, P.C., Babinski, M., 1995. U/Pb and Sm/Nd geochronologic studies of the eastern Borborema Province, Northeastern Brazil: initial conclusions: J. South Am. Earth Sci. 8, 267–288.
Vauchez, A., Neves, S., Caby, R., Corsini, M., Egydio-Silva, M., Arthaud, M.H., Amaro, V., 1995. The Borborema shear zone system, NE Brazil. J. South Am. Earth Sci. 8, 247–266.
Veríssimo, C.U.V., Santos, R.V., Parente, C.V., Oliveira, C.G., Cavalcanti, J.A.D., Nogueira Neto, J.A., 2010. Geoquímica Isotópica do Depósito de Fosfato e Uranio de Itataia, CE. In: X Cong. de Geoquimica dos Países de Língua Portuguesa e XVI Semana de Geoquímica, 2010, Porto. X Cong. de Geoquimica dos Países de Língua Portuguesa e XVI Semana de Geoquímica, pp. 883–889.
Wallace, A., Karlson, R., 1985. The schwartzwalder uranium deposit, in: Geology and structural controls on mineralization. Econ. Geol. 80, 1842–1857.